THE UNIVERSITY OF
WARWICK

AUTHOR: **Krishnan Rama** DEGREE: **Ph.D.**

TITLE: **Fermion Flavour Observables: Renormalisation Invariants and Model Building using Discrete Symmetries**

DATE OF DEPOSIT: .....

I agree that this thesis shall be available in accordance with the regulations governing the University of Warwick theses.

I agree that the summary of this thesis may be submitted for publication.

I **agree** that the thesis may be photocopied (single copies for study purposes only).

Theses with no restriction on photocopying will also be made available to the British Library for microfilming. The British Library may supply copies to individuals or libraries. subject to a statement from them that the copy is supplied for non-publishing purposes. All copies supplied by the British Library will carry the following statement:

> "Attention is drawn to the fact that the copyright of this thesis rests with its author. This copy of the thesis has been supplied on the condition that anyone who consults it is understood to recognise that its copyright rests with its author and that no quotation from the thesis and no information derived from it may be published without the author's written consent."

AUTHOR'S SIGNATURE: .....

USER'S DECLARATION

1. I undertake not to quote or make use of any information from this thesis without making acknowledgement to the author.
2. I further undertake to allow no-one else to use this thesis while it is in my care.

DATE SIGNATURE ADDRESS

.....

.....

.....

.....

.....

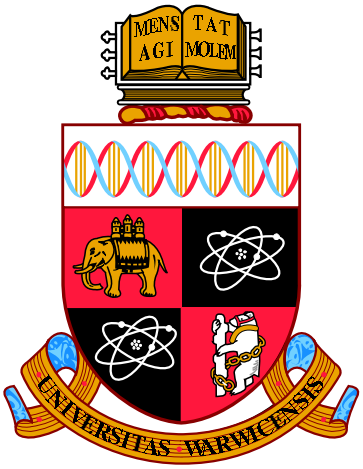

Fermion Flavour Observables: Renormalisation Invariants and Model Building using Discrete Symmetries

by

Krishnan Rama

Thesis

Submitted to the University of Warwick

for the degree of

Doctor of Philosophy

Department of Physics

October 2012

THE UNIVERSITY OF WARWICK

To
my little sister and best friend
Parvati Janaki

Contents

List of Tables

List of Figures

Acknowledgments

I thank my supervisors Prof. Paul Harrison and Prof. Bill for the wonderful support and guidance they provided in my research. I gratefully acknowledge the fruitful interactions I had with the staff and my friends in the Department of Physics that made my work a very pleasant experience. I also thank the University of Warwick and the Centre for Fundamental Physics at the Rutherford Appleton Laboratory for funding my research fellowship.

Declarations

The first chapter, "Introduction: Survey of the Field", does not contain any original work by the author. Here many figures from other publications have been used. The original research on renormalisation invariants described in Chapter 2 was done by the author under the guidance of Prof. Paul Harrison and Prof. Bill and it was published [1]. This material has been written verbatim in Sections 2.3-2.6. The results were also presented in the 35^{th} ICHEP conference (July 22-28, 2010, Paris). Model building and the accompanying research described in Chapter 3 and Chapter 4 were also done by the author under his supervisors' guidance. Some of the results in Chapter 3 were presented in the "NExT Meeting on Neutrino Physics and Particle Cosmology" (May 4, 2011, The University of Southampton). We have also submitted this work to PRD for publication. The main results from Chapter 4 were presented in the 36^{th} ICHEP conference (July 4-11, 2012, Melbourne) and "The LHC, Particle Physics and the Cosmos" (July 13-15, 2012, The University of Auckland). A paper with these results is currently under consideration for publication in JHEP.

Abstract

We very briefly review the current status of flavour physics with much of the emphasis on the experimental and the theoretical aspects of neutrino oscillations. Later we move on to study flavour symmetric constraints among observables like the Koide formula and present a novel speculation in this context. Our research on the renormalisation evolution of flavour symmetric observables leads us to the discovery of exact one-loop evolution invariants in the Standard Model. Then we shift our attention towards model building. We construct a model based on the discrete group $C_3 \times C_3 \rtimes C_3$ and successfully describe the flavour physics in the leptonic sector including the recent observation of non-zero mixing angle θ_{13}. Here both the charged-lepton and the neutrino mass matrices have a common circulant-plus-diagonal form. Later we use the previously published "Simplest Neutrino" texture as the starting point to construct another model based on the discrete group S_4. We redefine the flavour basis in a non-standard way and use the "μ-τ" rotated basis of S_4 in model building. Like in the previous model, here also we use the recent experimental data for fitting and make predictions.

Chapter 1

Introduction: Survey of the Field

Quarks and leptons which are the elementary fermions interact through the exchange of gauge bosons. The Standard Model of Particle Physics is the gauge theory that describes electroweak and strong interactions using the gauge group $SU(3) \times SU(2) \times U(1)$. The current formulation of the Standard Model was finalised in the mid 1970s with the confirmation of the existence of quarks. The discovery of the last of the fermions, the top quark (1995) and tau neutrino (2000), came later completing the picture of the three families. The apparent discovery of the Higgs boson, the last undiscovered particle in the Standard Model, came in 2012.

1.1 The Standard Model

In particle physics the fundamental interactions are described through local gauge theories. Here the Lagrangian is invariant under continuous local transformations formulated using the language of the Lie groups. Quantum electrodynamics is the simplest of these with a local abelian $U(1)$ gauge symmetry. This theory is extremely successful in predicting the electromagnetic interactions. In 1960 Sheldon Glashow discovered that the electromagnetic and the weak interactions can be combined in a single non-abelian gauge theory and later in 1967 Steven Weinberg and Abdus Salam incorporated the Higgs mechanism into Glashow's electroweak theory.

Fermions acquire mass through spontaneous symmetry breaking of the electroweak symmetry with the help of the Higgs mechanism. The Yukawa couplings give particles their corresponding masses and also bring about the phenomenon of flavour mixing. The Higgs mechanism also gives mass to the W and Z bosons, the only massive gauge bosons. The detection of the neutral weak currents caused by the Z boson exchange in 1973 and later the detection of W and Z particles in 1981 gave

the conclusive experimental confirmation for the electroweak theory. The masses of these gauge bosons were found to be the same as predicted by the theory.

Three flavours of quarks were first proposed by Gell-Mann in 1961 using his theory of eightfold way to explain the existence of a large number of hadrons and also to sort them into groups, but searches for free quarks failed. However high energy experiments proved that hadrons were indeed composed of constituent particles, also called partons. James Bjorken's theory of partons was verified at the Stanford Linear Accelerator. The explanation for the existence partons and the non-observation of free quarks came with the discovery that a non-abelian gauge theory leads to asymptotic freedom at high energies and confinement at low energies. David Gross, David Politzer and Frank Wilczek showed that the $SU(3)$ non-abelian gauge theory can successfully describe the strong interaction and this theory came to be known as the quantum chromodynamics. The evidence for the existence of gluons, the $SU(3)$ gauge bosons, came in jet events observed at the DESY collider facility.

The Higgs mechanism

The Higgs, H, is a scalar field and an $SU(2)$ doublet. The Higgs potential

$$V(H^\dagger H) = \frac{m^2}{2h_o^2}\left(H^\dagger H - h_o^2\right)^2 \tag{1.1}$$

has a continuous minimum at $H = (0, h_o)$ and this is the vacuum expectation value acquired by the Higgs field. Note that h_o is real; we have used the three degrees of freedom of the gauge group to force the first component of H to be 0 and the second component of H to be real. The Higgs particle is the excitation of the Higgs field away from its VEV.

The Higgs Lagrangian is given by

$$\mathcal{L}_H = (D_\mu H)^\dagger D^\mu H - V(H^\dagger H) \tag{1.2}$$

where

$$D_\mu H = \left(\partial_\mu + i\frac{g_1}{2}B_\mu + i\frac{g2}{2}W_\mu\right)H \tag{1.3}$$

with B_μ and W_μ being the $U(1)$ and $SU(2)$ gauge fields and g_1 and g_2 being the corresponding couplings. The field W_μ has three components W_μ^1, W_μ^2 and W_μ^3 when expanded as the coefficients of the three Pauli matrices.

It can be shown that after symmetry breaking by the Higgs mechanism, the

dynamical term in the Higgs field gives rise to the massive gauge fields

$$W_\mu^+ = \frac{W_\mu^1 - iW_\mu^2}{\sqrt{2}}, \qquad W_\mu^- = \frac{W_\mu^1 + iW_\mu^2}{\sqrt{2}}, \tag{1.4}$$

$$Z_\mu = W_\mu^3 \cos\theta_w - B_\mu \sin\theta_w \tag{1.5}$$

where

$$\cos\theta_w = \frac{g_2}{\sqrt{g_1^2 + g_2^2}}, \qquad \sin\theta_w = \frac{g_1}{\sqrt{g_1^2 + g_2^2}} \tag{1.6}$$

with the corresponding masses

$$M_w = \frac{h_o g_2}{\sqrt{2}}, \tag{1.7}$$

$$M_z = \frac{h_o \sqrt{g_1^2 + g_2^2}}{\sqrt{2}}. \tag{1.8}$$

Also we get a massless field

$$A_\mu = W_\mu^3 \sin\theta_w + B_\mu \cos\theta_w \tag{1.9}$$

which is nothing but the photon.

The Higgs also couple to the fermions. For the charged-leptons we have

$$\mathcal{L}_m^l = -\frac{m_e}{h_o} L^\dagger H e_R - \frac{m_\tau}{h_o} L^\dagger H \mu_R - \frac{m_\mu}{h_o} L^\dagger H \tau_R \tag{1.10}$$

where L is the left-handed lepton doublet, e_R, μ_R, τ_R are the right-handed charged-lepton fields. After symmetry breaking, the charged-leptons e, μ and τ get the masses m_e, m_μ and m_τ respectively. Neutrinos remain massless. However both the up-type and the down-type quarks are massive resulting in the phenomenon of mixing. This is explained in more detail in later sections.

1.1.1 Beyond the Standard Model

Here we list and briefly discuss some of the challenges facing the Standard Model.

The hierarchy problem and the supersymmetry

In the Standard Model the quantum corrections to the Higgs mass is quadratic resulting from fermionic loops in the Higgs propagator. Therefore at a very high scale such as the Grand Unification scale or the Plank scale, the corrections to the Higgs mass will become very high. The fact that the Higgs mass itself is much

small compared to this scale constitutes the hierarchy problem. In order to obtain the small Higgs mass, we would need incredible fine-tuning cancellation between the quadratic radiative corrections and the bare mass.

A possible solution to the hierarchy problem is through the introduction of supersymmetry. The loop contribution from the fermions and their superpartners cancel each other and the quadratic divergence is removed. None of the supersymmetric particles have been observed so far. The current experimental limit to the mass of squarks and gluinos are around 1.1 TeV and 0.5 TeV respectively. Coupled with the observation of a relatively large Higgs mass, the null result in the superparticle searches has made the minimal supersymmetric extension of the Standard Model rather "unnatural".

Neutrinos

In the original formalism of the Standard Model, the neutrinos are massless. However solar neutrino problem and the consequent discovery of the neutrino oscillations have shown that neutrinos are massive. The nature of the neutrino mass is unknown, i.e. whether the neutrinos are Dirac or Majorana. Also the oscillation experiments can measure only the mass-squared-differences and therefore the mass offset is yet to be measured. These developments necessitates extending the Standard Model to allow neutrino mass terms. How this can be done is still an open question.

Gauge unification and gravity

The Standard Model gauge group is the direct product group of $U(1)$, $SU(2)$ and $SU(3)$ with three independent gauge couplings. From a theoretic point of view, it is elegant to unify these three interactions into a single gauge group with a unified coupling constant. Such a Grand Unified Theory will also explain the quantisation of electric charge, the fact that all particles carry electric charges in exact multiples of $\frac{1}{3}$ of the elementary charge. The masses of the new particles predicted are of the order of the GUT scale, $\approx 10^{16}$ GeV, and hence they are not within the observational reach of the current collided experiments. However future observations such as proton decay, electric dipole moments of the elementary particles etc. may provide indirect evidence for the grand unification.

$SU(5)$ and $SO(10)$ are the most common gauge groups used in unification. For these cases, the renormalisation group running does not result in the accurate convergence of the Standard Model gauge couplings at a single point. Also $SU(5)$ grand unification of the Standard Model is ruled out by the current limits on the

proton decay rates. Hence the minimal supersymmetric extension of the Standard Model is often used which gives a better convergence of the gauge couplings as well as a longer proton lifetimes.

The Standard Model and also the Grand Unified Theories do not involve the gravitational force and the quantisation of gravity is a harder problem to solve. A quantum theory of general relativity may require a framework beyond the field theory itself like the string theory or the loop quantum gravity.

Cosmological problems: dark matter, baryon asymmetry etc.

Particles that do not interact electromagnetically and hence dark constitute the dark matter. Cold dark matter is essential to explain the structure formation in the universe and it is estimated that dark matter constitutes approximately 84% of the universe. Various candidates like the weakly interacting massive particles, axions etc have been proposed to account for the dark matter. Extensions of the Standard Model usually contain good dark matter candidates, but none has been experimentally detected so far.

Baryon asymmetry refers to the matter-antimatter imbalance in the observable universe. CP-violation is used for explaining this asymmetry. CP-violation ensures that matter and antimatter interact differently and if the Sakharov conditions are satisfied it results in baryogenesis. The Sakharov conditions are: 1. Baryon number violation, 2. C and CP violation and 3. Interactions out of thermal equilibrium. The Standard Model allows for CP-violation through the complex phase appearing in the CKM mixing matrix, but this is too small to account for the observed baryon asymmetry. A beyond Standard Model theory may provide larger CP-violation.

The flavour problem

The origin of flavour physics can be traced back to the concept of isospin introduced by Werner Heisenberg to describe the similarities of a proton and a neutron. They were together called nucleons and their masses were almost equal. The strong interaction did not seem to distinguish a proton from a neutron. Since they were almost identical (except for their charges), protons and neutrons can be thought of as different states of the same particle. They were assigned isospin projections $I_3 = +\frac{1}{2}$ and $I_3 = -\frac{1}{2}$ and as far as nuclear forces are concerned the effect of isospin can be safely neglected. Many newly discovered particles were observed to be isospin multiplets, e.g. a doublet, $I = \frac{1}{2}$, of K mesons (K^0 and $\bar{K}^0$), a triplet, $I = 1$, of Sigma

baryons (Σ^+,Σ^0,Σ^-), a singlet, $I = 0$, of Lambda baryon (Λ^0), a quartet, $I = \frac{3}{2}$, of Delta baryons (Δ^{++},Δ^+,Δ^0,Δ^-) etc. With the discovery of Kaons and the quantum number strangeness, the isospin symmetry was enlarged to include strangeness also. Murray Gell-Mann theorised the existence of SU(3) flavour symmetry with the up, the down and the strange belonging to its fundamental representation. The octet (the famous eight fold way) is simply the adjoint representation of the SU(3) flavour symmetry. Over time three more flavours, i.e. charm, bottomness (or beauty) and topness were discovered, but these quarks are much heavier and this makes the expanded SU(6) flavour symmetry badly broken.

Flavour physics involves the experimental as well as the theoretical study of the masses and mixing observables. In the Standard Model these observables are free parameters. The Standard Model consists of a total of 19 parameters (this excludes the case of massive neutrinos) and their numerical values appear to be unrelated and arbitrary. We search for beyond the Standard Model theories to describe and model these parameters through mechanisms like flavour symmetries and grand unification which lead to specific textures for the Yukawa couplings and thus to predictions for and/or relations among them.

1.1.2 Mixing in the quark sector

The mass term in the Standard Model containing the Yukawa couplings is given by

$$\mathcal{L}_Y = -Y^d_{ij}\bar{Q}_{Li}Hd_{Rj} - Y^u_{ij}\bar{Q}_{Li}\epsilon H^* u_{Rj} + hc. \tag{1.11}$$

where $Y^{u,d}$ are 3×3 complex matrices, H is the Higgs field, i, j are family labels, and ϵ is the 2×2 antisymmetric tensor. Q_L are the left-handed quark doublets and d_R and u_R are right-handed down- and up-type quark singlets, respectively, in the weak eigenstate basis. When the Higgs acquires a vacuum expectation value $(0, h_o)$, the Yukawa couplings in Eq. (1.11) give the mass matrices for the quarks. The weak eigenstates of the quarks are linear combinations of the mass eigenstates determined through the unitary matrices, $V^{u,d}_{L,R}$, which diagonalise the mass matrices,

$$M^f_{\text{diag}} = V^f_L Y^f V^{f\dagger}_R h_o \tag{1.12}$$

for $f = u, d$. Thus we obtain the Cabbibo-Kobayashi-Maskawa (CKM) matrix

$$V_{\text{CKM}} \equiv V^u_L V^{d\dagger}_L = \begin{pmatrix} V_{ud} & V_{us} & V_{ub} \\ V_{cd} & V_{cs} & V_{cb} \\ V_{td} & V_{ts} & V_{tb} \end{pmatrix} \tag{1.13}$$

whose elements are the couplings between the charged-current $W^{\pm}$ interactions and the physical states (mass eigenstates) of the quarks. The PDG [2] adopted the following convention in parametrising the unitary CKM matrix using three mixing angles and a CP-violating phase:

$$V = \begin{pmatrix} c_{12}c_{13} & s_{12}c_{13} & s_{13}e^{-i\delta} \\ -s_{12}c_{23} - c_{12}s_{23}s_{13}e^{i\delta} & c_{12}c_{23} - s_{12}s_{23}s_{13}e^{i\delta} & s_{23}c_{13} \\ s_{12}s_{23} - c_{12}c_{23}s_{13}e^{i\delta} & -c_{12}s_{23} - s_{12}c_{23}s_{13}e^{i\delta} & c_{23}c_{13} \end{pmatrix} \tag{1.14}$$

where $s_{ij} = \sin\theta_{ij}, c_{ij} = \cos\theta_{ij}$ and δ is the CP-violating phase. The angles θ_{ij} can be chosen to lie in the first quadrant, so $s_{ij}, c_{ij} \geq 0$.

To conveniently denote the experimentally observed hierarchy $s_{13} \ll s_{23} \ll s_{12} \ll 1$, Wolfenstein introduced the parametrisation [3],

$$s_{12} = \lambda = \frac{|V_{us}|}{\sqrt{|V_{ud}|^2 + |V_{us}|^2}} \tag{1.15}$$

$$s_{23} = A\lambda^2 = \lambda \left| \frac{V_{cb}}{V_{us}} \right| \tag{1.16}$$

$$s_{13}e^{i\delta} = V_{ub}^* = A\lambda^3(\rho + i\eta) = \frac{A\lambda^3(\bar{\rho} + i\bar{\eta})\sqrt{1 - A^2\lambda^4}}{\sqrt{1-\lambda^2}(1 - A^2\lambda^4(\bar{\rho} + i\bar{\eta}))}. \tag{1.17}$$

The parameter $\bar{\rho} + i\bar{\eta} = -(V_{ud}V_{ub}^*)/(V_{cd}V_{cb}^*)$ is phase-convention-independent. We can expand V_{CKM} to any order of λ, for example to $\mathcal{O}(\lambda^4)$ we have

$$V = \begin{pmatrix} 1 - \lambda^2/2 & \lambda & A\lambda^3(\rho - i\eta) \\ -\lambda & 1 - \lambda^2/2 & A\lambda^2 \\ A\lambda^3(1 - \rho - i\eta) & -A\lambda^2 & 1 \end{pmatrix} + \mathcal{O}(\lambda^4). \tag{1.18}$$

Note that the above matrix is unitary to $\mathcal{O}(\lambda^4)$. The experimental values [2] of these parameters are

$$\lambda = 0.22535 \pm 0.00065, \quad A = 0.811^{+0.022}_{-0.012}, \quad \bar{\rho} = 0.131^{+0.026}_{-0.013}, \quad \bar{\eta} = 0.345^{+0.013}_{-0.014}. \tag{1.19}$$

Using the unitarity conditions of the CKM matrix we get

$$\sum_k V_{ki}V_{kj}^* = \delta_{ij}, \quad \sum_j V_{ik}V_{jk}^* = \delta_{ij}. \tag{1.20}$$

When $i \neq j$ the summation vanishes and the three complex numbers in the summation can be represented as a triangle in the complex plane. The areas of all

these triangles are phase-convention-independent and equal to half of the Jarlskog invariant J [4], given by

$$\mathrm{Im}(V_{ij}V_{kl}V_{il}^{*}V_{kj}^{*}) = J\sum_{m,n}\epsilon_{ikm}\epsilon_{jln} \tag{1.21}$$

which measures the CP-violation.

In the literature the most commonly used unitarity triangle is the one formed using the first and last columns of the CKM matrix:

$$V_{ud}V_{ub}^{*} + V_{cd}V_{cb}^{*} + V_{td}V_{tb}^{*} = 0. \tag{1.22}$$

The above equation is divided by $V_{cd}V_{cb}^{*}$ and thus we get vertices at $(0,0)$, $(1,0)$ and $(\bar{\rho},\bar{\eta})$, using Eq. (1.17), as shown in Figure 1.1. The $\bar{\rho},\bar{\eta}$ plane is used to display various measurements of mixing. Overconstraining the unitarity triangle is a precise test for Standard Model and deviations from unitarity will provide insights to Beyond Standard Model theories.

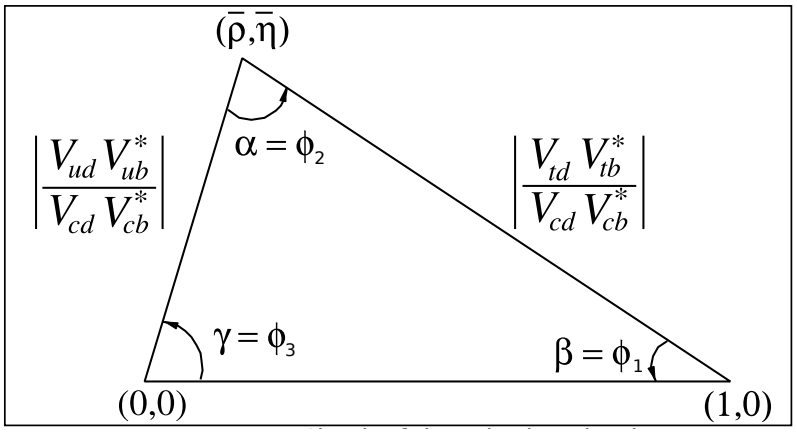

Figure 1.1: The unitarity triangle [2].

1.2 Neutrinos

The existence of neutrinos was postulated by Wolfgang Pauli to preserve energy-momentum conservation in beta decay. Neutrinos can interact with matter through charged current interactions and produce charged leptons. Hence a direct discovery of neutrinos should involve a detection of these charged leptons. Cowan and

Reines [5] used such an interaction

$$\bar{\nu}_e + p \rightarrow n + e^+ \tag{1.23}$$

to finally get irrefutable proof of the neutrino's existence. Antineutrinos produced at the Savannah River nuclear site interacted with protons in a tank of water in the detector producing positrons and neutrinos. The positron annihilates with an electron in the medium producing two gamma rays of about 0.5 MeV each. A scintillator in the tank of water and photomultiplier tubes were used to detect these gamma rays. Cd-108 was used to detect the neutrons. Excited Cd-109 is produced when the neutron is captured by the Cd-108 nucleus. The de-excitation produces a gamma ray which again is detected using the scintillator-photomultiplier set-up. The simultaneous detection of the positron annihilation and the neutron capture uniquely confirms the presence of an antineutrino interaction.

In 1962 muon neutrinos were observed by Lederman et al [6] at the Brookhaven Alternating Gradiant Synchrotron facility. These neutrinos were produced mostly through pion decays:

$$\pi^{\pm} \rightarrow \mu^{\pm} + (\nu/\bar{\nu}). \tag{1.24}$$

The neutrinos in turn were detected when they interacted with matter and produced muons and not electrons. This proved that these neutrinos were different from the previously discovered electron neutrinos. Separate electron and muon lepton number conservation laws were postulated which also helped to explain why decays like $\mu \rightarrow e + \gamma$ were not observed. In the detector, a spark chamber was used to identify muons.

Finally the tau neutrino (the last remaining fermion in the standard model) was discovered in 2000 by the DONUT collaboration [7]. An 800 GeV proton beam interacting with a one meter long tungsten beam dump was used to produce the tau neutrinos. D_S mesons produced in the beam dump undergo leptonic decay and produce tau leptons (τ) and tau antineutrinos ($\bar{\nu}_\tau$). The τs subsequently decay producing ν_τs. The ν_τ was detected in a nuclear emulsion: through the charged current interaction the ν_τ produces a τ and the identification of the τ as the only lepton created at the point of interaction provides a unique signature for ν_τ. Within a couple of millimetres after its creation, the τ decays typically producing a charged daughter particle. Thus a short track with a kink signifies the production and decay of a τ. If the daughter particles were an electron or a muon, they were detected using a charged particle spectrometer providing extra information.

1.2.1 Neutrino mass measurements

Beta decay experiments

A direct neutrino mass measurement can be done in principle, by analysing the energy spectrum of beta decay. Tritium having one of the least energic beta decays is an ideal candidate for this type of experiment. Here the total energy shared between the neutrino and the electron is only 18.6 keV. The maximum energy that the electron can carry is limited by the rest mass of the neutrino. The energy spectrum of the electrons will extend only up to the point which is the total energy of 18.6 keV minus the rest energy of the neutrino. The electron energy spectrum is shown in Figure 1.2.

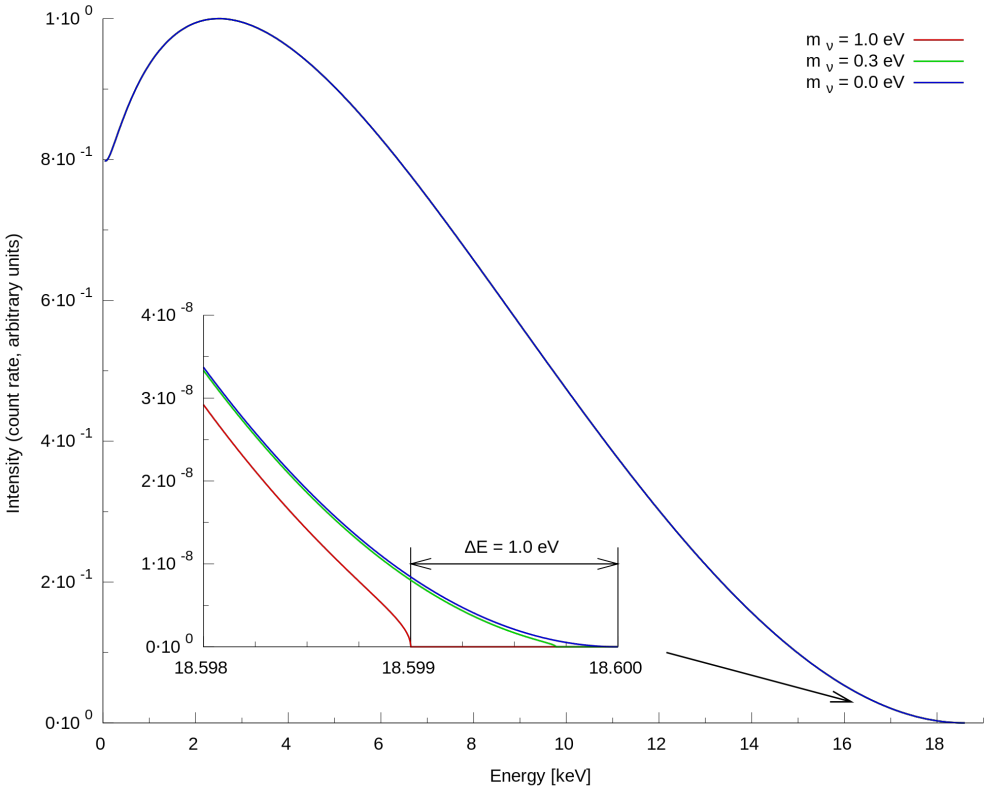

Figure 1.2: Beta decay spectrum of tritium [8]. Detection of neutrino mass requires a high precision measurement to analyse the end point of the spectrum.

The KATRIN (Karlsruhe Tritium Neutrino) Experiment can attain a sensitivity of 0.2 eV with the help of a special type of spectrometer called the MAC-E-Filter (Magnetic Adiabatic Collimation combined with an Electrostatic Filter).

Electrons are isotropically emitted from the source, but they are collimated using a slowly varying magnetic field into a beam moving almost parallel to the field lines. An electrostatic barrier acting as an integrating high-energy pass filter is used to separate the electrons above a given energy which are then re-accelerated and detected, thus providing the energy spectrum.

Using a set of recent tritium beta experiments, an upper limit of $m(\nu_e) < 2$ eV at 95% C.L. is obtained [9].

Neutrinoless double-beta decay

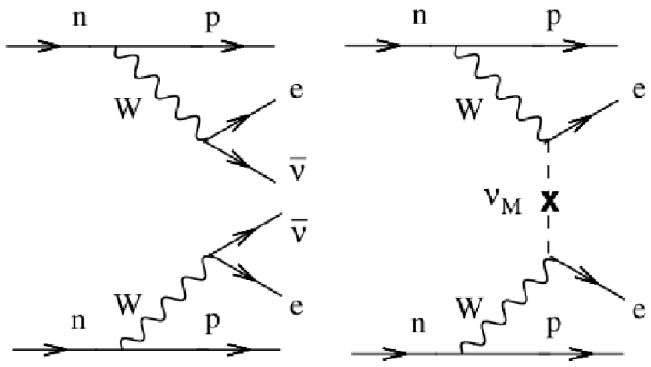

Figure 1.3: Double-beta decay processes, $\beta\beta2\nu$ and $\beta\beta0\nu$ respectively

Beta decay occurs when a neutron in a nucleus is converted into a proton (increasing the atomic number by one) with the emission of an electron and a neutrino. This can happen only if the binding energy of the final nucleus is more than that of the initial one. In some nuclei like Ge-76, the nucleus with the atomic number higher by one has lower binging energy, but the nucleus with atomic number higher by two has higher binding energy. Therefore they can not undergo a single beta decay, instead they can emit two betas and two neutrinos together (double beta decay), left of Figure 1.3. The two-neutrino double beta decay, $\beta\beta2\nu$

$$(Z, A) \rightarrow (Z + 2, A) + 2e + 2\bar{\nu}_e \tag{1.25}$$

conserves lepton number. If the neutrino is also its own antiparticle, it can be emitted as well as absorbed in simultaneous decays giving rise to neutrinoless double beta decay, right of Figure 1.3, $\beta\beta0\nu$:

$$(Z, A) \rightarrow (Z + 2, A) + 2e. \tag{1.26}$$

Neutrinoless double beta decay violates lepton number and is possible only if neutrinos are massive Majorana particles.

The shape of the total energy spectrum of the outgoing beta particles is determined by the phase space of all the light decay products [10]. In $\beta\beta2\nu$, some energy is carried away by the neutrinos and thus we get a continuous energy spectrum for the electrons below the maximum allowed end point energy (where the energy carried away by the neutrinos tends to zero). In the case $\beta\beta0\nu$, all the energy is carried by the electrons and so we get a single peak at the end point energy. The spectrum is shown in Figure 1.4.

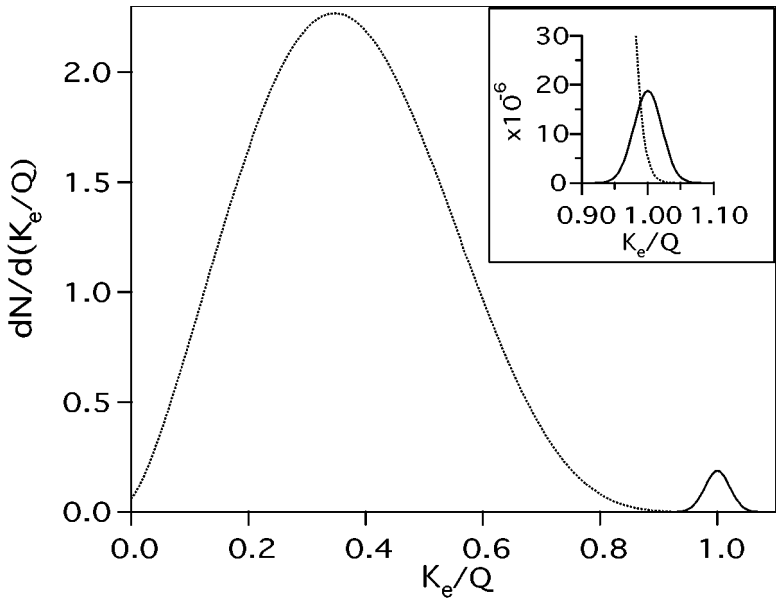

Figure 1.4: The spectrum of the total energy of the two electrons in a double beta decay. In the case of neutrinoless decay a bump appears centred at the end point of the main spectrum. The plot is made with an energy resolution of 5% [10] which smears the delta function into a bell-shaped curve.

Being a second-order process, $\beta\beta2\nu$ has a very long lifetime, 10 orders of magnitude longer than the typical lifetimes of trace radioactive impurities which also give betas of similar energy. So detecting double beta decays is quite challenging, not to mention even the rarer neutrinoless mode. But several cases of $\beta\beta2\nu$ have been detected and improvements in the sensitivity for the detection $\beta\beta0\nu$ have been made. These improvements lead to better limits on the effective neutrino mass, since the $\beta\beta0\nu$ rate is proportional to the square of the neutrino mass. The half-life for

the neutrinoless double beta decay is given by

$$\left(T^{0\nu}_{\frac{1}{2}}\right)^{-1} = G_{0\nu} \left|M^{0\nu}\right|^2 \langle m_{\beta\beta}\rangle^2 \tag{1.27}$$

where $G_{0\nu}$ is a phase space factor, $M^{0\nu}$ is the nuclear matrix element and $m_{\beta\beta}$ is the effective neutrino mass. Evaluation of the nuclear matrix element mainly depends on theoretical calculation and it is the source of the largest uncertainty to $m_{\beta\beta}$. The experimental upper limit of $m_{\beta\beta}$ is often quoted as a range of values which corresponds to the different models used to calculate the nuclear matrix element. Experiments like Heidelberg-Moscow, NEMO, COBRA, CUORE, GERDA etc. are aimed towards the goal of detecting $\beta\beta0\nu$ even though no conclusive evidence for it has been found so far. In 2001 a claim was made by a part of the Heidelberg-Moscow collaboration to have observed $\beta\beta0\nu$, but this is yet to be universally accepted by the larger scientific community. Various experiments have set limits on the effective Majorana neutrino mass. The NEMO-3 experiment [11] gives $|m_{\beta\beta}| < 0.47 - 0.96$ eV and $|m_{\beta\beta}| < 0.94 - 2.5$ eV corresponding to the isotopes Mo-100 and Se-82 respectively.

Cosmic neutrino background

There is a relic neutrino background with a temperature of 1.95K and a number density of 112cm^{-3}/flavour [12]. The corresponding energy density ($\Omega_\nu h^2 = \frac{m_\nu}{93\text{eV}}$) constitutes dark matter. From neutrino oscillation experiments we know that neutrinos have a minimum mass of about 0.05 eV which constitutes only 0.1% of dark matter. Tritium decay experiments set an upper bound on electron neutrino mass at around 2.2eV. A value close to this mass can contribute about 12% of dark matter. Neutrinos are classified as hot dark matter and they affect the large scale structure formation of the universe. Their large thermal energy hinders growth of clusters on a small scale. On the other hand both hot and cold dark matter can cluster at large scales. Knowledge of the large scale distribution and the galaxy power spectrum can be used to calculate an upper limit to the mass of the neutrinos. The WiggleZ Dark Energy Survey [13] gives the strongest cosmological limit on neutrino mass so far, $\sum m_\nu < 0.29$ eV.

1.2.2 Theory of neutrino mass and mixing

An excellent review of neutrino theory is given in [14] and this section is written mostly based on it.

Neutrinos are observed to change their flavour as they propagate. Neutrinos are weakly interacting particles and hence they are produced and detected as flavour eigenstates. As they propagate, the probabilistic contents of different flavours oscillate periodically. This phenomenon is called neutrino oscillation. In the original Standard Model neutrinos were assumed to be massless. Observation of neutrino oscillation has proved that they have mass and this necessitated adding extra neutrino mass terms.

For interactions involving the neutrino fields we have the charged current

$$j_\rho^{CC} = 2 \sum_{l=e,\mu,\tau} \overline{\nu_{lL}} \gamma_\rho l_L \tag{1.28}$$

and the neutral current

$$j_\rho^{NC} = \sum_{l=e,\mu,\tau} \overline{\nu_{lL}} \gamma_\rho \nu_{lL} \tag{1.29}$$

which couple with the W and the Z vector gauge bosons. Here ν_ls are the neutrino flavour fields, l_Ls are the left-handed charged-lepton fields and γ_ρ are the gamma matrices. In the Standard Model the charged current and the neutral current interactions are given by

$$L_I^{CC} = -\frac{g}{2\sqrt{2}} j_\rho^{CC} W^\rho + h.c. \tag{1.30}$$

$$L_I^{NC} = -\frac{g}{2\cos\theta_W} j_\rho^{NC} Z^\rho \tag{1.31}$$

where θ_W is the Weinberg angle and g is the $SU(2)_L$ gauge coupling constant. Charged current interactions define the neutrino flavour eigenstates ν_e, ν_μ, ν_τ : i.e. we may say that $\bar{\nu_e}$ is the particle produced in the decay $\pi^- \to e^- + \bar{\nu_e}$. Neutrinos are always produced and detected as flavour eigenstates.

The invisible width of the Z boson is used to determine the number of light neutrino flavours. LEP measurements gave it to be quite close to 3 with the most recent experimental value being 2.994 ± 0.012, confirming that no neutrino flavours other than e, μ, τ exist. The electron, the muon and the tau lepton numbers are conserved in the charged current and neutral current interactions. Precision measurements of branching ratios of various decays have been made to obtain strong bounds on the probabilities of lepton number violating processes and so far there has been no proof for Lepton number violation in any of these decays.

Non-zero neutrino masses and the phenomenon of neutrino mixing lead to violation of lepton number conservation. Let ν_{lL} be left-handed flavour neutrino fields and ν_{kL} be the left-handed neutrino

fields with definite masses m_k. The flavour eigenstates ν_{lL} are assumed to be superpositions of the mass eigenstates ν_{kL}:

$$\nu_{lL} = \sum_{k=1}^{n} U_{lk}\nu_{kL} \quad (l = e, \mu, \tau) \tag{1.32}$$

where U is the PMNS matrix responsible for mixing. In the simplest case the number of massive neutrino fields n is equal to 3. However if we postulate the existence of sterile neutrinos (which do not interact weakly as given in Eqs. (1.28, 1.29)) then n can be greater than 3.

Quarks interact weakly via the V-A current

$$\sum_{q'=u,c,t} \sum_{q=d,s,b} \overline{q'_L}\gamma_\rho V_{q'q} q_L \tag{1.33}$$

where V is the Cabibbo-Kobayashi-Maskawa matrix which leads to the observed mixing phenomenon in quarks. Even though the neutrino mixing relation, Eq. (1.32) is analogous to the quark mixing, Eq. (1.33), there is a fundamental difference. Unlike the quarks which are four component Dirac particles, the nature of the neutrinos is not well established. If they are also Dirac particles, neutrinos and antineutrinos will have opposite lepton numbers and hence the total lepton number

$$L = L_e + L_\mu + L_\tau \tag{1.34}$$

will be conserved. On the other hand if the massive neutrinos are two component Majorana particles then the total lepton number, Eq. (1.34), will not be conserved. Models can be constructed with different kinds of neutrino mass terms which lead to Dirac or Majorana neutrinos.

Dirac mass term

We have the Standard Model Higgs mechanism that generates the fermion masses through electroweak symmetry breaking via the Yukawa couplings of the Higgs to the fermions. A Dirac neutrino mass term is similar to the mass term for the up type quarks. The neutrino mass term, after electroweak symmetry breaking, takes the form

$$\mathcal{L}^D = -\sum_{l,l'} \overline{\nu_{lL}} M^D_{ll'} \nu_{l'R} + h.c. \tag{1.35}$$

where M^D is in general a complex 3×3 matrix.

Any complex 3×3 mass matrix can be diagonalised by using two unitary

matrices V and U which are left and right multiplied on the mass matrix:

$$M^D = U m_{\rm diag} V^\dagger. \tag{1.36}$$

The diagonal matrix, $m_{\rm diag}$, can be made positive definite, $m_{diag} = m_i \delta_{ij}$ with $m_i \geq 0$. In the diagonalised form the Dirac mass term, Eq. (1.35), takes the form

$$\mathcal{L}^D = -\sum_{k=1}^{3} m_k \overline{\nu_k} \nu_k + h.c. \tag{1.37}$$

where ν_{lL} is given by Eq. (1.32). Thus the left-handed components ν_{kL} of the three fields of neutrinos with masses $m_k\,(k = 1, 2, 3)$ are unitary linear combinations of the three flavour fields $\nu_{lL}\,(l = e, \mu, \tau)$. Similarly the right-handed components ν_{kR} are also linear combinations of the right-handed fields $\nu_{lR}\,(l = e, \mu, \tau)$ through the unitary matrix V:

$$\nu_{lR} = \sum_{k=1}^{3} V_{lk} \nu_{kR} \quad (l, e, \mu, \tau). \tag{1.38}$$

Right-handed fields, ν_{lR}, however, do not interact in the Standard Model and hence these sterile fields do not affect neutrino mixing.

For a Dirac field ν_k, the Lagrangian is invariant under global $U(1)$ transformation

$$\nu_l \to e^{i\phi} \nu_l, \quad l \to e^{i\phi} l \quad (l = e, \mu, \tau) \tag{1.39}$$

where the phase ϕ is the same for all the neutrino and charged lepton fields. Noether's theorem states that for every global symmetry there exists a conserved quantity. Here the conserved quantity is the total lepton number. A particle and its antiparticle have opposite lepton numbers. Thus a Dirac neutrino and its antineutrino can be distinguished by their lepton numbers. Even though processes like $\mu \to e + \gamma$, $\mu^- \to e^- + e^+ + e^-$ are allowed by the Dirac mass term, Eq. (1.35), the branching fractions of such decays are negligibly small.

A 3×3 unitary mixing matrix has 9 independent parameters, 3 angles and 6 phases. When these phases go to zero, the 3×3 unitary matrix is reduced to a 3 parameter 3×3 orthogonal matrix. In the Standard Model, out of the 9 parameters in the mixing matrix U, only four are observable. The charged current for the leptons in the Standard Model is given by

$$j_\rho^{CC\dagger} = 2 \sum_{l=e,\mu,\tau} \overline{l_L} \gamma_\rho \nu_{lL} = 2 \sum_{l=e,\mu,\tau} \sum_{k=1}^{3} \overline{l_L} \gamma_\rho U_{lk} \nu_{kL}. \tag{1.40}$$

It can be shown that five phases out of the six can be eliminated by absorbing them into the charged lepton and neutrino fields. The only remaining phase in U leads to CP-violation in the lepton sector.

A parametrization similar to the CKM mixing matrix for the quarks, Eq. (1.14), is adopted for the leptonic sector also:

$$V = \begin{pmatrix} c_{12}c_{13} & s_{12}c_{13} & s_{13}e^{i\delta} \\ -s_{12}c_{23} - c_{12}s_{23}s_{13}e^{i\delta} & c_{12}c_{23} - s_{12}s_{23}s_{13}e^{i\delta} & s_{23}c_{13} \\ s_{12}s_{23} - c_{12}c_{23}s_{13}e^{i\delta} & -c_{12}s_{23} - s_{12}c_{23}s_{13}e^{i\delta} & c_{23}c_{13} \end{pmatrix} \tag{1.41}$$

where $c_{ij} = \cos\theta_{ij}$ and $s_{ij} = \sin\theta_{ij}$ and δ is the CP-violating phase. In the above parametrisation we can see that the CP-violating term $e^{i\delta}$ is always multiplied with s_{13}. Therefore a small mixing mixing angle θ_{13} implies a comparative reduction in CP-violation. In fact this is applicable to any of the three mixing angles and if any of them goes to zero the CP-phase can be removed by redefining the lepton fields.

Dirac-Majorana mass term

A Dirac-Majorana mass term is the most general construction using a set of left-handed flavour fields ν_{lL} ($l = e, \mu, \tau$) and sterile right-handed fields ν_{sR} ($s = s_1, s_2, ...$). Here lepton numbers are not conserved. The Dirac-Majorana Lagrangian

$$\mathcal{L}^{D+M} = \mathcal{L}_L^M + \mathcal{L}^D + \mathcal{L}_R^M \tag{1.42}$$

has three parts with

$$\mathcal{L}^D = -\sum_{s,l} \overline{\nu_{sL}} M_{sl}^D \nu_{lR} + h.c. \tag{1.43}$$

$$\mathcal{L}_L^M = -\frac{1}{2}\sum_{l,l'} \overline{\nu_{lL}} M_{ll'}^L \nu_{l'L}^c + h.c. \tag{1.44}$$

$$\mathcal{L}_R^M = -\frac{1}{2}\sum_{s,s'} \overline{\nu_{sR}^c} M_{ss'}^R \nu_{s'R} + h.c.. \tag{1.45}$$

There are n_R sterile right-handed fields and in general n_R and the number of flavour fields (3) are different. The mass matrices M^D, M^L and M^R are complex. The charge-conjugation operation

$$(\nu_{lL})^c = \mathcal{C}\overline{\nu_{lL}}^T, \quad (\nu_{sR})^c = \mathcal{C}\overline{\nu_{sR}}^T, \tag{1.46}$$

where $\mathcal{C}$ is the charge-conjugation matrix, converts the left-handed field to right-handed and vice versa. The mass matrices M^L and M^R can be assumed to be symmetric without loss of generality. This is because

$$\overline{(\nu_{lL})^c}\nu_{l'L} = \overline{(\nu_{l'L})^c}\nu_{lL} \tag{1.47}$$

and thus any antisymmetric part in M^L and M^R becomes irrelevant.

A left-handed column vector

$$n_L \equiv \begin{pmatrix} \nu_L \\ (\nu_R)^c \end{pmatrix} \tag{1.48}$$

is defined with

$$\nu_L \equiv \begin{pmatrix} \nu_{eL} \\ \nu_{\mu L} \\ \nu_{\tau L} \end{pmatrix}, \quad \nu_R \equiv \begin{pmatrix} \nu_{s_1 R} \\ \nu_{s_2 R} \\ . \\ . \end{pmatrix}. \tag{1.49}$$

Since

$$\sum_{s,l} \overline{\nu_{sL}} M^D_{sl} \nu_{lR} = -\sum_{s,l} \nu^T_{lR} M^D_{sl} \overline{\nu_{sL}}^T = \sum_{s,l} \overline{(\nu_{lR})^c} (M^D)^T_{ls} (\nu_{sL})^c \tag{1.50}$$

and using the $(3+n_R)\times(3+n_R)$ matrix

$$M^{D+M} \equiv \begin{pmatrix} M_L & M^D \\ (M^D)^T & M^R \end{pmatrix} \tag{1.51}$$

we get

$$\mathcal{L}^{D+M} = -\frac{1}{2}\overline{n_L} M^{D+M} n^c_L + h.c.. \tag{1.52}$$

Note that the matrix M^{D+M} is symmetric.

We use the unitary matrix U to diagonalise the complex symmetric matrix M^{D+M}:

$$M^{D+M} = U m_{\text{diag}} U^T \tag{1.53}$$

where $(m_{\text{diag}})_{kj} = m_k \delta_{kj}$ and $m_k \geq 0$. With this substitution, the mass term, Eq. (1.52), takes the form

$$\mathcal{L}^{D+M} = -\frac{1}{2}\overline{N^c} m_{\text{diag}} N^c = -\frac{1}{2}\sum_{k=1}^{3+n_R} m_k \overline{\nu_k} \nu_k \tag{1.54}$$

where

$$N \equiv \begin{pmatrix} \nu_1 \\ \nu_2 \\ . \\ . \end{pmatrix} = U^\dagger n_L + \left(U^\dagger n_L\right)^c. \tag{1.55}$$

The fields ν_k are Majorana because

$$(\nu_k)^c = \nu_k \quad (k = 1, 2, 3, ..., 3 + n_R). \tag{1.56}$$

Therefore, when we have a Dirac-Majorana mass term with 3 neutrino flavours and n_R sterile right-handed fields, we get $3 + n_R$ Majorana fields with definite masses. A global phase transformation that keeps the mass term, Eq. (1.52), invariant does not exist; i.e. we do not have conserved quantities like lepton numbers that can differentiate particles and antiparticles.

Using Eq. (1.55), we can see that the left-handed neutrino fields, ν_{lL}, are unitary linear combinations of neutrino states with definite mass, ν_{kL},

$$\nu_{lL} = \sum_{k=1}^{3+n_R} U_{lk}\nu_{kL} \tag{1.57}$$

$$(\nu_{sR})^c = \sum_{k=1}^{3+n_R} U_{sk}\nu_{kL} \tag{1.58}$$

This leads to the observed mixing phenomenon among the flavour neutrinos ν_e, ν_μ and ν_τ. Eq. (1.57) implies that the flavour fields oscillate among themselves as was the case with the Dirac neutrinos. From Eq. (1.58) it is clear that the flavour neutrinos can also oscillate into unobservable sterile states.

It is well known that the Standard Model does not allow the term $\mathcal{L}_L^M$ in the Dirac-Majorana mass term, Eq. (1.42). We need models beyond the Standard Model like SO(10) GUT theories to get all richness of the Dirac-Majorana mass term.

Majorana mass term

A pure Majorana mass term is the only possibility if no neutrino field other than the three flavour fields $\nu_{lL}(l = e, \mu, \tau)$ exists. Then we have

$$\mathcal{L}^M = -\frac{1}{2}\sum_{l,l'} \overline{\nu_{lL}} M^L_{ll'} \nu^c_{l'L} \tag{1.59}$$

where M^L is a complex matrix which is also symmetric. The mixing relation is

$$\nu_{lL} = \sum_{k=1}^{3} U_{lk}\nu_{kL} \tag{1.60}$$

where ν_k is a Majorana field with mass m_k. Here we have only three massive neutrinos, equal to the number of flavour fields. The Majorana condition, Eq. (1.56) does not remain invariant under the rephasing of neutrino fields. Earlier, for the Dirac neutrinos, we could remove 5 out of 6 phases by redefining the lepton fields, Eq. (1.40). Here rephasing can be done only for the charged-lepton fields and this removes only 3 phases. Thus the Majorana case leaves three CP-violating phases in the mixing matrix U. But these extra phases do not cause any observable effect on neutrino oscillations.

The see-saw mechanism

Consider the Dirac-Majorana mass term, Eq. (1.42), and the resulting symmetric mass matrix, Eq. (1.51). Assume that $M^L = 0$, M^D is of the order of the weak scale and M^R is at a very high energy scale $\mathcal{M}$. The scale $\mathcal{M}$ is a model-dependent quantity. This can be very high, for example the grand unification scale $\approx 10^{15}$ GeV or even the Plank scale $\approx 10^{19}$ GeV or a comparatively low scale as low as the TeV scale. Under these conditions we will get a set of eigenvalues (neutrino masses) scaled inversely proportional to the large scale $\mathcal{M}$ resulting in very light neutrinos. Also we will have a set of heavy neutrinos hitherto unobserved. This process is known as the see-saw mechanism. The see-saw mechanism is quite attractive in the sense that it gives an explanation for the smallness of the neutrino masses compared to the masses of all other fermions. Of course it is the right-handed Majorana mass term at the high scale $\mathcal{M}$ that violates lepton number conservation.

The see-saw mechanism in the case of three families is analysed in detail below. Here we assume that M^D and M^R are 3×3 matrices in Eq. (1.51). As stated earlier M^L is assumed to be zero. Such a mass matrix can be brought into a block diagonalised form (up to corrections of order $(M^R)^{-1}M^D$) through the unitary transformation

$$W^T M^{D+M} W \approx \begin{pmatrix} M_{\text{light}} & 0 \\ 0 & M_{\text{heavy}} \end{pmatrix} \tag{1.61}$$

where

$$W \approx \begin{pmatrix} 1 - \frac{1}{2}(M^D)^*(M^R(M^R)^\dagger)^{-1}(M^D)^T & (M^D)^*(M^R)^{\dagger -1} \\ -(M^R)^{-1}(M^D)^T & 1 - \frac{1}{2}(M^R)^{-1}(M^D)^T(M^D)^*(M^R)^{\dagger -1} \end{pmatrix} \tag{1.62}$$

and

$$M_{\text{light}} \approx -M^D (M^R)^{-1} (M^D)^T, \quad M_{\text{heavy}} \approx M^R. \tag{1.63}$$

Three simple possibilities corresponding to specific choices of M^D and M^R are discussed below.

1. If $M^R = \mathcal{M}I$, where I is the identity, we will have the quadratic seesaw:

$$M_{\text{light}} \approx -\frac{M^D (M^D)^T}{\mathcal{M}} \tag{1.64}$$

and thus we have the light neutrino masses

$$m_k = \frac{\left(m_k^f\right)^2}{\mathcal{M}} \tag{1.65}$$

where m_k^f are the eigenvalues of M^D which are in weak scale. So the neutrino masses scale as the squares of the masses m_k^f

$$m_1 : m_2 : m_3 = (m_1^f)^2 : (m_2^f)^2 : (m_3^f)^2. \tag{1.66}$$

2. If $M^R = \frac{\mathcal{M}}{\mathcal{M}_W} M^D$, where $\mathcal{M}_W$ is the scale of M^D, we have the linear see-saw,

$$M_{\text{light}} \approx -\frac{\mathcal{M}_W}{\mathcal{M}} M^D \tag{1.67}$$

and thus we have the light neutrino masses.

$$m_k = \frac{\mathcal{M}_W}{\mathcal{M}} m_k^f \tag{1.68}$$

Here the neutrino masses scale as the masses m_k^f:

$$m_1 : m_2 : m_3 = m_1^f : m_2^f : m_3^f. \tag{1.69}$$

3. The third possibility is the one in which $M^D = \mathcal{M}_W I$. Let the eigenvalues of M^R be $\mathcal{M} m_k^R$. So we get

$$M_{\text{light}} \approx -\mathcal{M}_W^2 (M^R)^{-1} \tag{1.70}$$

with the light neutrino masses

$$m_k = \frac{\mathcal{M}_W^2}{\mathcal{M} m_k^R}\,. \tag{1.71}$$

So the neutrino masses scale inversely as the masses m_k^R:

$$m_1 : m_2 : m_3 = \frac{1}{m_1^R} : \frac{1}{m_2^R} : \frac{1}{m_3^R}\,. \tag{1.72}$$

1.2.3 Neutrino oscillations in vacuum

Let $|\nu_k\rangle$ be a neutrino mass eigenstate with mass m_k and assume that it is ultrarelativistic, $p \gg m_k$ i.e. we have

$$E_k = \sqrt{p^2 + m_k^2} \approx p + \frac{m_k^2}{2p}. \tag{1.73}$$

The flavour eigenstate, $|\nu_\alpha\rangle$, will be the coherent superposition of mass eigenstates:

$$|\nu_\alpha\rangle = \sum_{k=1}^{n} U_{\alpha k}^* |\nu_k\rangle. \tag{1.74}$$

The neutrinos are produced as flavour eigenstates and let the state shown in Eq. (1.74) be at time, $t = 0$. When propagating freely, the wavefunction of a particle with energy E_k evolves with a phase factor $\exp(-iE_k t)$ as described by the Schrodinger equation. Therefore when the neutrino, Eq. (1.74), reaches its destination after time t, its state is given by

$$|\nu_\alpha\rangle(t) = \sum_{k=1}^{n} U_{\alpha k} e^{(-iE_k t)} |\nu_k\rangle. \tag{1.75}$$

Just as they are produced, the neutrinos are also detected as flavour eigenstates. So we make the expansion

$$|\nu_\alpha\rangle(t) = \sum_{\beta} \mathcal{A}_{\nu_\alpha \to \nu_\beta}(t) |\nu_\beta\rangle \tag{1.76}$$

where

$$\mathcal{A}_{\nu_\alpha \to \nu_\beta}(t) = \sum_{k=1}^{n} U_{\alpha k} e^{(-iE_k t)} U_{\beta k}^*. \tag{1.77}$$

$\mathcal{A}_{\nu_\alpha \to \nu_\beta}(t)$ is the amplitude of $\nu_\alpha \to \nu_\beta$ oscillation after a time t or an equivalent distance, $L \simeq t$. The square of the amplitude gives the probability:

$$P_{\nu_\alpha \to \nu_\beta} = \left|\mathcal{A}_{\nu_\alpha \to \nu_\beta}(t)\right|^2 = \left| \sum_{k=1}^{n} U_{\alpha k} e^{-iE_k t} U_{\beta k}^* \right|^2 . \tag{1.78}$$

While deriving Eqs. (1.77, 1.78) we assumed that the state, $|\nu_\alpha\rangle$, belongs to one of the three flavours. But these formulae are valid for additional sterile neutrino

states also provided they are light particles (i.e. we have more than three light mass eigenstates). The presence of the sterile neutrinos is detectable indirectly through the disappearance of the flavour neutrinos. Note that in the case of the see-saw mechanism described earlier, with all the extra mass eigenstates being heavy, oscillations to sterile states do not happen. But it is possible to build models with light sterile states also, where flavour to sterile transitions become applicable. If the first n' mass eigenstates are light, ($n' < n$), and the rest are heavy, only the $n' \times n'$ submatrix of U takes part in neutrino oscillation. For the see-saw mechanism, this $n' \times n'$ submatrix is unitary to a good approximation. This is assumed in further discussions and we use n to mean n'.

For the antineutrino flavour state $|\bar{\nu}_\alpha\rangle$, using the relation Eq. (1.74), we have

$$|\bar{\nu}_\alpha\rangle = \sum_{k=1}^{n} U^*_{\alpha k} |\bar{\nu}_k\rangle. \tag{1.79}$$

Therefore for the antineutrino transition $\bar{\nu}_\alpha \to \bar{\nu}_\beta$ the amplitude is given by

$$\mathcal{A}_{\bar{\nu}_\alpha \to \bar{\nu}_\beta}(t) = \sum_{k=1}^{n} U^*_{\alpha k} e^{-iE_k t} U_{\beta k}. \tag{1.80}$$

Note that neutrino and antineutrino transition amplitudes differ only by the exchange of $U \to U^*$.

Using the unitarity relation, $\sum_{k=1}^{n} U^*_{\alpha k} U_{\beta k} = \delta_{\alpha\beta}$, and also the ultrarelativistic approximation, Eq. (1.73), the transition probability, Eq. (1.78), takes the form,

$$P_{\nu_\alpha \to \nu_\beta} = \left| \delta_{\alpha\beta} + \sum_{k=2}^{n} U^*_{\beta k} U_{\alpha k} \left(\exp\left(-i \frac{\Delta m^2_{k1} L}{2E} \right) - 1 \right) \right|^2 \tag{1.81}$$

where $\Delta m^2_{kj} \equiv m^2_k - m^2_j$. We can see that the quantity L/E, which is determined by the experimental set-up, is important in oscillation studies. The exponential part in Eq. (1.81) produces a noticeable oscillatory change only if

$$\Delta m^2 \gtrsim \frac{E}{L}. \tag{1.82}$$

So if the experimental set-up provides a large value for the parameter L/E, smaller values of Δm^2 can be probed, provided the corresponding mixing angle is not too small.

For both neutrinos and antineutrinos, the transition probabilities are invari-

ant under the phase transformation

$$U_{\alpha k} \to e^{-i\phi_\alpha} U_{\alpha k} e^{-i\psi_k}. \tag{1.83}$$

Since the Majorana CP-violating phase can be absorbed into the above mentioned phases, the Majorana and the Dirac cases can't be distinguished by observing neutrino oscillations.

From the expressions for the transition amplitudes of neutrinos and antineutrinos, Eq. (1.77) and Eq. (1.80), we get

$$P_{\nu_\alpha \to \nu_\beta} = P_{\bar{\nu}_\beta \to \bar{\nu}_\alpha}, \quad P_{\nu_\alpha \to \nu_\alpha} = P_{\bar{\nu}_\alpha \to \bar{\nu}_\alpha}. \tag{1.84}$$

This in turn is due to the fact that any local field theory is invariant under CPT transformation. In the special case of CP invariance in the leptonic sector, we get

$$P_{\nu_\alpha \to \nu_\beta} = P_{\bar{\nu}_\alpha \to \bar{\nu}_\beta}. \tag{1.85}$$

In this case, for massive Dirac neutrinos, we will be able to rephase the neutrino and the charged lepton fields to make U real. On the other hand, for Majorana neutrinos, we get

$$U^*_{\alpha k} = U_{\alpha k} \rho_k \tag{1.86}$$

with $\rho_k = -i\eta^{CP}_k = \pm 1$, where η^{CP} is the CP parity of the Majorana neutrinos having mass m_k.

For measuring CP-violation it is not easy to set up identical experiments with neutrinos and antineutrinos to compare the transition probabilities as given in Eq. (1.85). However, for a long baseline oscillation experiment, CP-violation modifies the pattern of oscillations as a function of neutrino energy. Thus we can measure CP-violation using neutrinos alone. For this purpose ν_e appearance experiments are the ideal candidates since they can unambiguously identify the oscillation as $\nu_\mu \to \nu_e$.

Oscillations in the two-neutrino case

The transition probability, Eq. (1.81), in the case of only two neutrino flavours, takes the form

$$P_{\nu_\alpha \to \nu_\beta} = \left| \delta_{\alpha\beta} + U_{\beta 2} U^*_{\alpha 2} \left(\exp\left(-i \frac{\Delta m^2 L}{2E} \right) - 1 \right) \right|^2 \tag{1.87}$$

where $\Delta m^2 = m_2^2 - m_1^2$ and α, β are e, μ or μ, τ etc. Usually neutrino oscillation data is analysed under this assumption. The elements of U appearing in Eq. (1.87)

connect the oscillating flavours with the mass eigenstate ν_2 (or ν_1). Note that the phase does not appear in Eq. (1.87) meaning CP violation is not observable in an oscillation scenario with only two flavours. This result can be demonstrated from Eq. (1.83) also. With the substitution, $U_{\alpha 2} = \sin\theta$, we get

$$P_{\nu_\alpha \to \nu_\beta} = \frac{1}{2}\sin^2 2\theta \left(1 - \cos\frac{\Delta m^2 L}{2E}\right) \quad (\alpha \neq \beta) \tag{1.88}$$

$$P_{\nu_\alpha \to \nu_\alpha} = P_{\nu_\beta \to \nu_\beta} = 1 - P_{\nu_\alpha \to \nu_\beta} \tag{1.89}$$

which is valid for neutrinos as well as antineutrinos. In experimentally applicable units we have

$$P_{\nu_\alpha \to \nu_\beta} = \frac{1}{2}\sin^2 2\theta \left(1 - \cos 2.53\frac{\Delta m^2 L}{E}\right) \quad (\alpha \neq \beta) \tag{1.90}$$

where L is in metres, E is in MeV and Δm^2 is in eV^2. Evidently the probability oscillates as a function of L/E with an amplitude of $\sin^2 2\theta$. The condition, Eq. (1.82), can be re-written using the oscillation length,

$$L^{\mathrm{osc}} = \frac{4\pi E}{\Delta m^2} \approx 2.38\frac{E(\mathrm{MeV})}{\Delta m^2 \mathrm{eV}^2}\mathrm{m}, \tag{1.91}$$

to give

$$L^{\mathrm{osc}} \lesssim L. \tag{1.92}$$

The transition probability, Eq. (1.88), with $\sin^2 2\theta = 1$ is plotted in Figure (1.5).

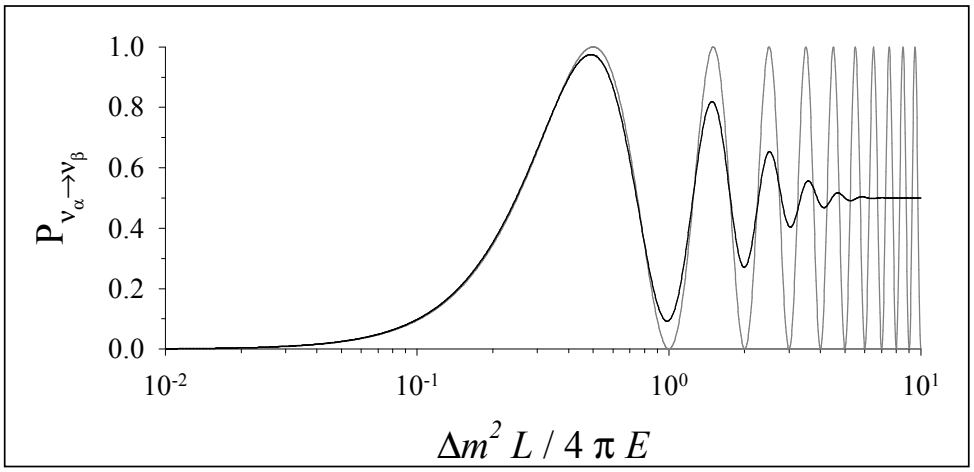

Figure 1.5: Transition probability for two flavour oscillations [14] is indicated using the grey line. The x-axis is in units of L/L^{osc}.

Since the incoming neutrinos have a range of energies, averaging over the neutrino energy distribution is required. The black line represents averaging over a gaussian distribution with mean value E and standard deviation $\sigma = E/10$. At the limit of large distances, the probability tends to a constant, $1 - \sin^2 2\theta/2$ for $L \gg L^{\text{osc}}$.

Analysis with three flavours is more complicated and is not discussed here.

1.2.4 Mikheyev-Smirnov-Wolfenstein (MSW) effect

The MSW effect [15] is the phenomenon of flavour conversion occurring to the neutrinos when they propagate through a medium. The vacuum Hamiltonian is modified because of the charged current and the neutral current interactions of neutrinos with the electrons and the nuclei in matter which in turn modifies the mass eigenstates and mixing angles. Electron neutrinos are born near the centre of the sun, where ambient densities modify the Hamiltonian such that the higher energy electron neutrinos are, to an excellent approximation locally, in a ν_2 mass eigenstate. The dynamics ensures that the mass eigenstate at a particular matter density remains an eigenstate as long as the density varies slowly (adiabatic condition). This is satisfied for high energy solar neutrinos and as a result the neutrino state emerging from the sun is ν_2, the mass eigenstate, which does not evolve with further propagation.

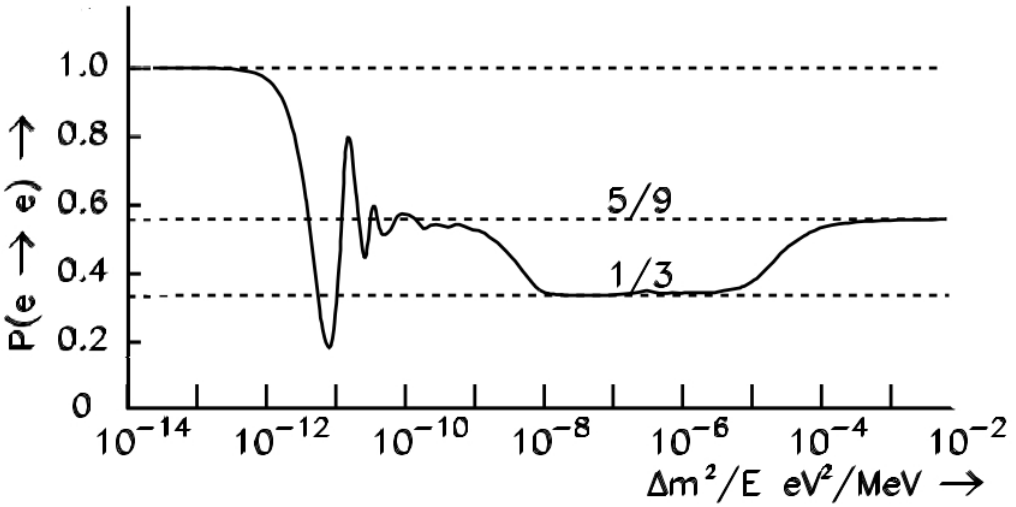

Figure 1.6: The MSW effect under the variation of neutrino energy. The plot [16] is made numerically with the assumption that $|U_{e2}|^2 = \frac{1}{3}$.

Thus for these neutrinos the survival probability is simply the overlap of the ν_2 eigenstate with the ν_e, i.e. $|U_{e2}|^2$. For other energies, the survival probability returns

to the vacuum expression, Eqs. (1.88, 1.89). The results of a numerical calculation are shown in Figure 1.6.

1.2.5 Neutrino oscillation experiments

Solar neutrinos

In the sun, most of the energy is produced through the fusion of hydrogen to form helium via different fusion chains. The Standard Solar Model (SSM) relates variables like radius, pressure, temperature, luminosity, density etc. using stellar structure equations. Numerically solving these equations with the help of the observed properties of the sun like its luminosity and surface abundances, we can predict the relative contributions of different nuclear fusion chains in the energy produced. This allows us to calculate the number of neutrinos produced at various energies. Figure 1.7 shows the neutrino energy spectrum predicted by the BP04 solar model [17].

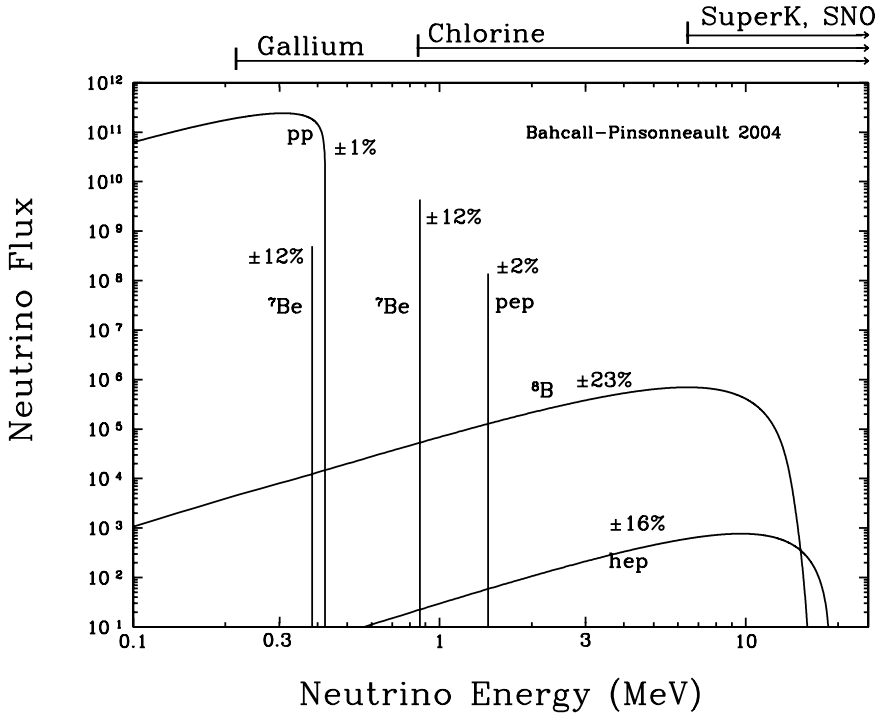

Figure 1.7: The predicted solar neutrino energy spectrum [17]. For continuum sources, the neutrino fluxes are given as the number of neutrinos per $cm^2 s^1 MeV^1$ at the Earth's surface. For line sources, the units are number of neutrinos per $cm^2 s^1$. The difficult-to-detect CNO neutrino fluxes are not shown here.

During the late 1960s, the Homestake experiment conducted by Raymond Davis Jr. and John N. Bahcall reported a deficit in the number of solar neutrinos. A 100,000 gallon tank filled with tetrachloroethylene kept in the Homestake gold mine was used as the neutrino target in the experiment. The chlorine (Cl-37) in the fluid gets converted into radioactive argon (Ar-37) by capturing a neutrino (threshold energy ~ 814 keV) on rare occasions. After running the experiment for a few weeks, argon was collected by bubbling Helium through the fluid. By measuring the amount of argon, the number of neutrinos was calculated. But only a third of the number expected by the SSM was observed and this came to be known as the solar neutrino problem. The high energy neutrinos detected at Homestake are subject to the MSW effect, the value of $\Delta m^2/E$ corresponding to roughly 2×10^{-5} on Figure 1.6. Thus, the observed survival probability $\simeq \frac{1}{3}$ corresponds to $|U_{e2}|^2 \simeq \sin^2\theta_{12} \simeq \frac{1}{3}$. The GALLEX experiment using gallium chloride solution with a lower threshold energy of 233.2 keV also confirmed the solar neutrino deficit. For the low neutrino energies which dominate these data, there is no MSW effect, the value of $\Delta m^2/E$ corresponding to roughly 2×10^{-4} on Figure 1.6. Thus, the vacuum formula, Eqs. (1.88, 1.89) applies, with the factor $\cos\left(\Delta m^2 L/2E\right)$ vanishing when averaged over the energy distribution. A measured survival probability $\simeq \frac{5}{9}$ here thus also indicates a value of $|U_{e2}|^2 \simeq \sin^2\theta_{12} \simeq \frac{1}{3}$.

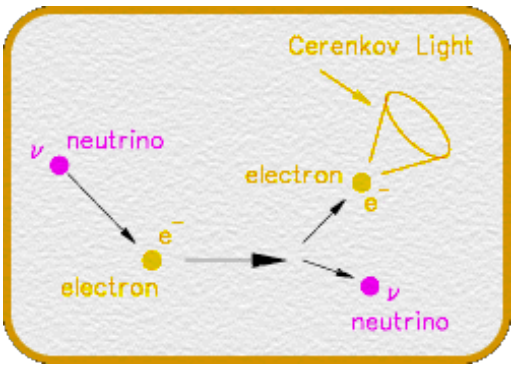

Figure 1.8: This is the primary mechanism in light water detectors like Kamiokande-2. Electron neutrinos, unlike the other flavours, can undergo both neutral and charged current interactions and thus electron neutrino interaction dominates by a factor six. The direction of cerenkov light provides the direction of the incoming neutrino.

The Kamiokande-2 experiment gave the first conclusive evidence that the neutrinos observed were indeed coming from the sun [18]. Being a water Cerenkov detector, the experiment could measure the direction of the incoming neutrinos. Also unlike the previous radiochemical experiments, it gave real time detection. All neutrino flavours can interact via neutral current interaction with the electrons and protons in water, but the charged current interaction channel is available only to election neutrinos, Figure (1.8). The neutrino energies are not high enough for the

production of muons and tau leptons, so ν_μ and ν_τ cannot interact via charged currents. The scattered charged particles moving faster than the speed of light in the medium emit Cerenkov light. Photomultiplier tubes amplify and measure this light, thus detecting the neutrino interactions. Kamiokande-2 had a much higher threshold of 7.15 MeV than the radiochemical experiments and the deficit observed was only about half of the value predicted by the SSM. The experiment also provided constraints on the oscillation parameters [19] with the assumption that neutrino oscillation was the reason for the deficit.

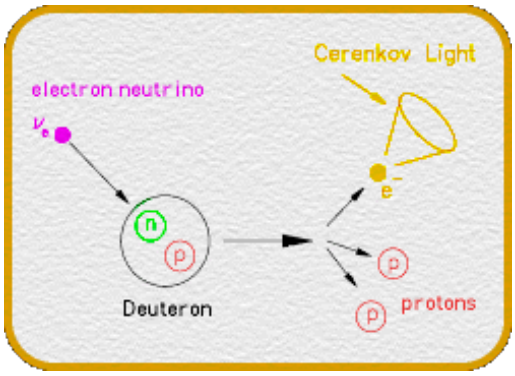

Figure 1.9: Through charged current interaction, the neutron in the deuterium is converted into a proton and the electron neutrino is converted into an electron. The electron with its smaller mass gets most of the energy and the electron which is superluminal in the medium emits Cerenkov light.

The SNO experiment using heavy water as the target material was sensitive to all neutrino flavours unlike previous detectors. The neutrons in heavy water nucleus (deuteron) increased the number of possibilities in which the incoming neutrinos can interact compared with a light water target. The neutrino interactions in SNO are shown in the Figures (1.8-1.10). SNO not only confirmed the electron neutrino deficit, but also showed that if all the neutrino flavours were combined, the result agreed with the number of neutrinos predicted by the SSM. This conclusively proved the neutrino oscillation hypothesis.

Again, the high energy neutrinos observed at Kamioka and SNO are subject to the MSW effect, the detected survival probabilities of electron neutrinos being $\sim \frac{1}{3}$, indicating again, a value of $|U_{e2}|^2 \sim \sin^2\theta_{12} \simeq \frac{1}{3}$. Combined analysis of solar neutrino data from all phases of operation of SNO carried out in a two-flavour neutrino oscillation framework yielded $\Delta m^2_{21} = (5.6^{+1.9}_{-1.4}) \times 10^{-5}\text{eV}^2$ and $\tan^2\theta_{12} = 0.427^{+0.033}_{-0.029}$ [20].

It is clear from Figure 1.7 that the Cerenkov detectors have a high threshold energy. To overcome this deficiency, new generation neutrino detectors like SNO+, Borexino, HERON etc. are designed. SNO+ is a liquid scintillator based detector. Scintillators produce much more light than the Cerenkov process and this decreases

the energy threshold so that the detection of pep solar neutrinos can be achieved. The Borexino detector is also scintillator based, but with still lower threshold of around 250 keV, small enough to detect Be-7 neutrinos. The HERON experiment also with a comparable threshold proposes to use superfluid helium as target. In these highly sensitive detectors ultrapure materials need to be used to minimise backgrounds.

Atmospheric neutrinos

High energy particles coming from outer space called cosmic rays were the most important tools in the study of particle physics before the advent of particle accelerators. In recent years cosmic rays began to play a major role again through atmospheric neutrinos whose production proceeds in three steps [14]. The first step involves the creation of charged pions and kaons directly or indirectly, when the cosmic rays bombard the nuclei in the upper atmosphere. The decays of these mesons produce a part of the atmospheric neutrino flux in the second step:

$$\pi^+ \to \mu^+ + \nu_\mu, \quad \pi^- \to \mu^- + \bar{\nu}_\mu$$
$$K^+ \to \mu^+ + \nu_\mu, \quad K^- \to \mu^- + \bar{\nu}_\mu. \tag{1.93}$$

Electron neutrino and antineutrino fluxes and further muon neutrino and antineutrino fluxes are produced in the third step:

$$\mu^+ \to e^+ + \nu_e + \bar{\nu}_\mu, \quad \mu^- \to e^- + \bar{\nu}_e + \nu_\mu. \tag{1.94}$$

It is clear from Eqs. (1.93, 1.94) that $(\nu_\mu + \bar{\nu}_\mu)/(\nu_e + \bar{\nu}_e) \approx 2$, where ν denotes neutrino flux. For neutrino en-

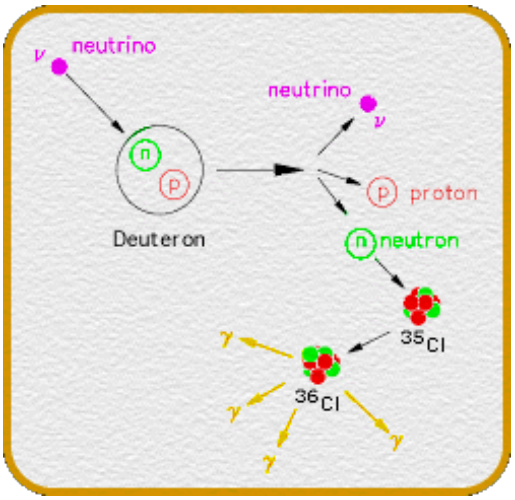

Figure 1.10: The Deuterium nucleus is broken apart as a result of a neutral current interaction. The liberated neutron is slowed down in the heavy water through scattering. The neutron is finally captured by another nucleus which emits gamma rays through de-excitation. The gamma rays will scatter electrons which in turn produce detectable light via the Cerenkov process. Cl-35 is more efficient in neutron capture than deuterium, so it was added in the later phase of detector operation.

ergies larger than 1 GeV, the corresponding muon's lifetime becomes large enough for them to reach the earth's surface before they decay, Eq.(1.94). Thus there will be relatively fewer electron neutrinos produced and the above ratio begins to rise with energy. Monte Carlo models of atmospheric neutrino production are able to predict individual electron and muon neutrino fluxes with only large uncertainties. But they can calculate the ratio of the fluxes with much better accuracy. Therefore in atmospheric neutrino oscillation studies the double ratio

$$R = \frac{R^{data}_{\nu_\mu/\nu_e}}{R^{MC}_{\nu_\mu/\nu_e}} \tag{1.95}$$

is used.

Most atmospheric neutrinos are produced at an altitude of 10km to 40 km above the earth. For a detector kept deep underground, observation of muons crossing the detector horizontally or upwards is an indication of atmospheric muon neutrinos. Experiments conducted in the Kolar gold field in India and also in South Africa were the first ones to report the detection of these atmospheric-neutrino-induced muons. Cerenkov detectors like the Kamiokande and iron plate calorimeters like the Soudan-2 could distinguish up and down going neutrinos. They were also able to differentiate electron and muon flavours. The ν_e and ν_μ events produced diffuse and sharp Cerenkov rings respectively in Cerenkov detectors and showers and tracks in iron calorimeters. They found that the ratio R, Eq. (1.95), is less than 1. This deficit, called the atmospheric neutrino anomaly, could be explained through the $\nu_\mu \to \nu_\tau$ oscillation hypothesis. The Super-Kamiokande detector, more than 10 times bigger than its predecessor Kamiokande, has been used in the detection of solar, atmospheric and beam neutrinos.

Using Eq. 1.90 along with the observed ν_μ deficit, the values of Δm^2_{23} and θ_{23} can be extracted. From the atmospheric data measured by Super-Kamiokande we get $1.9\,(1.7) \times 10^{-3} < \Delta m^2_{23} < 2.6\,(2.7) \times 10^{-3}\text{eV}^2$ and $0.407 \leq \sin^2\theta_{23} \leq 0.583$ [21].

Reactor neutrinos

Uranium-based nuclear reactors produce energy through the nuclear fission of U-235. The radioactive fission products often undergo beta decays before approaching the line of stability [22]. These beta decays produce around 6 antineutrinos per fission. The nuclear reactor fuel usually contains less then 5% of U-235. The rest, consisting of U-238, Pu-239, Pu-241 etc., also undergoes fission which again produces antineutrinos through beta decays. The neutrino flux can be calculated with the

knowledge of these decay chains, but these calculations have large errors. Early neutrino oscillation experiments like Goesgen (Switzerland), Ronvo (Russia) and Bugey (France) measured neutrino fluxes at varying distances from the reactor core, but only within a few tens of meters. Their measurements found no evidence for neutrino oscillations.

Reactor experiments, Chooz and Palo Verde, with a longer baseline of about a km were commissioned in the late nineties. They also did not find any evidence for neutrino oscillations. By probing the parameter region corresponding to $\Delta m^2_{\rm atm} \sim 10^{-3}{\rm eV}^2$, these experiments proved that the muon neutrino deficit in the Kamiokande atmospheric result was not due to $\nu_\mu \to \nu_e$ oscillations assuming CPT invariance. The Chooz experiment also provided the world's best constraint on the θ_{13} at that time: $\sin^2(2\theta_{13}) < 0.14$ at $\Delta m^2_{\rm atm} = 2.5 \times 10^{-3}{\rm eV}^2$. KamLAND was a long baseline reactor experiment with an average distance of around 180 km from the surrounding reactors, sensitive to probe $\Delta m^2_{\rm sol}$. KamLAND found evidence for oscillations compatible with solar neutrino experiments, thus linking oscillations of antineutrinos in vacuum to the flavour transformations through MSW matter effect in the sun.

Recently the Daya Bay Reactor Neutrino experiment [23] found that θ_{13} is non-zero. The experiment consists of three underground experimental halls connected with horizontal tunnels. The unique feature of this experiment is the use of the so-called movable detector. Antineutrino flux from six pressurised water reactors is detected in the two near (flux-weighted baseline 470 m and 576 m) and one far (1648 m) experimental halls. A 6% deficit was found in the far detector compared to the expected flux based on near hall measurements.

As in the case of the atmospheric neutrino deficit, here also we use Eq. 1.90 to express the observed neutrino disappearance (here $\bar{\nu}_e$) and to extract the mixing angle. The Daya Bay analysis yields $\sin^2 2\theta_{13} = 0.092 \pm 0.016({\rm stat}) \pm 0.005({\rm syst})$ [23]. Later RENO, a similar medium baseline reactor experiment in South Korea, also made a compatible measurement, $\sin^2 2\theta_{13} = 0.113 \pm 0.013({\rm stat.}) \pm 0.019({\rm syst.})$ [24].

Accelerator neutrinos

Neutrino beam experiments where one can control the properties of the beam can be used to study neutrinos better. The LSND experiment based at the Los Alamos National Laboratory was one of the earliest beam neutrino experiments. Liquid scintillators were used to detect the neutrinos produced and evidence for neutrino oscillation was found. But this was not consistent with solar and atmospheric neutrino oscillation data (assuming only three neutrino flavours) and this came to be

known as the LSND anomaly. Another accelerator-based experiment called KEK to Kamioka (K2K) was started in 1999. A proton accelerator was used in KEK to generate neutrinos and the observation was carried out at the Super-Kamiokande detector which was constructed 250 km away. A deficit of neutrinos was found compatible with previous observations of neutrino oscillation in atmospheric neutrinos.

A more advanced experiment called Tokai to Kamioka (T2K) with a baseline of 295 km is currently being conducted. This uses a high-intensity neutrino beam produced at J-PARC and the number of events detected at Super-Kamiokande is about 50 times more enabling the investigation of the additional neutrino oscillation mode, $\nu_\mu \rightarrow \nu_e$. The neutrino beam from J-PARC is directed at an angle 2.5° away from the Super-Kamiokande detector. The off-axis technique is used to tune the neutrino energy at oscillation maximum. From the direct beam to the off-axis beam, the peak energy shifts from around 2 GeV to < 1 GeV which is the ideal value. By observing the appearance of ν_e in a ν_μ beam T2K can measure the least known mixing angle θ_{13}. T2K can also measure the observables Δm^2_{23} and $\sin^2 2\theta_{23}$ more accurately than previously via ν_μ disappearance studies.

MiniBooNE is an ongoing neutrino beam experiment at Fermilab. One of the aims of the experiment was to independently verify the LSND anomaly. MiniBooNE found no appearance of electron neutrinos in the muon neutrino beam compatible with the two neutrino oscillation interpretation of LSND data. NuMI is the latest neutrino beam at Fermilab. Here a beam of protons is injected onto a carbon target. Mesons like pions and kaons are produced and are then focussed. The mesons decay into muons and neutrinos during their flight. A hadron absorber removes any left over hadrons and the subsequent earth shield removes the muons allowing only the neutrinos to pass through. This beam is used for experiments like MINOS, MINERνA etc. MINOS consists of a near detector at Fermilab and a far detector at the Soudan Mine 735 km away. Another experiment to utilise the NuMI beam is the proposed NuMI Off-Axis ν_e Appearance (NOνA) experiment. This experiment also has near and far detectors (at Fermilab and Northern Minnesota respectively), but with a longer baseline of 810 km and a better sensitivity to neutrino mass ordering.

The OPERA neutrino experiment in the underground Gran Sasso Laboratory (LNGS) is designed to detect the neutrino oscillations in the direct appearance mode in the $\nu_\mu \rightarrow \nu_\tau$ channel. The ν_μ beam is aimed from CERN to LNGS giving a baseline of 730 km. This experiment complements the atmospheric neutrino experiments which measure the mixing angle θ_{23} through the disappearance of ν_μ. At OPERA two ν_τ candidate events have been observed so far, one in 2010 and the other in 2012.

Feynman diagrams for the charged current and the neutral current interactions experienced by neutrinos and antineutrinos in ordinary matter are shown in Figure 1.11. Depending on the detector design we can observe a subset of these interactions.

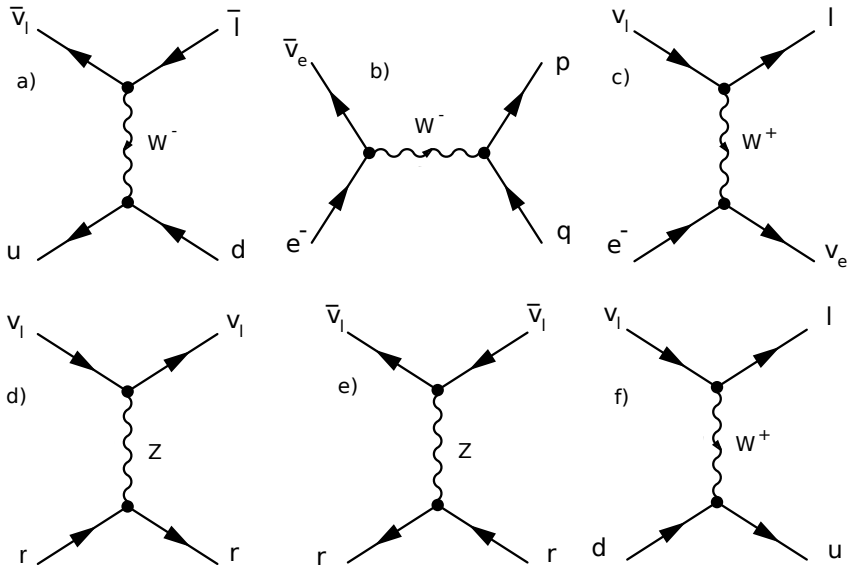

Figure 1.11: Feynman diagrams for the neutrino interactions in matter. The fermions (p, q) represents $(\bar{\nu}_l, l)$ or $(\bar{q}_{2/3}, q_{-1/3})$ and r represents e,u or d.

Using the global fit of oscillation experimental data [25] we get $\Delta m^2_{\rm sol} = 7.66 \pm 0.54 \times 10^{-5}$ eV^2 and $\Delta m^2_{\rm atm} = 2.53 \times 10^{-3} \pm 0.22$ eV^2 (normal hierarchy) or $= 2.43 \times 10^{-3} \pm 0.22$ eV^2 (inverted hierarchy) with 3σ errors. The results on the mixing angles can be converted into moduli-squared of the elements of the PMNS matrix elements. We get

$$|\mathrm{U_{PMNS}}|^2 = \begin{pmatrix} 0.61 - 0.72 & 0.26 - 0.37 & 0.017 - 0.034 \\ 0.04 - 0.32 & 0.15 - 0.53 & 0.35 - 0.67 \\ 0.05 - 0.35 & 0.16 - 0.56 & 0.31 - 0.63 \end{pmatrix}. \tag{1.96}$$

Chapter 2

Flavour Symmetric Observables and their Renormalisation Evolution

In the Standard Model, flavour physics is encoded in the Yukawa couplings between the fermions and the Higgs. Through the Higgs mechanism, the weak isospin symmetry is broken and the fermions acquire the observed masses and mixing properties depending on the choice of the Yukawa couplings. The values of these Yukawa couplings are ad hoc i.e. they are purely experimentally determined quantities. Specific forms of Yukawa couplings were postulated based on theoretical considerations like flavour symmetries and such theories lead to relations among masses and mixing observables. There are also phenomenological relations like the Koide formula [26]

$$\frac{m_e + m_\mu + m_\tau}{(\sqrt{m_e} + \sqrt{m_\mu} + \sqrt{m_\tau})^2} = \frac{2}{3} \tag{2.1}$$

discovered in 1981 which relates the masses of charged leptons. An important factor in the study of these relations among flavour observables (phenomenological or theoretical) is the effect of renormalisation evolution. The masses and mixing observables evolve with the change of energy scale through renormalisation. A phenomenological relation like the Koide formula which was originally proposed for the pole masses should also be valid for the renormalised values of masses. For the relation to be fundamental, we require it to be valid in a high energy scale where some unknown physics generates the relation in the first place. Likewise if we are constructing a theoretical model, the relations obtained will be applicable at the high energy scale of the theory. To test the model, we will have to evolve these down from the high

energy scale to the low energy experimental scale using renormalisation.

In this chapter we analyse the Koide formula and briefly discuss some of its possible extensions which are also flavour symmetric (invariant under the permutations of flavours). Later we study the renormalisation evolution of the flavour observables. This leads to the discovery of a set of renormalisation invariants in the Standard Model. We also discuss the possibilities of some pheneomenological relations motivated by these invariants. These results were published under the title "Exact One-Loop Evolution Invariants in the Standard Model" [1].

2.1 The Koide formula and its extensions

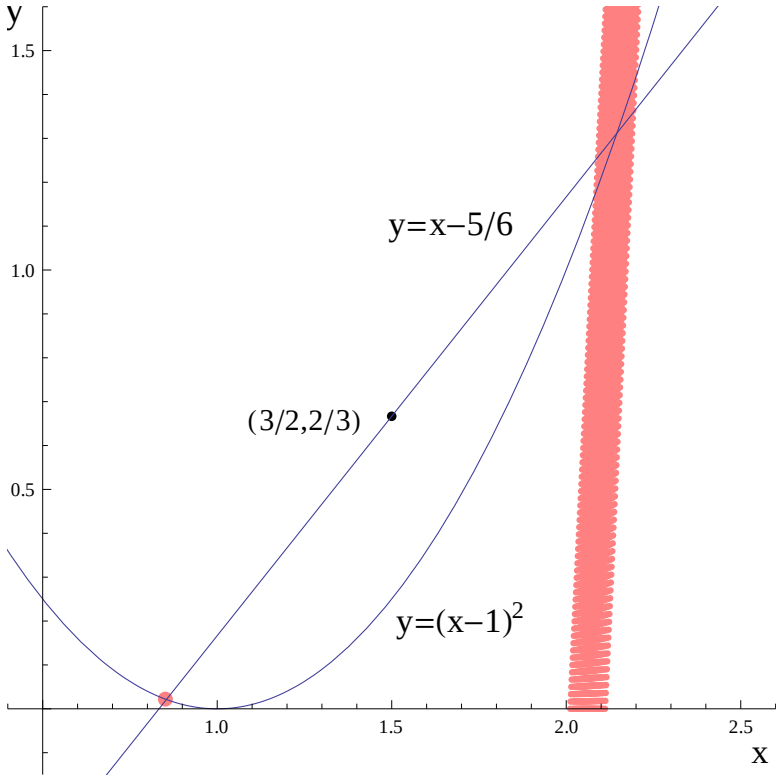

Figure 2.1: The modified Koide constraint (the parabola) and the line with the unit slope ($y = x - \frac{5}{6}$). It is interesting to note that the point $(\frac{3}{2}, \frac{2}{3})$ lies in the middle of the points of intersection of the parabola and the line.

With the accurate measurements of electron and muon masses, the Koide formula, Eq. (2.1), fixes the tau mass at 1776.96 MeV/c^2 and this is within the current experimentally allowed range, 1776.67 MeV/c^2 $\leftrightarrow$ 1777.01 MeV/c^2. The remarkable

accuracy of the formula, along with the fact that it is flavour permutation symmetric, motivates further search for similar relations that are not only applicable to the charged leptons, but also to the whole set of fermions.

The neutrino oscillation experiments provide the mass-squared differences of the neutrinos. This data rules out the Koide formula for neutrinos unless we include negative square roots of the masses. This limitation can be avoided if we remove the square roots from Eq. (2.1) by rearranging and squaring it twice. Thus we get a modified Koide formula which is valid for both leptons and neutrinos:

$$6DL_1 = \left(S - \frac{{L_1}^2}{16}\right)^2 \tag{2.2}$$

where

$$L_1 = m_e + m_\mu + m_\tau \tag{2.3}$$

$$S = m_e m_\mu + m_\mu m_\tau + m_\tau m_e \tag{2.4}$$

$$D = m_e m_\mu m_\tau \tag{2.5}$$

are flavour-permutation-symmetric functions of lepton masses. These three quantities are simply the coefficients of the eigenvalue equation of the charged lepton mass matrix. Dividing the equation with ${L_1}^4$ leads to

$$y = (x-1)^2 \tag{2.6}$$

where

$$y = \frac{6 \times 16^2 D}{{L_1}^3} \qquad \text{and} \qquad x = \frac{16S}{{L_1}^2}$$

are flavour-permutation-symmetric and dimensionless. Fixing a point in the x-y plane fixes the mass hierarchy. The modified Koide constraint, Eq. (2.2), forms a parabola in the x-y plane as shown in Figure 2.1. The point corresponding to the charged leptons (the pink dot) is more or less fixed by the accurate measurement of the charged lepton masses. The constraints on neutrino masses imposed by the oscillation experiments assuming normal hierarchy is shown as the pink band in Figure 2.1.

The uncertainties in the measurement of the neutrino mass-squared differences give some freedom for the choice of the neutrino point, i.e. a point in the parabola with in the pink band. We may draw a straight line joining the charged

lepton point with the neutrino point:

$$y = mx + c. \tag{2.7}$$

The slope of the line, m, is found to be in the range of $1.039 \leftrightarrow 0.911$ with a corresponding range of $-0.863 \leftrightarrow -0.754$ for the y intercept, c. If we fix the slope at 1, the y intercept has to be fixed at -0.829 to constrain the mass hierarchy accurately. The line $y = x - 5/6$ is a very good first approximation.

2.1.1 A Koide-like relation for the quarks

For leptons we have the Koide formula

$$\frac{m_e + m_\mu + m_\tau}{(\sqrt{m_e} + \sqrt{m_\mu} + \sqrt{m_\tau})^2} = \frac{m_{\nu_1} + m_{\nu_2} + m_{\nu_3}}{(\sqrt{m_{\nu_1}} + \sqrt{m_{\nu_2}} + \sqrt{m_{\nu_3}})^2} = \frac{2}{3}. \tag{2.8}$$

We have shown that the charged leptons satisfy the above equation to a high degree of accuracy and the neutrinos can have consistent solutions if we allow negative square roots. An analogous Koide-like formula can be written for the quarks:

$$\frac{m_u + m_c + m_t}{(\sqrt{m_u} + \sqrt{m_c} + \sqrt{m_t})^2} = \frac{m_d + m_s + m_b}{(\sqrt{m_d} + \sqrt{m_s} + \sqrt{m_b})^2} = \frac{1}{k} \tag{2.9}$$

where k is a constant. Of course the Koide formula is a special case of the above equation with $k = \frac{3}{2}$.

We may proceed in the same way as we did previously to get a generalised Koide parabola

$$y = (x - 1)^2 \tag{2.10}$$

where

$$y = \frac{64k}{(k-1)^4}\frac{D}{{L_1}^3} \qquad \text{and} \qquad x = \frac{4}{(k-1)^2}\frac{S}{{L_1}^2}.$$

We can fit this with the experimental data for quarks and the allowed range of k is obtained to be $k = 1.198 \leftrightarrow 1.219$. Large uncertainties in the measurement of the masses of quarks give more freedom for the choice of k compared to the leptons. Interestingly the line joining the up and down quark points with a slope=1 is phenomenologically allowed just like in the case of the leptons (even though the y-intercept of the line is different). This new constraint of unit slope further reduces the range of k for the quarks. Converting the Koide-like relation, Eq. (2.9), into the form given by Eq. (2.10) and the ansatz of using the line with unit slope (y=x+c)

A typical set of experimental values [27, 28]	Calculated values of k and the rest of the masses	Experimental values of the rest of the masses [27]
$m_e = 0.511$ MeV, $m_\mu = 105.66$ MeV, $m_\tau = 1776.82 \pm 0.16$ MeV	$k = 1.5$	
${m_{\nu_2}}^2 - {m_{\nu_1}}^2 = 75 \pm 2.0$ meV^2	$m_{\nu_1} = 0.39$ meV, $m_{\nu_2} = 8.7$ meV, $m_{\nu_3} = 48$ meV, ${m_{\nu_3}}^2 - {m_{\nu_1}}^2 = 2343$ meV^2	${m_{\nu_3}}^2 - {m_{\nu_1}}^2$ $= 2320^{+120}_{-80}$ meV^2
$m_u = 2.3^{+0.7}_{-0.5}$ MeV, $m_c = 1.77 \pm 0.14$ GeV, $m_t = 173.5 \pm 1.4$ GeV	$k = 1.21$	
$m_b = 4.91^{+0.12}_{-0.11}$ GeV	$m_d = 4.6$ MeV, $m_s = 97$ MeV	$m_d = 4.8^{+0.7}_{-0.3}$ MeV $m_s = 95 \pm 5$ MeV

Table 2.1: Predictions made using generalised Koide constraints. The errors in m_e and m_μ are insignificant for our calculations. For the quarks, relative errors are less for the up-type quarks. So we use their masses to calculate $k = 1.21$ for the quarks. Among the down-type quarks, m_b is the most accurately known. Therefore we use it as the input value. The value of k and the masses in the second column corresponds to the best fit.

are the original ideas presented in the above sections.

Thus we have a Koide parabola, Eq. (2.10) with $k = 1.500038 \leftrightarrow 1.499995$ for the leptons and $k = 1.198 \leftrightarrow 1.219$ for the quarks along with the lines of unit slope. These curves partially constrain the mass hierarchy for both leptons and quarks. The only remaining freedom is in fixing the y-intercepts of the lines. The masses of electron, muon and tau can be used to calculate the value of k and also the y-intercept for the leptons. This fully fixes the mass hierarchy for the neutrinos. Similarly we may use the masses of the up type quarks to calculate the value of k and the y-intercept for the quarks which in turn fixes the mass hierarchy for the down type quarks. Table 2.1 summarises these results. Note that for the charged leptons as well as for the heavy quarks we use the pole masses. Since the perturbative QCD calculation is not reliable in the low energy region of the light quarks, we use their $\overline{\text{MS}}$ masses at an accessible scale of $\mu \approx 2$ GeV [27].

2.1.2 Renormalisation effects on Koide formula

The Koide formula is intriguing and fascinating. But the fact that it relates pole masses instead of the renormalised ones makes us wonder if it is indeed fundamental

or just accidental. The importance of the effect of renormalisation on Koide-like relations becomes apparent in this context. Nan Li and Bo-Qiang Ma [29] studied the energy scale dependence of the Koide formula for the charged leptons and the Koide-like formulae for the other fermions. The parameters k_l, k_ν, k_u and k_d are used to describe the deviations from the Koide formula for leptons and quarks

$$k_l = \frac{m_e + m_\mu + m_\tau}{\frac{2}{3}(\sqrt{m_e} + \sqrt{m_\mu} + \sqrt{m_\tau})^2}. \tag{2.11}$$

Similarly the other parameters are also defined.

They solve the renormalisation group equations numerically. At energies much higher than the weak scale, the authors have considered two cases; one with Standard Model and the other with minimal SUSY. For the quarks general trend is a decrease in the renormalized mass with an increase in energy. For the up type quarks the value of k_u is in the range of $1.327 \leftrightarrow 1.359$ and for down type quarks the value of k_d is in the range of $1.025 \leftrightarrow 1.072$. For the charged leptons it is found that even at very high energies the value of k_l lies close to 1 (1.001881 at 2×10^{16} GeV for Standard Model). From these results they conclude that the Koide formula is more or less energy scale independent. For neutrinos, the allowed range of k_ν for the normal as well as the inverted hierarchies is $0.50 \leftrightarrow 0.85$. The authors also introduce a quark-lepton complementarity-hypothesis of the masses, i.e. a constraint that club the neutrinos with the up type quarks and the charged leptons with down type quarks. Some relations like $k_l + k_d \approx k_\nu + k_u \approx 2$ are proposed and using these the absolute neutrino masses are predicted.

2.2 Renormalisation

In this section we recapitulate the general theory of renormalisation quite briefly. Then we discuss the renormalisation of Standard Model parameters and find that directly using the RG evolution equations of masses and mixing parameters is less efficient in studying flavour symmetric constraints like the Koide formula. Therefore we develop a more suitable approach in which the evolving variables are flavour symmetric combinations of masses and mixing observables. This leads to the discovery of a set of one-loop renormalisation invariants which do not evolve under renormalisation.

The origin of renormalisation can be traced back to the perturbative calculations in Quantum Electrodynamics (QED). Amplitudes of Feynman diagrams containing loop integrals were found to be divergent. Loops consist of virtual particles

and to compute the amplitude we need to integrate over all possible four momenta of these particles. The divergences can be classified into ultraviolet divergences (which appear when energies of virtual particles tend to infinity) and infrared divergences (when energies tend to zero). To remove ultraviolet divergences we need to redefine or renormalise the parameters of the theory. Three kinds of ultraviolet divergences appear in QED (Figure 2.2); vacuum polarisation, electron self energy and vertex correction which correspond to the renormalisation of field strength, mass of electron and charge of electron respectively. Infrared divergences are less problematic and can be removed without the renormalisation of the parameters of the theory. For example infrared divergences in the vertex diagram can be cancelled by the addition of bremsstrahlung photons of energies tending to zero emitted from the electron legs.

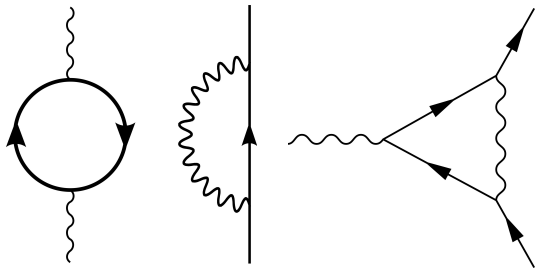

Figure 2.2: The three divergences in Quantum Electrodynamics: Vacuum polarisation, Electron self energy and Vertex correction respectively.

The technique of renormalisation can be summarised as follows [30]. The fields in the Lagrangian are rescaled to absorb the field strength renormalisations. Then each term is split into two parts. One is the physical part and the other is the counter term. Infinite unobservable shifts are contained in the counter terms. Physical quantities like the observed coupling constants and the masses are defined using the renormalisation conditions. Finally we can calculate the amplitudes using the new Feynman rules (with physical and counter terms) making sure that the renormalisation conditions are obeyed. The following equations show how the QED Lagrangian is split into physical and counter terms.
In the original QED Lagrangian,

$$\mathcal{L} = -\frac{1}{4}\left(F_{\mu\nu}\right)^2 + \overline{\psi}\left(i\partial\!\!\!/ - m_0\right)\psi - e_0\overline{\psi}\gamma^\mu\psi A_\mu, \tag{2.12}$$

we make the substitution $\psi = \sqrt{Z_2}\psi_r$ and $A^\mu = \sqrt{Z_3}A^\mu_r$ to absorb the field strength

renormalisation Z_2 and Z_3 and thus we get

$$\mathcal{L} = -\frac{1}{4} Z_3 \left(F_r^{\mu\nu}\right)^2 + Z_2 \overline{\psi}_r \left(i\partial\!\!\!/ - m_0\right) \psi_r - e_0 Z_2 \sqrt{Z_3} \overline{\psi}_r \gamma^\mu \psi_r A_{r\mu}. \tag{2.13}$$

Here ψ, A^μ and ψ_r, A_r^μ are the original and renormalised fields respectively. With the substitution $e_0 Z_2 \sqrt{Z_3} = e Z_1$, $\delta_3 = Z_3 - 1$, $\delta_2 = Z_2 - 1$, $\delta_m = Z_2 m_0 - m$ and $\delta_1 = Z_1 - 1 = (e_0/e) Z_2 \sqrt{Z_3} - 1$ the required splitting of the Lagrangian is attained:

$$\begin{aligned} \mathcal{L} = & -\frac{1}{4} \left(F_r^{\mu\nu}\right)^2 + \overline{\psi}_r \left(i\partial\!\!\!/ - m\right) \psi_r - e \overline{\psi}_r \gamma^\mu \psi_r A_{r\mu} \\ & - \frac{1}{4} \delta_3 \left(F_r^{\mu\nu}\right)^2 + \overline{\psi}_r \left(i\delta_2 \partial\!\!\!/ - \delta_m\right) \psi_r - e \delta_1 \overline{\psi}_r \gamma^\mu \psi_r A_{r\mu} \end{aligned} \tag{2.14}$$

where e_0, m_0 and e, m are the bare and physical quantities respectively.

2.2.1 Renormalisation Group

For describing electromagnetic interactions we may specify the effective charge, e, of the particle at a momentum scale μ, but since the scale is arbitrary we may use other momentum-charge pairs, $\{\mu', e'\}$, as well which gives the same physical results. The set of transformations of the physical parameters associated with the change in scale and necessary to keep the physics constant is called the Renormalisation Group (RG). The variation of the renormalised charge with an infinitesimal change in scale is described using the differential equation

$$\mu \frac{d\alpha(\mu)}{d\mu} = \beta\left(\alpha(\mu)\right), \qquad \beta(\alpha) = \beta_2 \alpha^2 + O(\alpha^3) \tag{2.15}$$

where the beta function, $\beta(\alpha)$, can be calculated as a series expansion in powers of α.

2.3 Standard Model Evolution

The one-loop renormalisation group equations for the gauge couplings g_is in the Standard Model (at high energies) are [31]:

$$\frac{dg_1}{dt} = \frac{41}{6} g_1^3, \quad \frac{dg_2}{dt} = -\frac{19}{6} g_2^3, \quad \frac{dg_3}{dt} = -7 g_3^3. \tag{2.16}$$

where $t = \frac{1}{16\pi^2} \ln\left(\mu/\mu_0\right)$ for renormalisation-scale μ. Here we use the $U(1)$ gauge coupling normalisation of [32, 33]. The evolution of the couplings is shown in Figure 2.3.

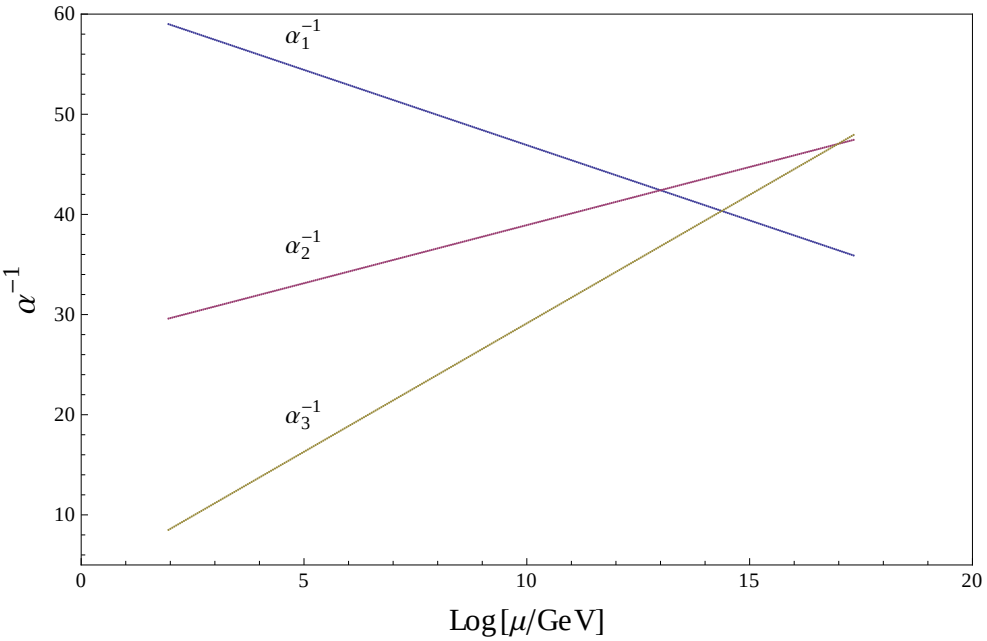

Figure 2.3: Renormalization evolution of the Standard Model gauge couplings. We have $\alpha_i^{-1} = \frac{4\pi}{g_i^2}$ where g_is evolve according to Eqs. (2.16)

We define the Hermitian squares of the Yukawa coupling matrices for charge $+\frac{2}{3}$ (U) and charge $-\frac{1}{3}$ (D) quarks respectively:

$$\mathcal{U} = U^\dagger U, \qquad\qquad \mathcal{D} = D^\dagger D \tag{2.17}$$

and the variables:

$$T = Tr(3\mathcal{U} + 3\mathcal{D} + \mathcal{N} + \mathcal{L}), \tag{2.18}$$

$$G_U = \frac{17}{12}g_1^2 + \frac{9}{4}g_2^2 + 8g_3^2, \tag{2.19}$$

$$G_D = \frac{5}{12}g_1^2 + \frac{9}{4}g_2^2 + 8g_3^2 \tag{2.20}$$

One-loop RG equations for the quark Yukawa coupling matrices in the Standard Model [34] are given by

$$U^{-1}\frac{dU}{dt} = \gamma_u + \frac{3}{2}(\mathcal{U} - \mathcal{D}), \tag{2.21}$$

$$D^{-1}\frac{dD}{dt} = \gamma_d + \frac{3}{2}(\mathcal{D} - \mathcal{U}) \tag{2.22}$$

where

$$\gamma_u = T - G_U; \qquad \gamma_d = T - G_D, \tag{2.23}$$

Neglecting $\mathcal{N}$ and $\mathcal{L}$ which correspond to neutrinos and charged leptons, we can solve the evolution equations, Eqs. (2.16, 2.21, 2.22), numerically. We extract the values of the quark masses from this solution and the result is shown in Figure 2.4.

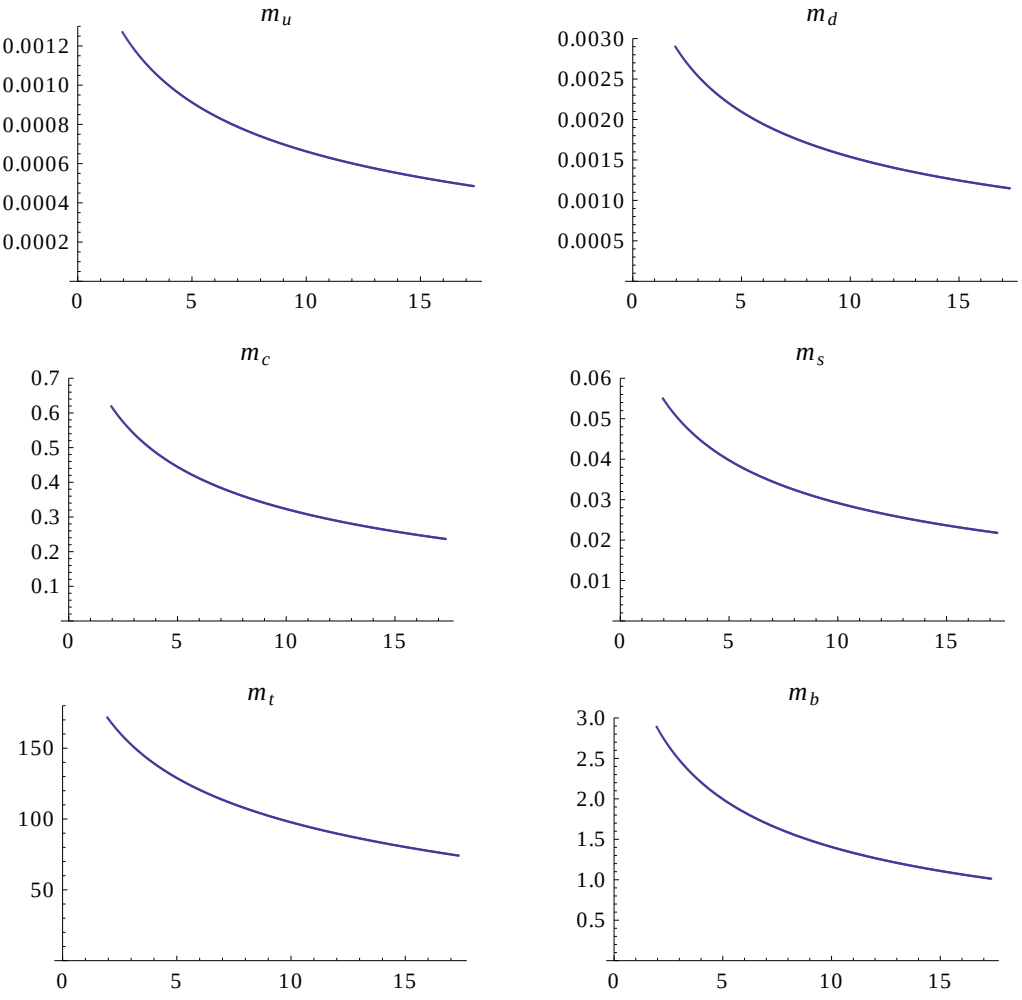

Figure 2.4: Renormalization evolution of the quark masses. The x-axis is in units of Log(μ/GeV) and the y-axis in GeV. All masses decrease continuously from the weak scale to the GUT scale under Standard Model evolution.

From Figure 2.4 it is clear that all quark masses decrease with increase in energy scale and they evolve more or less at the same rate. Therefore the evolution of the ratios of quark masses should be much slower. This is shown in Figure 2.5.

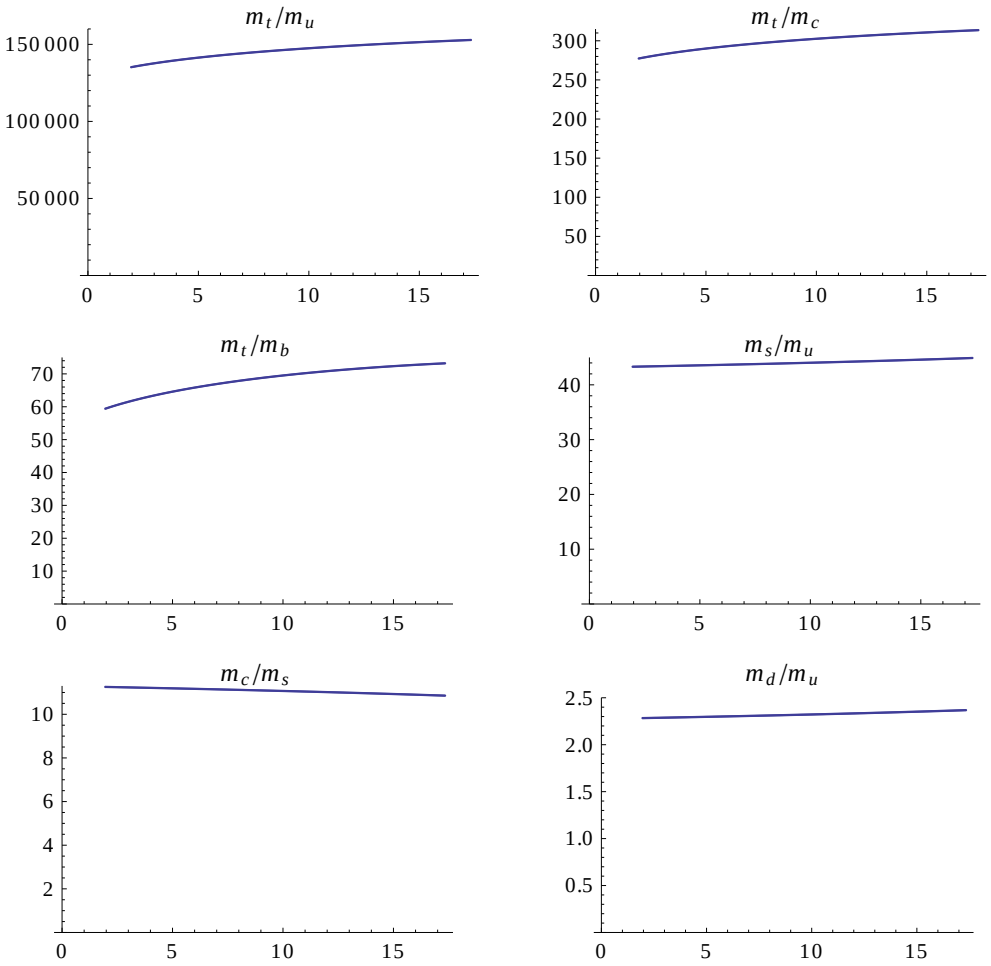

Figure 2.5: Renormalization evolution of the ratios of the quark masses. The mass ratios evolve much slower compared to the masses. The x-axis is in units of Log(μ/GeV).

Recently, there has been interest in evolution invariants [35, 36, 37, 38], combinations of observables which do not evolve under the renormalisation group. Applications have thus far been primarily focussed beyond the Standard Model [35, 36], although approximate evolution invariants of the Standard Model have also been identified [37, 38]. Any empirical relations among evolution invariants are more likely to be fundamental than relations valid at a particular scale between observables which evolve differently with energy such as the Koide formula.

The RG evolution equations of the Yukawa couplings are compactly written as matrix equations [34, 39], since the problem is intrinsically flavour-symmetric - all flavours are treated equivalently. Conventional flavour observables, such as the quark

and lepton masses (proportional to the eigenvalues of the Yukawa coupling matrices) or their mixing angles, break the flavour symmetry so that their RG equations are more complicated [32, 33, 38]. This complexity has meant that in most cases, only quantities that are invariant in certain approximations have been found, eg. assuming no fermion mixing [35], assuming only two generations of fermions [37], or neglecting the contributions of light quark masses [38]. Motivated by the earlier work on flavour-symmetric variables [40, 41], we introduce a set of flavour-symmetric observables whose one-loop RG equations in the Standard Model are especially simple. These lead straightforwardly without approximation to Standard Model evolution invariants which, for the first time, are exact (at this order). This new approach might find further application beyond the Standard Model. For illustration, we consider primarily the quarks, but our considerations are equally valid for the leptons in the case that neutrinos are Dirac particles, in which case more invariants follow.

The evolution equations for $\mathcal{U}$ and $\mathcal{D}$, the Hermitian-squared matrices of Eq. (2.17), are:

$$\frac{d\mathcal{U}}{dt} = 2\gamma_u \mathcal{U} + 3\mathcal{U}^2 - \frac{3}{2}\{\mathcal{U}, \mathcal{D}\}, \tag{2.24}$$

$$\frac{d\mathcal{D}}{dt} = 2\gamma_d \mathcal{D} + 3\mathcal{D}^2 - \frac{3}{2}\{\mathcal{U}, \mathcal{D}\}. \tag{2.25}$$

We introduce a complete set of ten flavour-symmetric invariants (each is invariant under independent $S3$ permutations of the (u, c, t) and/or the (d, s, b) flavour labels):

$$\begin{aligned}
\mathcal{T}_{+0} &= Tr(\mathcal{U}) & \mathcal{T}_{0+} &= Tr(\mathcal{D}) \\
\mathcal{T}_{-0} &= Tr(\mathcal{U}^{-1}) & \mathcal{T}_{0-} &= Tr(\mathcal{D}^{-1}) \\
\mathcal{T}_{++} &= Tr(\mathcal{U}\mathcal{D}) & \mathcal{T}_{+-} &= Tr(\mathcal{U}\mathcal{D}^{-1}) \\
\mathcal{T}_{-+} &= Tr(\mathcal{U}^{-1}\mathcal{D}) & \mathcal{T}_{--} &= Tr(\mathcal{U}^{-1}\mathcal{D}^{-1}) \\
\mathcal{D}_{\mathcal{U}} &= \mathrm{Det}(\mathcal{U}) & \mathcal{D}_{\mathcal{D}} &= \mathrm{Det}(\mathcal{D}).
\end{aligned} \tag{2.26}$$

The set is complete in the sense that these ten variables are fully determined by the physical masses and mixings, and are in turn, sufficient to fully determine them (up to discrete permutations of the flavour labels). A further ten analogous variables can be similarly constructed using Hermitian squares of Yukawa matrices for the neutrinos ($\mathcal{N}$) and the charged leptons ($\mathcal{L}$).

Differentiating Eqs. (2.26) and using Eqs. (2.24) and (2.25), we obtain the

separate evolution equations of our ten flavour-symmetric observables:

$$\frac{d\mathcal{T}_{+0}}{dt} = 2\gamma_u\mathcal{T}_{+0} + 3(\mathcal{T}_{+0}^2 - 2\mathcal{T}_{-0}\mathcal{D}_{\mathcal{U}} - \mathcal{T}_{++}) \tag{2.27a}$$

$$\frac{d\mathcal{T}_{0+}}{dt} = 2\gamma_d\mathcal{T}_{0+} + 3(\mathcal{T}_{0+}^2 - 2\mathcal{T}_{0-}\mathcal{D}_{\mathcal{D}} - \mathcal{T}_{++}) \tag{2.27b}$$

$$\frac{d\mathcal{T}_{-0}}{dt} = -2\gamma_u\mathcal{T}_{-0} - 9 + 3\mathcal{T}_{-+} \tag{2.27c}$$

$$\frac{d\mathcal{T}_{0-}}{dt} = -2\gamma_d\mathcal{T}_{0-} - 9 + 3\mathcal{T}_{+-} \tag{2.27d}$$

$$\frac{d\mathcal{T}_{++}}{dt} = 2(\gamma_u + \gamma_d)\mathcal{T}_{++} \tag{2.27e}$$

$$\frac{d\mathcal{T}_{--}}{dt} = -2(\gamma_u + \gamma_d)\mathcal{T}_{--} \tag{2.27f}$$

$$\begin{aligned}\frac{d\mathcal{T}_{+-}}{dt} &= 2(\gamma_u - \gamma_d + 3\mathcal{T}_{+0})\mathcal{T}_{+-} - 6\mathcal{T}_{+0} \\ &\quad + 6\mathcal{D}_{\mathcal{U}}(\mathcal{T}_{--} - \mathcal{T}_{-0}\mathcal{T}_{0-})\end{aligned} \tag{2.27g}$$

$$\begin{aligned}\frac{d\mathcal{T}_{-+}}{dt} &= 2(-\gamma_u + \gamma_d + 3\mathcal{T}_{0+})\mathcal{T}_{-+} - 6\mathcal{T}_{0+} \\ &\quad + 6\mathcal{D}_{\mathcal{D}}(\mathcal{T}_{--} - \mathcal{T}_{-0}\mathcal{T}_{0-})\end{aligned} \tag{2.27h}$$

$$\frac{d\mathcal{D}_{\mathcal{U}}}{dt} = 3\mathcal{D}_{\mathcal{U}}[2\gamma_u + (\mathcal{T}_{+0} - \mathcal{T}_{0+})] \tag{2.27i}$$

$$\frac{d\mathcal{D}_{\mathcal{D}}}{dt} = 3\mathcal{D}_{\mathcal{D}}[2\gamma_d - (\mathcal{T}_{+0} - \mathcal{T}_{0+})]. \tag{2.27j}$$

Here we make the following observations. Most of the variables' evolutions have two parts: 1) A part proportional to the variable itself, whose coefficient depends at most on γ_u, γ_d, $\mathcal{T}_{+0}$ and $\mathcal{T}_{0+}$. We call this the "pure" part; 2) A part which depends more generally on the other variables - the "mixed" part. The four variables $\mathcal{D}_{\mathcal{U}}$, $\mathcal{D}_{\mathcal{D}}$, $\mathcal{T}_{++}$ and $\mathcal{T}_{--}$ have only pure parts (this is also the case for Jarlskog's determinant [4, 42], which was the main result of Ref. [43]). This feature seems to be peculiar to the Standard Model - we will rely on it in the next stage of our derivation.

2.4 Standard Model Evolution Invariants

Exploiting the opportunity to cancel the terms involving $\mathcal{T}_{+0}$ and $\mathcal{T}_{0+}$ in Eqs. (2.27i) and (2.27j), we note that the quantity $\mathrm{Det}(\mathcal{UD}) = (\mathcal{D}_{\mathcal{U}}\mathcal{D}_{\mathcal{D}})$ has a pure evolution with exactly a factor three times the coefficient which appears in Eqs. (2.27e) and (2.27f):

$$\frac{d}{dt}\ln\mathrm{Det}(\mathcal{UD}) = 6(\gamma_u + \gamma_d). \tag{2.28}$$

We may thus form two independent combinations which are exact evolution invariants at one loop order:

$$\mathcal{I}^q_{TD} \equiv \frac{\mathcal{T}_{++}}{(\mathcal{D}_{\mathcal{U}}\mathcal{D}_{\mathcal{D}})^{\frac{1}{3}}} \equiv \frac{Tr(\mathcal{U}\mathcal{D})}{\mathrm{Det}^{\frac{1}{3}}(\mathcal{U}\mathcal{D})}; \qquad \frac{d\mathcal{I}^q_{TD}}{dt} = 0, \tag{2.29}$$

$$\mathcal{I}^q_{PD} \equiv \mathcal{T}_{--}(\mathcal{D}_{\mathcal{U}}\mathcal{D}_{\mathcal{D}})^{\frac{1}{3}} \equiv Tr(\mathcal{U}\mathcal{D})^{-1}\mathrm{Det}^{\frac{1}{3}}(\mathcal{U}\mathcal{D}); \qquad \frac{d\mathcal{I}^q_{PD}}{dt} = 0. \tag{2.30}$$

The pure evolutions expressed by Eqs. (2.27e), (2.27f) and (2.28), and the two resulting RG invariants, Eqs. (2.29)-(2.30), are the key results of this chapter. Our notation for $\mathcal{I}^q_{TD}$ and $\mathcal{I}^q_{PD}$ is based on which of the coefficients of the eigenvalue equation of the matrix $\mathcal{U}\mathcal{D}$ the RG invariant may be constructed from, e.g. $\mathcal{I}^q_{PD} = P(\mathcal{U}\mathcal{D})/\mathrm{Det}^{\frac{2}{3}}(\mathcal{U}\mathcal{D})$, where $P(\mathcal{U}\mathcal{D})$ is defined in Eq. (2.46). $\mathcal{I}^q_{TD}$ and $\mathcal{I}^q_{PD}$ appear to be the only exact RG invariants that can be constructed from the quark Yukawa coupling matrices alone in the Standard Model case. We have not succeeded in finding similar exact RG invariants involving only Yukawa couplings in the MSSM or the 2 Higgs doublet model (2HDM).

We can construct entirely analogous evolution invariants using $\mathcal{N}$ and $\mathcal{L}$, the (Hermitian squares of the) Yukawa coupling matrices for the leptons (in the Dirac neutrino case). The RG evolution equations of $\mathcal{N}$ and $\mathcal{L}$ are analogous to those in Eqs. (2.24)-(2.25) with γ_ν and γ_ℓ defined as in Eq. (2.23) with the same value of T (Eq. (2.18)) and the gauge contributions, Eqs. (2.19) and (2.20), modified to $G_N = \frac{3}{4}g_1^2 + \frac{9}{4}g_2^2$ and $G_L = \frac{15}{4}g_1^2 + \frac{9}{4}g_2^2$. The leptonic analogue of the "pure" evolution rate $2(\gamma_u + \gamma_d)$, Eqs. (2.27e-2.27f) and (2.28), is just $2(\gamma_\nu + \gamma_\ell)$, being the pure evolution rate of $Tr(\mathcal{N}\mathcal{L})$ and $\mathrm{Det}^{\frac{1}{3}}(\mathcal{N}\mathcal{L})$. Thus two more invariants follow, which we call $\mathcal{I}^\ell_{TD}$ and $\mathcal{I}^\ell_{PD}$ respectively, having definitions in terms of $\mathcal{N}$ and $\mathcal{L}$ analogous to those in Eqs. (2.29) and (2.30).

For completeness, we present here other exact one-loop evolution invariants of the Standard Model. The T-dependence cancels in the ratio of any corresponding pair of purely-evolving quark and lepton observables, leaving only a dependence on gauge couplings, g_i ($i = 1..3$). Thus e.g. using Eq. (2.28), together with its leptonic analogue and Eq. (2.16), we have that:

$$\mathcal{I}^{ql}_{\mathrm{prod}} \equiv \frac{\mathrm{Det}(\mathcal{U}\mathcal{D})}{\mathrm{Det}(\mathcal{N}\mathcal{L})} g_1^{-\frac{96}{41}} g_3^{-\frac{96}{7}} \tag{2.31}$$

is also an exact one-loop evolution invariant.

We note that by combining Eqs. (2.27i) and (2.27j), to form the pure-evolving $\mathrm{Det}(\mathcal{U}\mathcal{D})$, we have effectively removed one independent evolution equation from the

complete set, Eqs. (11). Thus, we may add the (independent) Jarlskog commutator [4, 42] which also has a pure RG evolution equation [43]:

$$\frac{d}{dt}\ln(\mathrm{Det}[\mathcal{U},\mathcal{D}]) = 3[2(\gamma_u+\gamma_d)+Tr(\mathcal{U})+Tr(\mathcal{D})] \tag{2.32}$$

and likewise for the leptons. Noting the definition of T, Eq. (2.18), and using Eqs. (2.28), (2.32), their leptonic analogues, and Eq. (2.16), we find another RG invariant:

$$\mathcal{I}^{ql}_{\mathrm{comm}} \equiv \frac{\mathrm{Det}^3[\mathcal{U},\mathcal{D}]\mathrm{Det}[\mathcal{N},\mathcal{L}]}{\mathrm{Det}^3(\mathcal{U}\mathcal{D})\mathrm{Det}^{\frac{5}{4}}(\mathcal{N}\mathcal{L})} g_1^{-\frac{81}{82}} g_2^{\frac{81}{38}}. \tag{2.33}$$

Using Eqs. (2.16), two more RG invariants can be constructed from gauge couplings alone:

$$\mathcal{I}^{g}_{12} \equiv \frac{6}{41}g_1^{-2} + \frac{6}{19}g_2^{-2}, \tag{2.34}$$

$$\mathcal{I}^{g}_{13} \equiv \frac{6}{41}g_1^{-2} + \frac{1}{7}g_3^{-2}. \tag{2.35}$$

Finally, we note the Standard Model RG evolution equation of the Higgs vacuum expectation value, v [44]:

$$\frac{dv}{dt} = v\left(-T + \frac{3}{4}g_1^2 + \frac{9}{4}g_2^2\right). \tag{2.36}$$

Since its product with any Yukawa coupling gives a mass term, we have that if we use mass matrices directly, rather than Yukawa matrices, the T- and g_2-dependences of the γ_i, Eq. (2.23), are exactly cancelled leaving only the dependences on g_1 and g_3. Thus, using v together with purely-evolving quantities, and the gauge couplings, allows the construction of other RG invariants, e.g.

$$\mathcal{I}^{q}_{DV} \equiv \mathrm{Det}^{\frac{1}{3}}(\mathcal{U}\mathcal{D})\, v^4 g_1^{\frac{4}{41}} g_3^{-\frac{32}{7}}. \tag{2.37}$$

Of course, only one of these invariants involving v is independent of the set already defined.

2.5 Evaluation

In constructing our RG invariants, we have used only four of the variables defined in Eq. (2.26), namely $\mathcal{D}_{\mathcal{U}}$, $\mathcal{D}_{\mathcal{D}}$, $\mathcal{T}_{++}$ and $\mathcal{T}_{--}$. While $\mathrm{Det}(\mathcal{U}\mathcal{D}) = \mathcal{D}_{\mathcal{U}}\mathcal{D}_{\mathcal{D}}$ is simply the product of all six eigenvalues, variables of the form $Tr(\mathcal{U}^n\mathcal{D}^m)$ depend also on the mixing matrix elements. It is easy to show that such quantities are simple

mass moment transforms [45] of the "P-matrix" [46] of transition probabilities $|V_{\alpha i}|^2$. Writing $u = m_u^2/v^2$, etc., with analogous expressions for the charge $-\frac{1}{3}$ quarks:

$$\begin{aligned} Tr(\mathcal{U}^n\mathcal{D}^m) &= \begin{pmatrix} u^n, & c^n, & t^n \end{pmatrix} \cdot \begin{pmatrix} |V_{ud}|^2|V_{us}|^2|V_{ub}|^2 \\ |V_{cd}|^2|V_{cs}|^2|V_{cb}|^2 \\ |V_{td}|^2|V_{ts}|^2|V_{tb}|^2 \end{pmatrix} \cdot \begin{pmatrix} d^m \\ s^m \\ b^m \end{pmatrix} \\ &= \sum_{\alpha i} m_\alpha^{2n} m_i^{2m} |V_{\alpha i}|^2 / v^{2(m+n)} \quad \forall\, m, n, \end{aligned} \tag{2.38}$$

(with $\alpha = u, c, t$ and $i = d, s, b$) in which terms, the flavour-symmetry property is manifest. We may now expand our new RG invariants explicitly. From Eq. (2.29):

$$\mathcal{I}_{TD}^q = \sum_{\alpha i} \frac{m_\alpha^2 m_i^2 |V_{\alpha i}|^2}{(m_u m_c m_t m_d m_s m_b)^{\frac{2}{3}}} = \sum_{\alpha\neq\beta\neq\gamma, i\neq j\neq k} \left(\frac{m_\alpha^2}{m_\beta m_\gamma} \frac{m_i^2}{m_j m_k} \right)^{\frac{2}{3}} |V_{\alpha i}|^2. \tag{2.39}$$

From Eq. (2.30):

$$\begin{aligned} \mathcal{I}_{PD}^q &= (m_u m_c m_t m_d m_s m_b)^{\frac{2}{3}} \sum_{\alpha i} m_\alpha^{-2} m_i^{-2} |V_{\alpha i}|^2 \\ &= \sum_{\alpha\neq\beta\neq\gamma, i\neq j\neq k} \left(\frac{m_\beta m_\gamma}{m_\alpha^2} \frac{m_j m_k}{m_i^2} \right)^{\frac{2}{3}} |V_{\alpha i}|^2. \end{aligned} \tag{2.40}$$

Analogous formulae are obtained for the leptonic RG invariants, $\mathcal{I}_{TD}^\ell$ and $\mathcal{I}_{PD}^\ell$. From Eq. (2.31):

$$\mathcal{I}_{\rm prod}^{ql} = \frac{m_u m_c m_t m_d m_s m_b}{m_1 m_2 m_3 m_e m_\mu m_\tau} g_1^{-\frac{96}{41}} g_3^{-\frac{96}{7}}, \tag{2.41}$$

while from Eq. (2.33):

$$\mathcal{I}_{\rm comm}^{ql} = J_q^3 f^3(u) f^3(d) \times J_\ell f(\nu) f(\ell) \times (y_1 y_2 y_3 y_e y_\mu y_\tau)^{-\frac{1}{4}} g_1^{-\frac{81}{82}} g_2^{\frac{81}{38}}, \tag{2.42}$$

with $f(u) = (m_t^2 - m_c^2)(m_c^2 - m_u^2)(m_t^2 - m_u^2)/(m_t^2 m_c^2 m_u^2)$ and similar definitions for the charge $-\frac{1}{3}$ quarks, and the leptons. The y_ν and y_ℓ are the eigenvalues of $\mathcal{N}$ and $\mathcal{L}$.

For brevity, we limit the following discussion to $\mathcal{I}_{TD}^q$ and $\mathcal{I}_{PD}^q$, the RG invariants constructed only from quark Yukawa matrices. Using the experimental values of the quark masses [28], and the Wolfenstein parameters [3], λ, A, ρ and η for the CKM matrix, we find both invariants to be of the order of 10^8, as shown in Figure 2.6, with their ratio $(\mathcal{I}_{PD}^q/\mathcal{I}_{TD}^q) = 0.7^{+1.1}_{-0.4}$, consistent with unity.

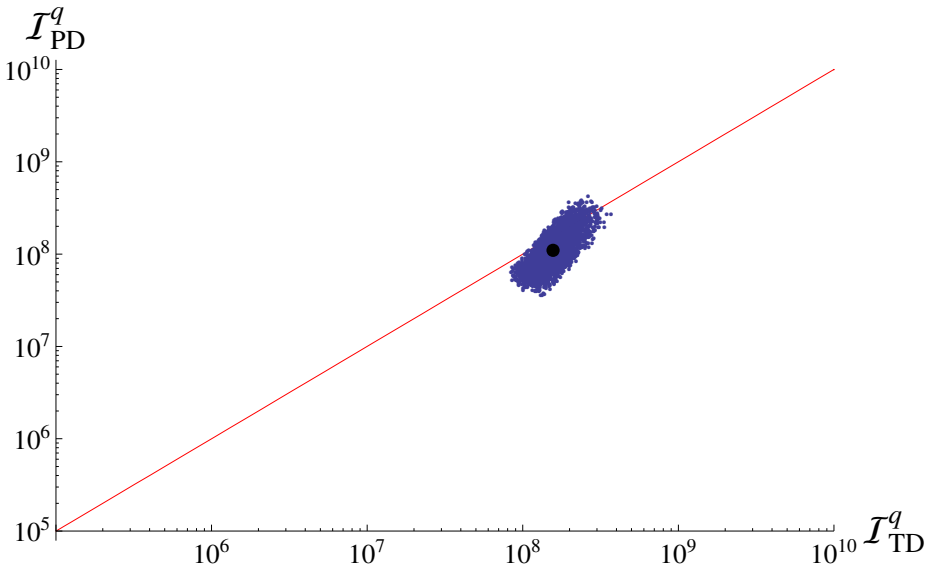

Figure 2.6: The black point shows the values of the RG invariants $\mathcal{I}^q_{TD}$ and $\mathcal{I}^q_{PD}$ found using quark masses from [28] and measured values of the CKM mixings (all renormalised to M_Z). The cluster of points indicates the range allowed by experimental and theoretical uncertainties. The straight line shows the hypothesis $\mathcal{I}^q_{TD} = \mathcal{I}^q_{PD}$ suggested by the data.

The strongly hierarchical quark masses and the small CKM mixing angles mean that each of them is dominated by a single leading term. We find at next-to-leading order in small quantities (small mass ratios and λ^2):

$$\mathcal{I}^q_{TD} \approx \left(\frac{m_t}{m_u}\frac{m_t}{m_c}\frac{m_b}{m_d}\frac{m_b}{m_s}\right)^{\frac{2}{3}} \left(1+\lambda^2\left(\frac{m_c}{m_t}\frac{m_s}{m_b}\right)^2\right), \tag{2.43}$$

$$\mathcal{I}^q_{PD} \approx \left(\frac{m_t}{m_u}\frac{m_c}{m_u}\frac{m_b}{m_d}\frac{m_s}{m_d}\right)^{\frac{2}{3}} (1-\lambda^2). \tag{2.44}$$

Since for $\mathcal{I}^q_{TD}$, Eq. (2.43), the leading term is several orders of magnitude larger than the next-to-leading term, the combination $\left(m_t^2 m_b^2/m_u m_c m_d m_s\right)^{\frac{2}{3}}$ is itself invariant to a very good approximation. At next-to-leading order, the $\mathcal{O}(1)$ invariant ratio is:

$$\frac{\mathcal{I}^q_{PD}}{\mathcal{I}^q_{TD}} \approx \left(m_c^2 m_s^2/m_t m_u m_b m_d\right)^{\frac{2}{3}} (1-\lambda^2). \tag{2.45}$$

From the weak scale to the GUT scale, the various quark masses evolve by typically 55-65% (Figure 2.4). The different mass ratios, on the other hand, vary at a slower rate, eg. m_b/m_s changes by ∼16% and m_s/m_d by ∼1.8% (Figure 2.5). As

stated earlier we have numerically solved Eqs. (2.21) and (2.22) together with the RG equations for the gauge couplings, Eq. (2.16), and here using that solution we have verified that the RG invariants do not evolve at all. We have similarly verified that the leading terms of our RG invariants given in Eqs. (2.43) and (2.44) change by 0.05% or less as shown in Figure 2.7.

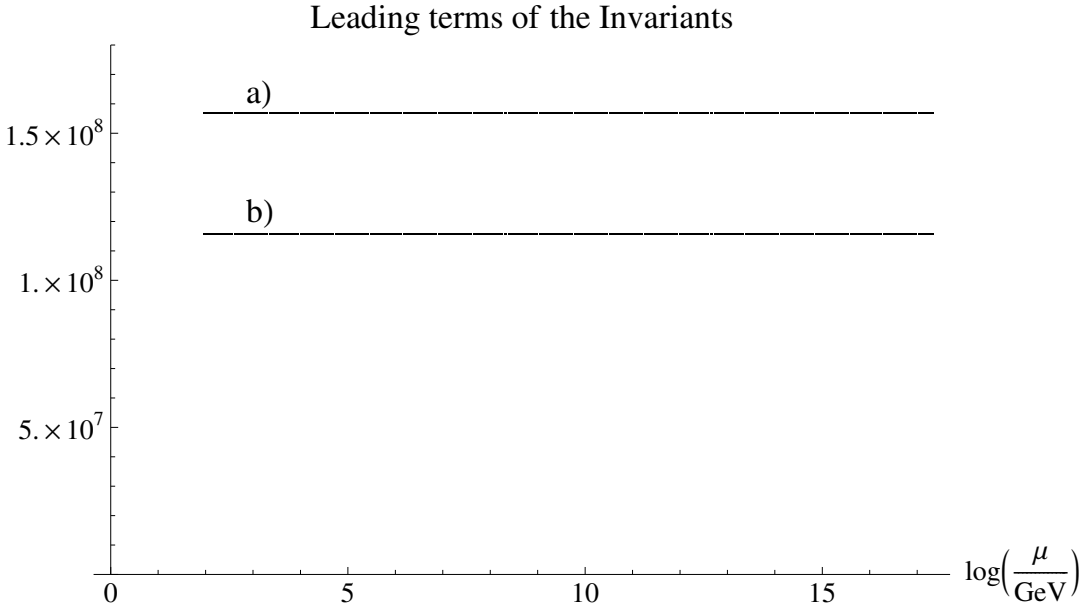

Figure 2.7: Evolution of the leading terms of the RG invariants $\mathcal{I}^q_{TD}$ and $\mathcal{I}^q_{PD}$. Numerical analysis indicates that the leading terms of the RG invariants a) the RHS of Eq. (2.43) and b) the RHS of Eq. (2.44) practically remain unchanged from weak scale to GUT scale

2.6 Interpretation

While the Yukawa coupling matrices $\mathcal{U}$ and $\mathcal{D}$ separately have the mixed and coupled evolutions given by Eqs. (2.24) and (2.25), it is an interesting feature, apparently peculiar to the Standard Model, that the eigenvalues, λ_i, of the *product* matrix $\mathcal{UD}$ have pure evolutions with common rate, leaving the eigenvalue *ratios* RG-invariant (There is no significance to the choice of the product order $\mathcal{UD}$ over $\mathcal{DU}$, since the eigenvalues are the same in each case. All our results are equally applicable to both cases). This follows since $\mathcal{T}_{++} = Tr(\mathcal{UD})$ and $\mathrm{Det}(\mathcal{UD})$ with pure RG evolution equations given in Eqs. (2.27e) and (2.28), are simply the order-one and order-three coefficients in the eigenvalue equation of the matrix $\mathcal{UD}$, while $\mathcal{T}_{--} = Tr(\mathcal{UD})^{-1}$,

with pure evolution given by Eq. (2.27f), is simply $P(\mathcal{UD})/\mathrm{Det}(\mathcal{UD})$ where:

$$P(\mathcal{UD}) \equiv \frac{1}{2}\left[Tr^2(\mathcal{UD}) - Tr(\mathcal{UD})^2\right] \tag{2.46}$$

$(= \lambda_1\lambda_2 + \lambda_2\lambda_3 + \lambda_3\lambda_1)$ is the corresponding order-two coefficient. From Eqs. (2.27e), (2.27f) and (2.28), we thus see that each of the coefficients in the eigenvalue equation of $\mathcal{UD}$ has a pure RG evolution equation with an evolution rate which is simply given by the order of the coefficient times the same basic rate, $2(\gamma_u + \gamma_d)$. Since the three eigenvalues of $\mathcal{UD}$ are all order-one in terms of these coefficients via the formula for the roots of a cubic, it follows that they also have pure RG evolution equations with common evolution rate $2(\gamma_u + \gamma_d)$. We thus conclude that the ratios of the eigenvalues of $\mathcal{UD}$, λ_i/λ_j $(i \neq j)$, are also each RG invariants (although clearly they are not individually flavour-symmetric).

While it is an undoubted mystery why the two independent invariants, $\mathcal{I}^q_{TD} \approx (\lambda_3^2/\lambda_1\lambda_2)^{\frac{1}{3}}$ and $\mathcal{I}^q_{PD} \approx (\lambda_2\lambda_3/\lambda_1^2)^{\frac{1}{3}}$, should be so large ($\mathcal{O}(10^8)$), it is also a puzzle why they should be so nearly equal to each other - the proximity to unity of their observed ratio, $(\mathcal{I}^q_{PD}/\mathcal{I}^q_{TD}) \simeq 0.7^{+1.1}_{-0.4}$ (see Figure 2.6), represents a significant fine-tuning of Standard Model parameters. Moreover, it is interesting to observe that if this ratio were exactly unity, then the spectrum of the product matrix $\mathcal{UD}$ would be geometric, i.e.

$$\mathcal{I}^q_{TD} = \mathcal{I}^q_{PD} (= \mathcal{I}, \text{ say}) \Rightarrow \lambda_3/\lambda_2 = \lambda_2/\lambda_1 \approx \mathcal{I}, \tag{2.47}$$

relations which are then valid at all scales. Indeed, one might reasonably postulate that nature requires the spectrum of the matrix $\mathcal{UD}$ to be exactly geometric, $(\mathcal{I}^q_{PD}/\mathcal{I}^q_{TD}) \equiv 1$, at some (presumably high) energy scale, the data being fully consistent with this. Of course, the separate spectra of the $\mathcal{U}$ and $\mathcal{D}$ matrices have long been known [47] to be approximately geometric: $m_c^2/(m_u m_t) \sim \mathcal{O}(1)$, $m_s^2/(m_d m_b) \sim \mathcal{O}(1)$. However, such separate relations are not RG-invariant and are therefore a priori less interesting and generally more difficult to test experimentally.

We consider briefly why the Standard Model admits RG invariants constructed from the Yukawa couplings, but the MSSM does not. As we did in Eqs. (2.17, 2.26) for the Standard Model, here also we define a similar set of ten flavour symmetric observables. The RG evolution equations for the MSSM [43] are

$$U^{-1}\frac{dU}{dt} = -G_U + 3\mathcal{T}_{+0} + (3U^\dagger U + D^\dagger D) \tag{2.48}$$

$$D^{-1}\frac{dD}{dt} = -G_D + 3\mathcal{T}_{0+} + (3D^\dagger D + U^\dagger U) \tag{2.49}$$

where

$$G_U = \frac{16}{3}g_3^2 + 3g_2^2 + \frac{13}{9}g_1^2 \tag{2.50}$$

$$G_D = \frac{16}{3}g_3^2 + \frac{7}{9}g_1^2. \tag{2.51}$$

The evolution equations for the ten flavour symmetric observables in the MSSM are given by

$$\frac{1}{2}\frac{d\mathcal{T}_{+0}}{dt} = \mathcal{T}_{+0}(-G_U + 3\mathcal{T}_{+0}) + 3\mathcal{T}_{+0}^2 - 6\mathcal{T}_{-0}\mathcal{D}_{\mathcal{U}} + \mathcal{T}_{++} \tag{2.52a}$$

$$\frac{1}{2}\frac{d\mathcal{T}_{0+}}{dt} = \mathcal{T}_{0+}(-G_D + 3\mathcal{T}_{0+}) + 3\mathcal{T}_{0+}^2 - 6\mathcal{T}_{0-}\mathcal{D}_{\mathcal{D}} + \mathcal{T}_{++} \tag{2.52b}$$

$$\frac{1}{2}\frac{d\mathcal{T}_{-0}}{dt} = -\mathcal{T}_{-0}(-G_U + 3\mathcal{T}_{+0}) - 9 - \mathcal{T}_{-+} \tag{2.52c}$$

$$\frac{1}{2}\frac{d\mathcal{T}_{0-}}{dt} = -\mathcal{T}_{0-}(-G_D + 3\mathcal{T}_{0+}) - 9 - \mathcal{T}_{+-} \tag{2.52d}$$

$$\frac{1}{2}\frac{d\mathcal{D}_{\mathcal{U}}}{dt} = \mathcal{D}_{\mathcal{U}}(3(-G_U + 3\mathcal{T}_{+0}) + 3\mathcal{T}_{+0} + \mathcal{T}_{0+}) \tag{2.52e}$$

$$\frac{1}{2}\frac{d\mathcal{D}_{\mathcal{D}}}{dt} = \mathcal{D}_{\mathcal{D}}(3(-G_D + 3\mathcal{T}_{0+}) + 3\mathcal{T}_{0+} + \mathcal{T}_{+0}) \tag{2.52f}$$

$$\frac{1}{2}\frac{d\mathcal{T}_{++}}{dt} = \mathcal{T}_{++}(-G_U - G_D + 7(\mathcal{T}_{+0} + \mathcal{T}_{0+})) + 4\mathcal{D}_{\mathcal{U}}(\mathcal{T}_{-+} - \mathcal{T}_{-0}\mathcal{T}_{0+}) + 4\mathcal{D}_{\mathcal{D}}(\mathcal{T}_{+-} - \mathcal{T}_{+0}\mathcal{T}_{0-}) \tag{2.52g}$$

$$\frac{1}{2}\frac{d\mathcal{T}_{--}}{dt} = -\mathcal{T}_{--}(-G_U - G_D + 3(\mathcal{T}_{+0} + \mathcal{T}_{0+})) - 4(\mathcal{T}_{-0} + \mathcal{T}_{0-}) \tag{2.52h}$$

$$\frac{1}{2}\frac{d\mathcal{T}_{+-}}{dt} = \mathcal{T}_{+-}(G_D - G_U + 3(\mathcal{T}_{+0} - \mathcal{T}_{0+}) + 2\mathcal{T}_{+0}) - 2\mathcal{T}_{+0} + 2\mathcal{D}_{\mathcal{U}}(\mathcal{T}_{--} - \mathcal{T}_{-0}\mathcal{T}_{0-}) \tag{2.52i}$$

$$\frac{1}{2}\frac{d\mathcal{T}_{-+}}{dt} = \mathcal{T}_{-+}(G_U - G_D + 3(\mathcal{T}_{0+} - \mathcal{T}_{+0}) + 2\mathcal{T}_{0+}) - 2\mathcal{T}_{0+} + 2\mathcal{D}_{\mathcal{D}}(\mathcal{T}_{--} - \mathcal{T}_{-0}\mathcal{T}_{0-}). \tag{2.52j}$$

For the Standard Model it can be seen from Eqs. (2.24) and (2.25), that the mixed parts of the evolution equations for the Yukawa coupling matrices $\mathcal{U}$ and $\mathcal{D}$ have balanced positive and negative coefficients. These are exploited in the evolution of the product $\mathcal{U}\mathcal{D}$ where these terms cancel on taking the trace of simple powers. The existence of balanced coefficients in the Standard Model can be traced back to the use of the conjugate Higgs for the Yukawa couplings of the charge $\frac{2}{3}$ quarks, by contrast with the MSSM and the 2HDM, which use independent Higgs fields in each charge sector, resulting in mixed evolutions, Eqs. (2.52), with coefficients all having the same sign, so that no such cancellation is possible.

We have recast the Standard Model RG equations using flavour-symmetric weak-basis invariant functions of the Yukawa coupling matrices, leading to the identification of exact one-loop RG invariants in the Standard Model. We have identified two such invariants involving quark Yukawas alone, and two similar ones for leptons in the case of Dirac neutrinos. The Standard Model seems at least somewhat unusual in allowing such RG invariants - we have not been able to find any in the MSSM or 2HDM. Despite the fact that the evolutions of $\mathcal{U}$ and $\mathcal{D}$ are coupled and mixed, the weak-basis invariants of their product matrix $\mathcal{U}\mathcal{D}$ have pure evolutions with a rate simply proportional to their order, so that its eigenvalue-ratios are RG-invariant, and are furthermore experimentally observed to be consistent with a geometric spectrum.

Chapter 3

A Model for Lepton Yukawa Matrices based on the Discrete Symmetry $C_3 \times C_3 \rtimes C_3$

In this chapter we construct a model for Yukawa mass matrices motivated by the observation of small mixing angles in the quark sector and mostly large mixing in the leptonic sector. After the introductory section, we move on to study our flavour group $C_3 \times C_3 \rtimes C_3$. Some basic group theoretical techniques essential in model building are also explained. In the next section we construct the lepton flavour model in the Standard Model framework. Then we do a phenomenological analysis and make predictions. Finally we briefly discuss the applicability of the model in the quark sector.

3.1 Introduction

In the Standard Model of particle physics, fermions acquire mass through the Higgs mechanism. The Yukawa couplings are responsible for the different values of masses the fermions have and also for the phenomenon of flavour mixing. If all the Yukawa matrices are diagonal there is no mixing. On the other hand, if the Yukawa matrices are non-diagonal, their unitary diagonalising matrices in general lead to flavour mixing ($U_u U_d^\dagger$ for the quarks and $U_l U_\nu^\dagger$ for the leptons). Mixing observables in the quark sector are expressed using the CKM matrix and in the leptonic (neutrino) sector using the PMNS matrix respectively. On a rough approximation we might say that the mixing is close to minimal for quarks (CKM matrix is close to the identity) and close to maximal for neutrinos. To be more precise neutrino mixing is

characterised by two large mixing angles, the solar angle ($\tan^2\theta_{12} = 0.47^{+0.06}_{-0.05}$ [48]) and the atmospheric angle ($\sin^2 2\theta_{23} > 0.92$ [49]), together with the relatively small reactor mixing angle, θ_{13} [23, 24]. The Tribimaximal (TBM) mixing scheme [50], having $\tan^2\theta_{12} = \frac{1}{2}$ and $\sin^2 2\theta_{23} = 1$, has proved a useful first approximation to the data.

It is reasonable to assume that a unified description of fermion mixing should include elements of both maximal and minimal mixing along with a mechanism that pushes it towards minimal mixing for the quarks and maximal mixing for the leptons. We have $U_{CKM} = U_u U_d^\dagger$ and $U_{PMNS} = U_l U_\nu^\dagger$ where U_u, U_d, U_l and U_ν are the unitary matrices that diagonalise the Yukawa matrices corresponding to charge $+\frac{2}{3}$ quarks, charge $-\frac{1}{3}$ quarks, charged leptons and neutrinos respectively. Here we assume that the Yukawa matrices are hermitian.

A circulant Yukawa matrix

$$Y_{circ} = \begin{pmatrix} 0 & A & A^* \\ A^* & 0 & A \\ A & A^* & 0 \end{pmatrix} \tag{3.1}$$

is diagonalised by the Trimaximal mixing matrix [51, 52]

$$T = \frac{1}{\sqrt{3}} \begin{pmatrix} 1 & 1 & 1 \\ 1 & \omega & \bar{\omega} \\ 1 & \bar{\omega} & \omega \end{pmatrix} \tag{3.2}$$

where ω and $\bar{\omega}$ are the complex cube roots of unity, $-\frac{1}{2} + i\frac{\sqrt{3}}{2}$ and $-\frac{1}{2} - i\frac{\sqrt{3}}{2}$ respectively. Trimaximal matrix with all its elements equal in modulus ($\frac{1}{\sqrt{3}}$) can be considered as the maximal form of mixing. On the other hand, a diagonal Yukawa matrix

$$Y_{diag} = \begin{pmatrix} -B-\epsilon & 0 & 0 \\ 0 & 2B & 0 \\ 0 & 0 & -B+\epsilon \end{pmatrix} \tag{3.3}$$

does not contribute to mixing at all. Note that the circulant and the diagonal Yukawa matrices in Eq. (3.1) and Eq. (3.3) are written as traceless. This is because adding a part proportional to identity to a matrix does not change its diagonalising matrix. A model that incorporates circulant as well as diagonal parts in the Yukawa matrices may be suited to describe mixing in both the quark and the leptonic sectors. So we

postulate that the Yukawa matrices have the general circulant-plus-diagonal form

$$Y = KI + \begin{pmatrix} -B-\epsilon & A & A^* \\ A^* & 2B & A \\ A & A^* & -B+\epsilon \end{pmatrix}. \tag{3.4}$$

It should be noted that it is not straightforward to obtain a highly hierarchical set of masses from the above mass matrix, Eq. (3.4), and we require some fine tuning of the parameters. For simplicity let us ignore the circulant part. First we fine tune the parameter K (coefficient of the identity) so that it is very close to $2B$, but has the opposite sign. This gives the smallest mass, $K + 2B$. The other eigenvalues are $K - B - \epsilon$ and $K - B + \epsilon$. Now, appropriate fine tuning is applied to the parameter ϵ also to obtain the other two masses satisfying the large hierarchy.

3.1.1 Circulant-plus-diagonal Yukawa matrices and Tribimaximal mixing

The TBM mixing matrix in terms of the moduli of its elements is given by

$$|\text{TBM}| \equiv \begin{pmatrix} \frac{\sqrt{2}}{\sqrt{3}} & \frac{1}{\sqrt{3}} & 0 \\ \frac{1}{\sqrt{6}} & \frac{1}{\sqrt{3}} & \frac{1}{\sqrt{2}} \\ \frac{1}{\sqrt{6}} & \frac{1}{\sqrt{3}} & \frac{1}{\sqrt{2}} \end{pmatrix}. \tag{3.5}$$

In many models of neutrino mixing, the TBM pattern arises from the neutrino mass matrix alone, while the charged lepton mass matrix is assumed to be diagonal. But when it was originally proposed [50], the TBM mixing was modelled as the product of Trimaximal matrix, Eq. (3.2) and the 2×2-maximal matrix

$$\begin{pmatrix} \frac{1}{\sqrt{2}} & 0 & -\frac{1}{\sqrt{2}} \\ 0 & 1 & 0 \\ \frac{1}{\sqrt{2}} & 0 & \frac{1}{\sqrt{2}} \end{pmatrix}. \tag{3.6}$$

In this scenario, diagonalisation of the charged lepton and neutrino mass matrices should lead to Trimaximal and 2×2-maximal matrices respectively whose product gives rise to TBM mixing.

For circulant-plus-diagonal mass matrices, we assume that in the case of charged leptons, the traceless diagonal part is very small compared to the circulant part, Eq. (3.7). We also impose the condition that the phase of the circulant elements

is small. Thus we have

$$Y_l = K_l I + \begin{pmatrix} -B_l - \epsilon_l & A_l & A_l^* \\ A_l^* & 2B_l & A_l \\ A_l & A_l^* & -B_l + \epsilon_l \end{pmatrix} \tag{3.7}$$

with

$$|\epsilon_l|, |B_l| << \mathrm{Im}(A_l) << |A_l|. \tag{3.8}$$

The above condition, Eq. (3.8), makes sure that the diagonalising matrix for the charged-lepton Yukawa matrix, Eq. (3.7), is close to the Trimaximal pattern.

For the neutrinos on the other hand, the circulant part should be very small compared to the traceless diagonal part. Here also we need to impose another condition, namely, the circulant elements should be large compared to the difference between diagonal elements, i.e. ϵ in Eq. (3.4). Thus we have

$$Y_\nu = K_\nu I + \begin{pmatrix} -B_\nu - \epsilon_\nu & A_\nu & A_\nu^* \\ A_\nu^* & 2B_\nu & A_\nu \\ A_\nu & A_\nu^* & -B_\nu + \epsilon_\nu \end{pmatrix} \tag{3.9}$$

with

$$|\epsilon_\nu| << |A_\nu| << |B_\nu|. \tag{3.10}$$

The condition, Eq. (3.10), makes sure that the diagonalising matrix for the neutrino Yukawa matrix, Eq. (3.9), is close to the 2×2-maximal pattern, Eq. (3.6).

3.1.2 Theory of finite groups - A primer

A set of objects with the definition of the operation of multiplication constitute a group. Multiplication should be associative and the group should be closed under multiplication. A multiplicative identity as well as multiplicative inverses for all the group elements should exit. The number of elements in a group is called the order of the group and a finite group is the one with a finite order. For every element of the group, $a \in G$, we have $a^{h_a} = e$ where e is the identity element and h_a is said to be the order of the element a.

Let f be a map from a group G to another G'. This map is homomorphic only if it preserves the multiplicative structure, i.e. $f(a)f(b) = f(ab)$. The special case where the map is one-to-one is known as the isomorphic map. The element $g^{-1}ag$ for $g \in G$ is called the element conjugate to a. The set of all the elements conjugate to a form a conjugacy class of G, i.e. $g^{-1}ag, \forall g \in G$. All elements in a

conjugacy class have the same order. Every group can be divided into a specific number of conjugacy classes.

If the subset H of a group G is itself a group, then H is said to be the subgroup of G. If a subgroup N of G satisfies $g^{-1}Ng = N$ for any element g of G, then N is called a Normal subgroup of G. Let H and N be a subgroup and a normal subgroup of G respectively. The group HN is defined as

$$\{h_i n_i | h_i \in H, n_i \in N\} \tag{3.11}$$

It can be shown that $HN = NH$ and this group is a subgroup of G. The normal subgroup is important in the definition of semidirect product of two groups. In the special case where $G = HN = NH$ with $H \cap N = \{e\}$, the semidirect product $N \rtimes H$ is isomorphic to G. Let $a_1, a_2 \in N$ and $b_1, b_2 \in H$. The multiplication rule for the semidirect product $N \rtimes H$ is given by

$$(a_1, a_2)(b_1, b_2) = (a_1, f_{a_2}(b_1), a_2 b_2) \tag{3.12}$$

where $f_{a_2}(b_1)$ denotes the homomorphic map

$$f_{a_2}(b_1) = a_2 b_1 a_2^{-1} \tag{3.13}$$

from H to N. The definition of direct product is simpler. Let $a_1, a_2 \in G_1$ and $b_1, b_2 \in G_2$, where G_1, G_2 are two groups. The multiplication rule for the direct product $G_1 \times G_2$ is given by

$$(a_1, a_2)(b_1, b_2) = (a_1 b_1, a_2 b_2). \tag{3.14}$$

A representation of G is a homomorphic map from the abstract elements g of G onto matrices $D(g)$. The representation is said to be faithful if the map is injective, i.e. if all the representation matrices are distinct. The vector space on which the representation matrices act is said to the representation space and the dimension of the vector space is the dimension of the representation. If v_j constitute a subspace of the representation space and $D(g)_{ij} v_j \forall g$ also lies in the same subspace, then it is called an invariant subspace. A representation with an invariant subspace is reducible, and one without is irreducible. Every reducible representation can be block diagonalised into irreducible representations using similarity transformations. In other words, every reducible representation is a direct sum of the constituting

irreducible representations:

$$D(g) = \sum_{\alpha=1}^{r} \oplus D_\alpha(g) \tag{3.15}$$

where $D(g)$ is reducible and $D_\alpha(g)$ are the various irreducible representations. Given two irreducible representations, we may obtain the tensor product of the corresponding irreducible vector spaces. The tensor product representation acting on this tensor product space in general is reducible:

$$D_m(g) \otimes D_n(g) = \sum_{\alpha=1}^{r} \oplus D_\alpha(g) \tag{3.16}$$

Character $\chi_D(g)$ of a representation $D(g)$ is the trace of the representation matrix $D(g)$. Similarity transformations do not change the character. By the same logic, all the elements in a conjugacy class have the same character. The number of irreducible representations for a group will be equal to the number of its conjugacy classes. In a character table, characters of all the conjugacy classes for all the irreducible representations are tabulated.

Suppose we are given the tensor product of any two irreducible representations and we need the decomposition of the direct product into the direct sum of irreducible representations. As a first step, we can use the character table and the orthogonality relationship for characters to enumerate the irreducible representations contained in the direct sum. Let D_a and D_b be two irreducible representations. The orthogonality relation [53] for characters is

$$\frac{1}{N} \sum_{g \in G} \chi_{D_a}(g)^* \chi_{D_b}(g) = \delta_{ab} \tag{3.17}$$

where N is the order of the group G and χs are the characters. The direct product $a \otimes b$ can be represented using the Kronecker product of matrices D_a and D_b. So the characters of the direct product representation will be the product of the characters of the representations D_a and D_b.

Let $D_{a\otimes b}$ be the representation of the direct product of two irreducible representations, D_a and D_b. Let $\chi_{D_{a\otimes b}}(g)$ be the characters of this direct product representation. Since $D_{a\otimes b}$ is a reducible representation, it will contain each of the irreducible representations (D_c) some integer number of times, m_c. We can use the orthogonality relation, Eq. (3.17), to compute m_c:

$$m_c = \frac{1}{N} \sum_{g \in G} \chi_{D_c}(g)^* \chi_{D_{a\otimes b}}(g) = \frac{1}{N} \sum_{g \in G} \chi_{D_c}(g)^* \chi_{D_a}(g) \chi_{D_b}(g). \tag{3.18}$$

3.2 The flavour group - $C_3 \times C_3 \rtimes C_3$

We assume that both left and right handed fermions fall in the same representation of the flavour group. Higgs(H) is assumed to be a flavour singlet. Consider the mass term in the Standard Model Lagrangian

$$\psi_L^\dagger Y H \psi_R \tag{3.19}$$

and a flavour transformation

$$\psi_L \to g_c \psi_L, \quad \psi_R \to g_c \psi_R \tag{3.20}$$

where g_c is an element of the defining representation of the cyclic group C_3, $g_c \in \{1, c, c^2\}$ with

$$c = \begin{pmatrix} 0 & 0 & 1 \\ 1 & 0 & 0 \\ 0 & 1 & 0 \end{pmatrix}. \tag{3.21}$$

The mass term, Eq. (3.19), will remain invariant under the transformation, Eq. (3.2), only if Y is a circulant matrix because

$$g_c Y_{circ} g_c^\dagger = Y_{circ}. \tag{3.22}$$

The defining representation of C_3 can be diagonalised using the Trimaximal mixing matrix (T), Eq. (3.2). So we have

$$T c T^\dagger = d \tag{3.23}$$

where

$$d = \begin{pmatrix} 1 & 0 & 0 \\ 0 & \omega & 0 \\ 0 & 0 & \bar{\omega} \end{pmatrix}. \tag{3.24}$$

The matrix d contains the irreducible representations of C_3 which are 1, ω and $\bar{\omega}$. It is also obvious that if the Yukawa matrix is diagonal, then

$$d Y_{diag} d^\dagger = Y_{diag}. \tag{3.25}$$

Because of these observations we use c and d as the generators to construct our flavour group and it turns out to be $C_3 \times C_3 \rtimes C_3$. This group was used in model building in earlier studies [54, 55, 56].

$C_3 \times C_3 \rtimes C_3$ also known as $\Delta(27)$ has 27 elements. This group belongs to a class of groups named as $\Delta(3N^2)$ which is isomorphic to $C_N \times C'_N \rtimes C_3$. For $\Delta(27)$, we have $N = 3$. Let a, a' and b be the generators of C_N, C'_N and C_3 respectively. Using these generators we can write the following presentation for the group $\Delta(3N^2)$.

$$\begin{aligned} a^N = a'^N = b^3 = e, \qquad aa' = a'a, \\ bab^{-1} = a^{-1}a'^{-1}, \qquad ba'b^{-1} = a. \end{aligned} \tag{3.26}$$

All the $3N^2$ elements of $\Delta(3N^2)$ take the following simple form in terms of the above mentioned generators

$$g = b^k a^m a'^n \tag{3.27}$$

for $k = 0$, 1, 2 and m, $n = 0$, 1, 2, ..., $N-1$. We mentioned earlier that the matrices c, Eq. (3.21), and d, Eq. (3.24) generate $\Delta(27)$. Therefore c and d can be used to construct the generators a, a' and b for the specific case of $\Delta(27)$:

$$a = \omega d, \qquad a' = \bar{\omega} d, \qquad b = c. \tag{3.28}$$

$C_3 \times C_3 \rtimes C_3$ consists of 11 conjugacy classes. So we have 11 irreducible representations. Two of those are the defining representation $\mathbf{3}$ and its conjugate representation $\overline{\mathbf{3}}$. All the other representations are one-dimensional. This includes the trivial representation $\mathbf{1}$ and eight others which are not faithful representations. We provide the characters of the group representations in Table 3.1. The eight non-trivial one-dimensional representations are named based on the group element under which the representation transforms trivially. For example $\mathbf{1_c}$ transforms trivially under c which is quite evident from the character table. It transforms like the irreducible representations of C_3 under the remaining generator d. Others are also named analogously.

3.2.1 Direct product of representations

Once we have the irreducible representations and the character table, the next step in building the model is to construct invariants out of the representations. For that we need the direct product expansion of the various irreducible representations. The direct product of one-dimensional representations can be obtained trivially from the character table. For example $\mathbf{1_c} \times \overline{\mathbf{1_c}} = \mathbf{1}$ and $\mathbf{1_c} \times \mathbf{1_d} = \mathbf{1_{cd}}$. For the three-dimensional representations ($\mathbf{3}$ and $\overline{\mathbf{3}}$) of $C_3 \times C_3 \rtimes C_3$, the tensor product decomposition can be calculated using Eq. (3.18) and the results are shown in Table 3.2.

	e	$1C_3^{(1)}$	$1C_3^{(2)}$	$3C_3^{(1)}$	$3C_3^{(2)}$	$3C_3^{(3)}$	$3C_3^{(4)}$	$3C_3^{(5)}$	$3C_3^{(6)}$	$3C_3^{(7)}$	$3C_3^{(8)}$
$\chi_{\mathbf{1}}$	1	1	1	1	1	1	1	1	1	1	1
$\chi_{\mathbf{1_c}}$	1	1	1	1	1	$\bar{\omega}$	ω	$\bar{\omega}$	ω	ω	$\bar{\omega}$
$\chi_{\overline{\mathbf{1_c}}}$	1	1	1	1	1	ω	$\bar{\omega}$	ω	$\bar{\omega}$	$\bar{\omega}$	ω
$\chi_{\mathbf{1_d}}$	1	1	1	$\bar{\omega}$	ω	1	1	$\bar{\omega}$	ω	$\bar{\omega}$	ω
$\chi_{\overline{\mathbf{1_d}}}$	1	1	1	ω	$\bar{\omega}$	1	1	ω	$\bar{\omega}$	ω	$\bar{\omega}$
$\chi_{\mathbf{1_{cd}}}$	1	1	1	ω	$\bar{\omega}$	$\bar{\omega}$	ω	1	1	$\bar{\omega}$	ω
$\chi_{\overline{\mathbf{1_{cd}}}}$	1	1	1	$\bar{\omega}$	ω	ω	$\bar{\omega}$	1	1	ω	$\bar{\omega}$
$\chi_{\mathbf{1_{c\bar{d}}}}$	1	1	1	$\bar{\omega}$	ω	$\bar{\omega}$	ω	ω	$\bar{\omega}$	1	1
$\chi_{\overline{\mathbf{1_{c\bar{d}}}}}$	1	1	1	ω	$\bar{\omega}$	ω	$\bar{\omega}$	$\bar{\omega}$	ω	1	1
$\chi_{\mathbf{3}}$	3	3ω	$3\bar{\omega}$	0	0	0	0	0	0	0	0
$\chi_{\overline{\mathbf{3}}}$	3	$3\bar{\omega}$	3ω	0	0	0	0	0	0	0	0

Table 3.1: Character table for the group $C_3 \times C_3 \rtimes C_3$. The conjugacy classes are given in the form $nC_h^{(j)}$ where n is the number of elements in the class, h is the order of each element in the class and j is the index to differentiate otherwise identical classes.

Tensor product	Decomposition
$\mathbf{3} \times \mathbf{3}$	$\overline{\mathbf{3}} + \overline{\mathbf{3}} + \overline{\mathbf{3}}$
$\overline{\mathbf{3}} \times \overline{\mathbf{3}}$	$\mathbf{3} + \mathbf{3} + \mathbf{3}$
$\mathbf{3} \times \overline{\mathbf{3}}$	$\mathbf{1} + \mathbf{1_c} + \overline{\mathbf{1_c}} + \mathbf{1_d} + \overline{\mathbf{1_d}} + \mathbf{1_{cd}} + \overline{\mathbf{1_{cd}}} + \mathbf{1_{c\bar{d}}} + \overline{\mathbf{1_{c\bar{d}}}}$

Table 3.2: Tensor product expansion of three-dimensional representations of $C_3 \times C_3 \rtimes C_3$

The next step is to calculate the explicit expressions of the irreducible representations contained in the direct product representation. The technique is called the method of canonical decomposition [53].

3.2.2 The Canonical decomposition of a representation

Let D be a representation of the group G acting on the vector space V. Let $\chi_1, ..., \chi_h$ be the distinct characters of the irreducible representations $W_1, ..., W_h$ of G and $n_1, ..., n_h$ their degrees. The method of canonical decomposition follows two steps. First we obtain a direct sum decomposition of V which is "coarser" than the decomposition into irreducible representations, but which has the advantage of being unique. Let this decomposition be

$$V = V_1 \oplus V_2 \oplus ... \oplus V_h. \tag{3.29}$$

In the second step we decompose each of the V_is into irreducible spaces:

$$V_i = V_i^1 \oplus V_i^2 \oplus ... \oplus V_i^m \tag{3.30}$$

where each of V_i^1, V_i^2... transform under a representation isomorphic to W_i. In other words, we have decomposed V into a direct sum of irreducible representations and collected together the isomorphic representations. We use the projection operator p_i to decompose V into V_is:

$$p_i = \frac{n_i}{N} \sum_{g \in G} \chi_i(g)^* D(g). \tag{3.31}$$

Now consider the second step i.e. the decomposition V_i into its subspaces, Eq. (3.30). However this decomposition is not unique. It can be done in infinitely many ways. But a method for explicitly constructing a decomposition of V_i into a direct sum of subrepresentations isomorphic to W_i is explained below. Let $r_{\alpha\beta}(g)$ be the matrix elements of W_i. For each pair of integers α and β taken from 1 to n_i, let $p_{\alpha\beta}$ denote a linear map of V into V defined by

$$p_{\alpha\beta} = \frac{n_i}{N} \sum_{g \in G} r_{\beta\alpha}(g^{-1}) D(g). \tag{3.32}$$

The map $p_{\alpha\alpha}$ is a projection whose image $V_{i,\alpha}$ is contained in V_i and in fact V_i is the direct sum of $V_{i,\alpha}$ for α from 1 to n_i. Let $(x_1^1, ..., x_1^m)$ be a basis of $V_{i,1}$. Let $x_\alpha^1 = p_{\alpha 1}(x_1^1)$. The vector space spanned by x_α^1s for α from 1 to n_i is stable under G. Thus using the mapping $p_{\alpha\beta}$, m such vector spaces can be generated from $(x_1^1, ..., x_1^m)$. Thus we have decomposed the space V_i into subspaces $V_i^1, ..., V_i^m$.

In the model using $C_3 \times C_3 \rtimes C_3$ described in the next section, the relevant

Representation	Expression
$\mathbf{1}$	$\psi_L^\dagger \psi_R$
$\mathbf{1_c}$	$\psi_L^\dagger c \psi_R$
$\overline{\mathbf{1_c}}$	$\psi_L^\dagger \bar{c} \psi_R$
$\mathbf{1_d}$	$\psi_L^\dagger d \psi_R$
$\overline{\mathbf{1_d}}$	$\psi_L^\dagger \bar{d} \psi_R$
$\mathbf{1_{cd}}$	$\psi_L^\dagger cd \psi_R$
$\overline{\mathbf{1_{cd}}}$	$\psi_L^\dagger \bar{c}\bar{d} \psi_R$
$\mathbf{1_{c\bar{d}}}$	$\psi_L^\dagger c\bar{d} \psi_R$
$\overline{\mathbf{1_{c\bar{d}}}}$	$\psi_L^\dagger \bar{c} d \psi_R$

Table 3.3: Explicit expressions of the tensor decomposition of $\overline{\mathbf{3}} \times \mathbf{3}$

tensor product is $\mathbf{3} \times \overline{\mathbf{3}}$. So we do its canonical decomposition here. Let

$$\psi_L = \begin{pmatrix} \psi_{L1} \\ \psi_{L2} \\ \psi_{L3} \end{pmatrix}, \quad \psi_R = \begin{pmatrix} \psi_{R1} \\ \psi_{R2} \\ \psi_{R3} \end{pmatrix} \tag{3.33}$$

transform as $\mathbf{3}$s. The explicit expressions of the irreducible representations ($\mathbf{1}$, $\mathbf{1_c}$, $\overline{\mathbf{1_c}}$, $\mathbf{1_d}$, $\overline{\mathbf{1_d}}$, $\mathbf{1_{cd}}$, $\overline{\mathbf{1_{cd}}}$, $\mathbf{1_{c\bar{d}}}$, $\overline{\mathbf{1_{c\bar{d}}}}$) contained in the direct product $\overline{\mathbf{3}} \times \mathbf{3}$ of $\psi_L^\dagger(\overline{\mathbf{3}})$ and $\psi_R(\mathbf{3})$ are given in Table 3.3.

3.3 The Flavon Model

Flavons have been postulated [57, 58, 59, 60] as a means of explaining the observed patterns in fermion masses and mixing. In model building, flavour symmetries are mostly implemented using scalar fields called the flavons. The simplest case involves promoting the Yukawa couplings to gauge singlet scalars. The flavons are usually invariant under the gauge group of the underlying theory either Standard Model or GUT and they transform only under the flavour symmetry group. Since their masses are typically much larger than the electroweak scale, they introduce a further energy scale in the model. The mass matrices arise from the spontaneous breaking of the flavour symmetry by means of the VEVs of the flavon fields, the VEVs define the symmetry breaking energy scale. The mass terms appearing at the electroweak

scale are obtained from the terms in the flavon model which couple the flavons with the fermions. We also have the flavon potential terms involving the self couplings among the flavons. A discrete flavour symmetry leads to a discrete set of values for the flavon fields corresponding to the minima of the potential. When the field acquires one of these values, the symmetry is spontaneously broken. It should be noted that in the case of a continuous symmetry, spontaneous symmetry breaking produces Goldstone bosons. Discrete flavour symmetries avoid this problem. Flavon models often involve dimension-5 and higher operators. These are non-renormalisable and hence are regularised using the cut-off scale. The lowest dimensional terms correspond to the mass matrices at the lowest order. Higher dimensional terms produce higher order corrections to the mass matrices.

3.3.1 Circulant-plus-diagonal Yukawa matrix using $C_3 \times C_3 \rtimes C_3$ flavons

A circulant-plus-diagonal mass matrix can be obtained by postulating three flavons ϕ_ι, ϕ_c and ϕ_d that transform as a $\mathbf{1}$, $\mathbf{1_c}$ and $\mathbf{1_d}$ respectively. These flavons are scalar fields and are neutral under the Standard Model gauge group. As shown in Table 3.3, we construct terms that transform as $\mathbf{1}$, $\mathbf{1_c}$ and $\mathbf{1_d}$ using the fermions $\psi_L^\dagger$ and ψ_R:

$$\mathbf{1} \equiv \psi_{L1}^\dagger \psi_{R1} + \psi_{L2}^\dagger \psi_{R2} + \psi_{L3}^\dagger \psi_{R3} \tag{3.34a}$$

$$\mathbf{1_c} \equiv \psi_{L1}^\dagger \psi_{R3} + \psi_{L2}^\dagger \psi_{R1} + \psi_{L3}^\dagger \psi_{R2} \tag{3.34b}$$

$$\mathbf{1_d} \equiv \psi_{L1}^\dagger \psi_{R1} + \bar{\omega} \psi_{L2}^\dagger \psi_{R2} + \omega \psi_{L3}^\dagger \psi_{R3}. \tag{3.34c}$$

Using the flavons and the fermions we construct the following invariant:

$$\begin{aligned}
&\phi_\iota(\psi_{L1}^\dagger \psi_{R1} + \psi_{L2}^\dagger \psi_{R2} + \psi_{L3}^\dagger \psi_{R3}) + \\
&\phi_d^*(\psi_{L1}^\dagger \psi_{R1} + \bar{\omega} \psi_{L2}^\dagger \psi_{R2} + \omega \psi_{L3}^\dagger \psi_{R3}) + \phi_d(\psi_{L1}^\dagger \psi_{R1} + \bar{\omega} \psi_{L2}^\dagger \psi_{R2} + \omega \psi_{L3}^\dagger \psi_{R3})^* + \\
&\phi_c^*(\psi_{L1}^\dagger \psi_{R3} + \psi_{L2}^\dagger \psi_{R1} + \psi_{L3}^\dagger \psi_{R2}) + \phi_c(\psi_{L1}^\dagger \psi_{R3} + \psi_{L2}^\dagger \psi_{R1} + \psi_{L3}^\dagger \psi_{R2})^*.
\end{aligned} \tag{3.35}$$

The above expression takes the matrix form

$$\begin{pmatrix} \psi_{L1} \\ \psi_{L2} \\ \psi_{L3} \end{pmatrix}^\dagger \begin{pmatrix} \phi_\iota + \phi_d + \phi_d^* & \phi_c & \phi_c^* \\ \phi_c^* & \phi_\iota + \omega\phi_d + \bar{\omega}\phi_d^* & \phi_c \\ \phi_c & \phi_c^* & \phi_\iota + \bar{\omega}\phi_d + \omega\phi_d^* \end{pmatrix} \begin{pmatrix} \psi_{R1} \\ \psi_{R2} \\ \psi_{R3} \end{pmatrix} \tag{3.36}$$

which is indeed a circulant-plus-diagonal matrix. For future reference it is convenient to express the above matrix in terms of the phases of the flavons θ_c and θ_d:

$$\phi_\iota I + \begin{pmatrix} 2|\phi_d|\mathrm{Cos}(\theta_d) & |\phi_c|e^{i\theta_c} & |\phi_c|e^{-i\theta_c} \\ |\phi_c|e^{-i\theta_c} & 2|\phi_d|\mathrm{Cos}(\frac{2\pi}{3}+\theta_d) & |\phi_c|e^{i\theta_c} \\ |\phi_c|e^{i\theta_c} & |\phi_c|e^{-i\theta_c} & 2|\phi_d|\mathrm{Cos}(\frac{-2\pi}{3}+\theta_d) \end{pmatrix}. \tag{3.37}$$

We note that the form of Eq. (3.37) corresponds to the postulated form of Yukawa matrices, Eq. (3.4).

3.3.2 The Flavon Model in the Standard Model framework

Here the model is constructed in the Standard Model framework, even though it can be extended to a beyond Standard Model theory. The mass term for the charged leptons is given by

$$\begin{aligned} &\frac{y_{l\iota}\phi_{l\iota}}{\Lambda}(L_e^\dagger e_R + L_\mu^\dagger \mu_R + L_\tau^\dagger \tau_R)H + \\ &\frac{y_{lc}\phi_{lc}^*}{\Lambda}(L_e^\dagger \tau_R + L_\mu^\dagger e_R + L_\tau^\dagger \mu_R)H + \frac{y_{lc}\phi_{lc}}{\Lambda}H^\dagger(\tau_R^\dagger L_e + e_R^\dagger L_\mu + \mu_R^\dagger L_\tau) + \\ &\frac{y_{ld}\phi_{ld}^*}{\Lambda}(L_e^\dagger e_R + \bar{\omega}L_\mu^\dagger \mu_R + \omega L_\tau^\dagger \tau_R)H + \frac{y_{ld}\phi_{ld}}{\Lambda}H^\dagger(e_R^\dagger L_e + \omega\mu_R^\dagger L_\mu + \bar{\omega}\tau_R^\dagger L_\tau). \end{aligned} \tag{3.38}$$

For the neutrinos we assume a similar Dirac mass term:

$$\begin{aligned} &\frac{y_{\nu\iota}\phi_{\nu\iota}}{\Lambda}(L_e^\dagger \nu_{eR} + L_\mu^\dagger \nu_{\mu R} + L_\tau^\dagger \nu_{\tau R})\epsilon H^* + \\ &\frac{y_{\nu c}\phi_{\nu c}^*}{\Lambda}(L_e^\dagger \nu_{\tau R} + L_\mu^\dagger \nu_{eR} + L_\tau^\dagger \nu_{\mu R})\epsilon H^* + \frac{y_{\nu c}\phi_{\nu c}}{\Lambda}H^T\epsilon(\nu_{\tau R}^\dagger L_e + \nu_{eR}^\dagger L_\mu + \nu_{\mu R}^\dagger L_\tau) + \\ &\frac{y_{\nu d}\phi_{\nu d}^*}{\Lambda}(L_e^\dagger \nu_{eR} + \bar{\omega}L_\mu^\dagger \nu_{\mu R} + \omega L_\tau^\dagger \nu_{\tau R})\epsilon H^* + \frac{y_{\nu d}\phi_{\nu d}}{\Lambda}H^T\epsilon(\nu_{eR}^\dagger L_e + \omega\nu_{\mu R}^\dagger L_\mu + \bar{\omega}\nu_{\tau R}^\dagger L_\tau). \end{aligned} \tag{3.39}$$

Here L is the left handed lepton doublet, H is the Standard Model Higgs doublet with ϵ being the antisymmetric matrix $\begin{pmatrix} 0 & 1 \\ -1 & 0 \end{pmatrix}$, Λ is the cut-off scale, $\phi_{l\iota}, \phi_{\nu\iota}$, $\phi_{lc}, \phi_{\nu c}$ and $\phi_{ld}, \phi_{\nu d}$ are the invariant, the circulant and the diagonal flavons for the charged leptons and the neutrinos respectively and $y_{l\iota}$, y_{ld}, y_{lc}, $y_{\nu\iota}$, $y_{\nu d}$, $y_{\nu c}$ are real constants.

It is well known that the Higgs gets a vacuum expectation value $\begin{pmatrix} 0 \\ h_o \end{pmatrix}$ at the weak scale. Similarly through spontaneous symmetry breaking at a higher en-

ergy scale, the flavons also acquire vacuum expectation values. For the flavon ϕ_ι, extremising a potential of the form $\phi_\iota^4 - 2v^2\phi_\iota^2$ will provide a non-zero vacuum expectation value $\pm v$. For the flavons ϕ_c and ϕ_d suppose we write potentials of the form $(\phi^*\phi)^2 - 2v^2\phi^*\phi$. They are the "Mexican hat" potentials invariant under $U(1)$ transformation $\phi \to e^{i\alpha}\phi$ and they give a VEV with $|\phi| = v$. Such a potential is not very interesting to us. What we need is something which is C_3-invariant only. So we may introduce the following potential:

$$\frac{1}{\Lambda^2}\left|\phi^3 - v^3\right|^2 \tag{3.40}$$

which is obviously invariant under the transformation $\phi \to e^{i\frac{2n\pi}{3}}\phi$, n being an integer. This potential is shown in Figure 3.1. There are three minima, corresponding to ϕ equal to v , $ve^{i\frac{2\pi}{3}}$ and $ve^{i\frac{4\pi}{3}}$. Here we have assumed the parameter v to be real.

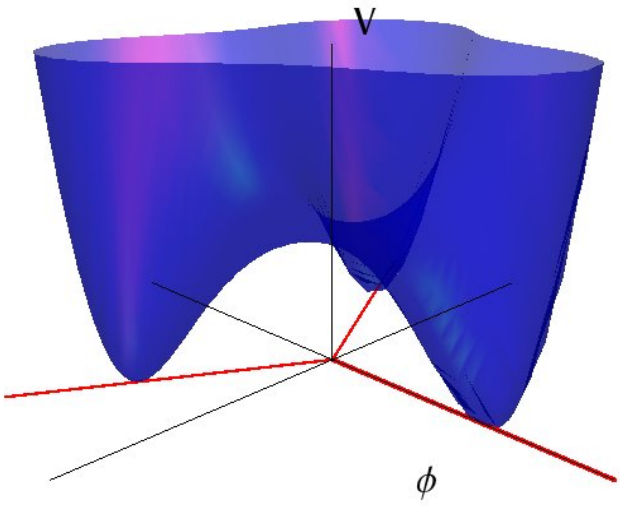

Figure 3.1: C_3 invariant potential

Through spontaneous symmetry breaking, each of the complex flavons (ϕ_{lc}, $\phi_{\nu c}$, ϕ_{ld}, $\phi_{\nu d}$) acquire one of the above VEVs and they along with the VEVs of invariant flavons ($\phi_{l\iota}$, $\phi_{\nu\iota}$) generate the fermion Yukawa matrices. For the charged leptons we get the following mass matrix:

$$Y_l = \mathbf{y}_{l\iota} I + \begin{pmatrix} 2\mathbf{y}_{ld}\cos\left(\frac{2n_{ld}\pi}{3}\right) & \mathbf{y}_{lc}e^{i\frac{2n_{lc}\pi}{3}} & \mathbf{y}_{lc}e^{-i\frac{2n_{lc}\pi}{3}} \\ \mathbf{y}_{lc}e^{-i\frac{2n_{lc}\pi}{3}} & 2\mathbf{y}_{ld}\cos\left(\frac{2(n_{ld}+1)\pi}{3}\right) & \mathbf{y}_{lc}e^{i\frac{2n_{lc}\pi}{3}} \\ \mathbf{y}_{lc}e^{i\frac{2n_{lc}\pi}{3}} & \mathbf{y}_{lc}e^{-i\frac{2n_{lc}\pi}{3}} & 2\mathbf{y}_{ld}\cos\left(\frac{2(n_{ld}-1)\pi}{3}\right) \end{pmatrix} \tag{3.41}$$

where n_{lc} and n_{ld} are integers and $\mathbf{y}_{l\iota} = y_{l\iota}\langle\phi_{l\iota}\rangle/\Lambda$, $\mathbf{y}_{lc} = y_{lc}|\langle\phi_{lc}\rangle|/\Lambda$, $\mathbf{y}_{ld} = y_{ld}|\langle\phi_{ld}\rangle|/\Lambda$ with $\langle\rangle$ representing a VEV.

The above equation is in the form of Eq. (3.7) as expected. But to realise the condition specified in Eq. (3.8) we require the phases appearing in the Yukawa matrix, Eq. (3.41), to be small, unlike multiples of $\frac{2\pi}{3}$ generated above. Therefore we allow the VEVs to acquire a small non-trivial phase away from $\frac{2n\pi}{3}$ by slightly perturbing the previous potential to the following form:

$$\frac{1}{\Lambda^2}\left|\phi^3 - \left(ve^{i\alpha}\right)^3\right|^2 \tag{3.42}$$

where α is the small phase. The resulting potential is shown in Figure 3.2. Here we have made a simplifying assumption that the expression for the potential, Eq. (3.42), is the same for all complex flavons, i.e. the small phase α is common to all the flavons. This decreases the number of free parameters in the model and makes it predictive.

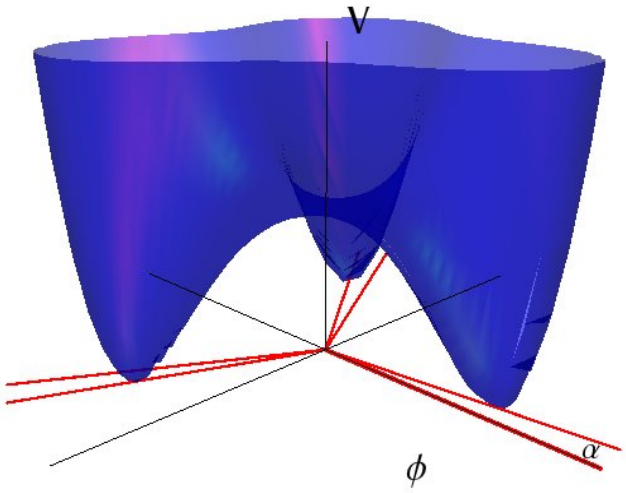

Figure 3.2: C_3 invariant potential perturbed by a small phase α

With this modification of having a phase $\frac{2n\pi}{3} + \alpha$ for the flavon VEVs, we obtain the Yukawa matrices for the charged leptons:

$$Y_l = \mathbf{y}_{l\iota}I + \begin{pmatrix} 2\mathbf{y}_{ld}\cos\left(\frac{2n_{ld}\pi}{3}+\alpha\right) & \mathbf{y}_{lc}e^{i\left(\frac{2n_{lc}\pi}{3}+\alpha\right)} & \mathbf{y}_{lc}e^{-i\left(\frac{2n_{lc}\pi}{3}+\alpha\right)} \\ \mathbf{y}_{lc}e^{-i\left(\frac{2n_{lc}\pi}{3}+\alpha\right)} & 2\mathbf{y}_{ld}\cos\left(\frac{2(n_{ld}+1)\pi}{3}+\alpha\right) & \mathbf{y}_{lc}e^{i\left(\frac{2n_{lc}\pi}{3}+\alpha\right)} \\ \mathbf{y}_{lc}e^{i\left(\frac{2n_{lc}\pi}{3}+\alpha\right)} & \mathbf{y}_{lc}e^{-i\left(\frac{2n_{lc}\pi}{3}+\alpha\right)} & 2\mathbf{y}_{ld}\cos\left(\frac{2(n_{ld}-1)\pi}{3}+\alpha\right) \end{pmatrix} \tag{3.43}$$

and for the neutrinos:

$$Y_\nu = \mathbf{y}_{\nu\iota} I + \begin{pmatrix} 2\mathbf{y}_{\nu d}\cos\left(\frac{2n_{\nu d}\pi}{3}+\alpha\right) & \mathbf{y}_{\nu c}e^{i\left(\frac{2n_{\nu c}\pi}{3}+\alpha\right)} & \mathbf{y}_{\nu c}e^{-i\left(\frac{2n_{\nu c}\pi}{3}+\alpha\right)} \\ \mathbf{y}_{\nu c}e^{-i\left(\frac{2n_{\nu c}\pi}{3}+\alpha\right)} & 2\mathbf{y}_{\nu d}\cos\left(\frac{2(n_{\nu d}+1)\pi}{3}+\alpha\right) & \mathbf{y}_{\nu c}e^{i\left(\frac{2n_{\nu c}\pi}{3}+\alpha\right)} \\ \mathbf{y}_{\nu c}e^{i\left(\frac{2n_{\nu c}\pi}{3}+\alpha\right)} & \mathbf{y}_{\nu c}e^{-i\left(\frac{2n_{\nu c}\pi}{3}+\alpha\right)} & 2\mathbf{y}_{\nu d}\cos\left(\frac{2(n_{\nu d}-1)\pi}{3}+\alpha\right) \end{pmatrix}. \tag{3.44}$$

A small but non-zero α, along with the integer $n_{lc} = 0$ ensures the conditions, Eq. (3.8), on the parameters of Y_l. For the neutrino case, the first inequality of Eq. (3.10) is taken care of by the smallness of α, since $\alpha \to 0$ makes two diagonal elements equal. Clearly the extreme limit

$$\frac{\mathbf{y}_{ld}}{\mathbf{y}_{lc}} << \alpha << \frac{\mathbf{y}_{\nu c}}{\mathbf{y}_{\nu d}} << 1 \tag{3.45}$$

leads to TBM, with deviations from this mixing pattern calculable, in principle, in terms of these "small" parameters. Overall, the model has 7 independent parameters, $\mathbf{y}_{l\iota}, \mathbf{y}_{lc}, \mathbf{y}_{ld}, \mathbf{y}_{\nu\iota}, \mathbf{y}_{\nu c}, \mathbf{y}_{\nu d}$ and α, which determine 10 observables. This constrains the parameter space of the masses and the mixing observables. In the next section we fit these parameters to the 8 currently-measured experimental observables (three charged-lepton masses, two neutrino mass-squared differences and three leptonic mixing angles) and make predictions for those yet to be measured (the lightest neutrino mass and the CP phase).

3.4 Fitting the model with experimental data

Rather than making a fit numerically through brute force, we first approach the problem analytically and use a parametrisation that separates the masses from the mixing observables. This makes the final numerical analysis easy and also helps to get a better understanding of the parameter space.

3.4.1 Parametrising circulant-plus-diagonal matrices

In general a matrix which is the sum of circulant and diagonal parts, Eq. (3.37), is proportional to

$$I + \begin{pmatrix} 2k_d\cos(\theta_d) & k_c e^{i\theta_c} & k_c e^{-i\theta_c} \\ k_c e^{-i\theta_c} & 2k_d\cos(\frac{2\pi}{3}+\theta_d) & k_c e^{i\theta_c} \\ k_c e^{i\theta_c} & k_c e^{-i\theta_c} & 2k_d\cos(\frac{-2\pi}{3}\theta_d) \end{pmatrix}. \tag{3.46}$$

The characteristic equation for the above matrix is

$$\lambda^3 - 3\lambda^2 + 3(1 - k_c^2 - k_d^2)\lambda + 2(1 - k_c^3 \cos 3\theta_c - k_d^3 \cos 3\theta_d) - 3(1 - k_c^2 - k_d^2) = 0. \quad (3.47)$$

Let us rewrite Eq. (3.47) in the following way

$$\lambda^3 - 3\lambda^2 + 3(1 - x^2)\lambda + 2(1 - x^3 y) - 3(1 - x^2) = 0 \quad (3.48)$$

where

$$x^2 = k_c^2 + k_d^2 \quad (3.49a)$$
$$x^3 y = k_c^3 \cos 3\theta_c + k_d^3 \cos 3\theta_d. \quad (3.49b)$$

Eliminating x from Eq. (3.49b) using Eq. (3.49a) we get

$$y = (\cos\zeta)^3 \cos 3\theta_c + (\sin\zeta)^3 \cos 3\theta_d \quad (3.50)$$

where ζ is defined using the following equations:

$$k_c = x \cos\zeta \quad (3.51a)$$
$$k_d = x \sin\zeta. \quad (3.51b)$$

Let the eigenvalues of matrix (3.46) be e_1, e_2 and e_3. We have

$$e_1 + e_2 + e_3 = 3 \quad (3.52a)$$
$$e_1 e_2 + e_2 e_3 + e_3 e_1 = 3(1 - x^2) \quad (3.52b)$$
$$e_1 e_2 e_3 = 3(1 - x^2) - 2(1 - x^3 y). \quad (3.52c)$$

We define two flavour symmetric quantities r_1 and r_2:

$$r_1 = \frac{e_1 e_2 + e_2 e_3 + e_3 e_1}{(e_1 + e_2 + e_3)^2} \quad (3.53a)$$
$$r_2 = \frac{e_1 e_2 e_3}{(e_1 + e_2 + e_3)^3}. \quad (3.53b)$$

These dimensionless quantities “measure" the hierarchy of the eigenvalues or the masses.

The parameters x and y in terms of r_1 and r_2 are given by

$$x^2 = 1 - 3r_1 \tag{3.54a}$$

$$y^2 = \frac{(2 - 9r_1 + 27r_2)^2}{4(1 - 3r_1)^3}. \tag{3.54b}$$

Thus x and y can be calculated if the fermion masses are experimentally known. Mixing information is contained in the variables θ_c, θ_d and ζ along with the constraint given through Eq. (3.50). This completes our discussion on the parametrisation of a circulant-plus-diagonal matrix.

3.4.2 Monte Carlo analysis

In the model both the charged-lepton and the neutrino mass matrices are circulant-plus-diagonal. Correspondingly we have two sets of variables and equations. Moreover θ_c and θ_d are α plus an integer multiple of $\frac{2\pi}{3}$ for both charged leptons as well as neutrinos. Thus we end up with the following set of equations:

Charged Leptons:

$$r_{l1} = \frac{m_e m_\mu + m_\mu m_\tau + m_\tau m_e}{(m_e + m_\mu + m_\tau)^2} \tag{3.55a}$$

$$r_{l2} = \frac{m_e m_\mu m_\tau}{(m_e + m_\mu + m_\tau)^3} \tag{3.55b}$$

$$x_l^2 = 1 - 3r_{l1} \tag{3.55c}$$

$$y_l^2 = \frac{(2 - 9r_{l1} + 27r_{l2})^2}{4(1 - 3r_{l1})^3} \tag{3.55d}$$

$$y_l = \left(\cos^3\zeta_l + \sin^3\zeta_l\right)\cos 3\alpha \tag{3.55e}$$

Neutrinos:

$$r_{\nu 1} = \frac{m_1 m_2 + m_2 m_3 + m_3 m_1}{(m_1 + m_2 + m_3)^2} \tag{3.56a}$$

$$r_{\nu 2} = \frac{m_1 m_2 m_3}{(m_1 + m_2 + m_3)^3} \tag{3.56b}$$

$$x_\nu^2 = 1 - 3r_{\nu 1} \tag{3.56c}$$

$$y_\nu^2 = \frac{(2 - 9r_{\nu 1} + 27r_{\nu 2})^2}{4(1 - 3r_{\nu 1})^3} \tag{3.56d}$$

$$y_\nu = \left(\cos^3\zeta_\nu + \sin^3\zeta_\nu\right)\cos 3\alpha \tag{3.56e}$$

where m_1, m_2, m_3 are the masses of the neutrino mass eigenstates.

We do a Monte Carlo analysis with two random variables α and ζ_ν. Let us first consider Eqs. (3.56). Using Eq. (3.56e) and the random variables α and ζ_ν, we calculate y_ν. Squared differences of neutrino masses are known experimentally, Table 3.4. We use this information and the previously calculated value of y_ν along with Eqs. (3.56a, 3.56b, 3.56d) to solve for the unknown neutrino mass offset (or equivalently the lightest neutrino mass). Finally we calculate x_ν and the neutrino mass matrix. Now consider the Eqs. (3.55). Masses of charged leptons are known, Table 3.4. So we can calculate the values of x_l and y_l using Eqs. (3.55a - 3.55d). This value of y_l and the random variable α are used in Eq. (3.55e) to calculate ζ_l. Thus we generate the charged lepton mass matrix also.

Lepton	Mass
m_e	0.4959MeV
m_μ	104.7MeV
m_τ	1780MeV
$m_2^2 - m_1^2$	91meV^2
$\lvert m_3^2 - m_2^2 \rvert$	2900meV^2

Table 3.4: Masses of leptons renormalised at 1 TeV [28]. We need to use the values renormalised at the unknown scale Λ. But in the previous chapter we have seen that even though the masses vary considerably through renormalisation evolution, the mass ratios remain more or less constant. Since our fit depends only on the mass ratios, it will remain valid not just at 1 TeV, but even to energy scales a few orders of magnitude higher.

Observable	Best fit $\pm 1\sigma$
$\sin^2\theta_{12}$	$0.312^{+0.017}_{-0.015}$
$\sin^2\theta_{23}$	0.51 ± 0.06 (normal hierarchy)
	0.52 ± 0.06 (inverted hierarchy)

Table 3.5: Experimental values of the large neutrino mixing angles θ_{12} and θ_{23} along with 1σ errors [61].

In the next step we compute the PMNS matrix from the mass matrices. Experimental neutrino oscillation data for large mixing angles with 1σ errors is given in Table 3.5. For the small mixing angle θ_{13}, we use the weighted average of the Daya Bay and RENO observations:

$$\sin^2\theta_{13} = 0.025^{+0.003}_{-0.003}. \tag{3.57}$$

The values of $\sin^2\theta_{12}$, $\sin^2\theta_{23}$ and $\sin^2\theta_{13}$ are extracted from the computed PMNS matrix and they are fitted with the experimental data using a χ^2 goodness of fit variable:

$$\chi^2 = \sum_{\theta=\theta_{12},\theta_{23},\theta_{13}} \left(\frac{(\sin^2\theta)_{\text{model}} - (\sin^2\theta)_{\text{expt}}}{\sigma_{\text{expt}}} \right)^2 \tag{3.58}$$

where σ_{expt} is the experimental error on $\sin^2\theta$.

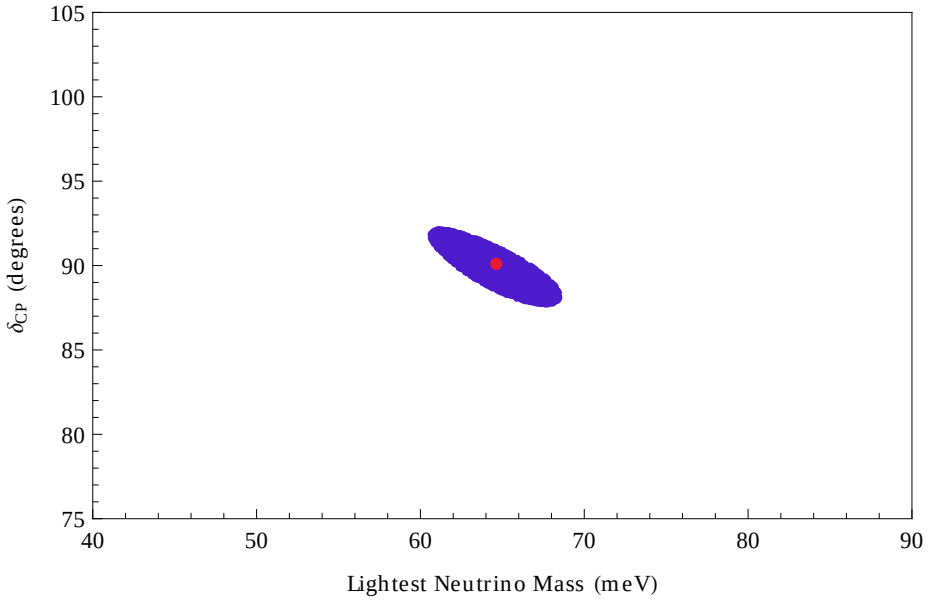

Figure 3.3: Predicted values of δ_{CP} vs. the mass of the lightest neutrino mass eigenstate. The shaded region denotes $\Delta\chi^2 \equiv (\chi^2 - \chi^2_{\text{min}}) \leq 1$, and the best fit is indicated by the red dot.

As stated earlier the model has 7 parameters while there are 10 masses and mixing observables. Two of these observables, the overall neutrino mass offset and the CP-violating phase δ_{CP} have not been measured yet. So the model is used to predict the values of these unknown observables. The remaining 8 observables are fitted with the 7 parameters of the model. It is obvious that the fit is over-constrained

by one degree of freedom. The earlier discussion described how we make this fit: first separate out and fit the mass observables, then fit the 3 mixing observables with two random variables of the model, α, ζ_ν, using Monte Carlo analysis and χ^2 goodness of fit method. The predictions made using this analysis are given in Figure 3.3. We note that our numerical analysis does not give an acceptable χ^2 for any normal hierarchy, whereby an inverted hierarchy ($(m_3^2 - m_2^2) < 0$) can be said to be a prediction of our model, given the measured observables. The best fit gives a lightest neutrino mass $m_3 \simeq 64.6$ meV ($m_1 \simeq 83.6$ meV and $m_2 \simeq 84.1$ meV).

The best fit is given (at high precision) by $\mathbf{y}_{l\iota}$=628.31, $\mathbf{y}_{lc}$=576.43, $\mathbf{y}_{ld}$=9.30, $\mathbf{y}_{\nu\iota}$=21.36, $\mathbf{y}_{\nu c}$=7.884, $\mathbf{y}_{\nu d} = -52.44$, $\alpha = -2.944°$, along with the integers n_{lc}, n_{ld}, $n_{\nu c}$, $n_{\nu d}$ equal to $0, 1, 1, -1$ respectively. The values of $\mathbf{y}_{l\iota}$, $\mathbf{y}_{lc}$, $\mathbf{y}_{ld}$ are in units of MeV/h_o and $\mathbf{y}_{\nu\iota}$, $\mathbf{y}_{\nu c}$, $\mathbf{y}_{\nu d}$ are in meV/h_o where h_o is the Standard Model Higgs VEV. After diagonalisation, the charged lepton mass matrix gives the electron, muon and tau lepton masses given in Table 3.4. The diagonalisation of the neutrino mass matrix, $U_\nu Y_\nu U_\nu^\dagger$, gives

$$\begin{pmatrix} 83.59 & 0 & 0 \\ 0 & -84.13 & 0 \\ 0 & 0 & 64.63 \end{pmatrix}. \tag{3.59}$$

Note that the negative sign of second eigenvalue can be removed by absorbing it into the unobservable right diagonalising matrix. i.e. $\nu_{\text{masses}} = U_\nu Y_\nu S U_\nu^\dagger$, where S is a diagonal matrix with entries 1,-1,1. The neutrino masses $m_1 = 83.59$, $m_2 = 84.13$ and $m_3 = 64.63$ agree with the mass-squared differences given in Table 3.4.

The moduli-squared of the elements of the PMNS matrix corresponding to the best fit is given below:

$$\text{PMNS Matrix} \equiv \begin{pmatrix} 0.670 & 0.305 & 0.025 \\ 0.161 & 0.339 & 0.500 \\ 0.169 & 0.356 & 0.475 \end{pmatrix}. \tag{3.60}$$

This gives $\sin^2\theta_{12} = 0.313$, $\sin^2\theta_{23} = 0.513$, $\sin^2\theta_{13} = 0.025$ as expected. We also get CP-violating phase, $\delta_{CP} = 90.1°$ with the Jarlskog CP-violating invariant, $J = 0.0357$ (to be compared with its theoretical maximum value, $J_{\max} \simeq 0.0962$).

Approximate analytic predictions can be derived as series expansions in the "small" parameters of our model, $\beta_l \equiv \frac{\mathbf{y}_{ld}}{\mathbf{y}_{lc}} \simeq 0.016$, $\alpha \simeq -0.051$ and $\beta_\nu \equiv \frac{\mathbf{y}_{\nu c}}{\mathbf{y}_{\nu d}} \simeq -0.15$. For example, starting from the expression:

$$J = \frac{i\text{Det}[M_l, M_\nu]}{2\text{Discr}_l \text{Discr}_\nu} \tag{3.61}$$

where M_l and M_ν are the leptonic mass matrices, $\text{Discr}_l = (m_e - m_\mu)(m_\mu - m_\tau)(m_\tau - m_e)$ and $\text{Discr}_\nu = (m_1 - m_2)(m_2 - m_3)(m_3 - m_1)$, we find

$$J \approx \frac{\alpha}{6\beta_\nu}\left(1 + \frac{\beta_l\beta_\nu}{4\alpha^2} - \frac{3\alpha^2}{2\beta_\nu^2} + \frac{\beta_\nu}{3} + \frac{27\alpha^4}{8\beta_\nu^4} - \frac{3\beta_l}{8\beta_\nu}\ldots\right) = 0.0360 \tag{3.62}$$

in close agreement with our numerical results above.

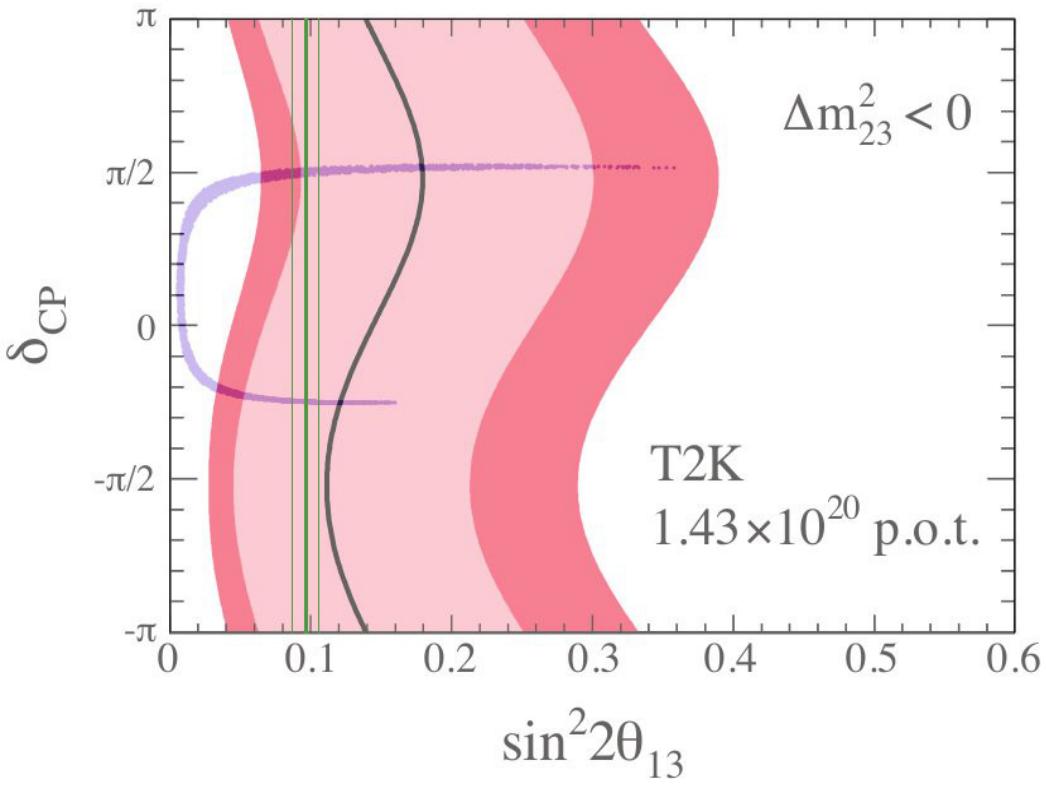

Figure 3.4: Blue region denotes the correlation between θ_{13} and δ_{CP} predicted by the model with $\Delta\chi^2 \leq 1$. The plot is superimposed with the T2K figure [62] for 68% and 90% C.L. regions obtained experimentally. For large θ_{13} the model predicts $\delta_{CP} \approx \frac{\pi}{2}$. Note that in the lower blue region we have $\delta_{CP} \approx -\frac{\pi}{4}$ consistent with the experiment, but this region vanishes for $\Delta\chi^2 \leq 0.3$. The best fit lies in the upper blue region and we have analysed only this solution. The vertical lines represent the latest world average value for θ_{13} with 1σ error range.

Even though the fit gives a close-to-maximal CP phase, we note that the large CP phase is not a generic prediction arising from the structure of the model itself. Rather, the value of δ_{CP} depends on several of the parameters and these are

constrained here by the measured values of other observables. In fact δ_{CP} is strongly correlated with θ_{13} and comes out close to $\frac{\pi}{2}$ for large values of θ_{13} as indicated by recent experiments. Figure 3.4 illustrates these points. The model constrains the observable to the blue region which corresponds to $\Delta\chi^2 \equiv (\chi^2 - \chi^2_{\rm min}) \leq 1$ (but unlike in the previous analysis here we keep θ_{13} as an unknown variable, i.e. for calculating χ^2 we use only θ_{12} and θ_{23} in Eq. (3.58)). A value for δ_{CP} close to $\frac{\pi}{2}$ offers the potential for large observable CP-violating asymmetries in future neutrino oscillation experiments, with Jarlskog's CP-violating invariant, J, assuming close to 40% of its theoretical maximum value.

3.5 Quark masses and the CKM matrix

Quark masses are strongly hierarchical, especially for the charge $\frac{2}{3}$ quarks, given the very large mass of the top quark. From Eq. (3.54b) it is clear that y goes to the limiting value 1 when r_1 and r_2 tend to 0, i.e. when one of the quark masses becomes very large. A value of y very close to 1, severely restricts the allowed range of ζ, θ_c and θ_d as can be seen from Eq. (3.50). Then ζ tends to $\frac{n\pi}{2}$ and θ_c or θ_d tends to $\frac{n\pi}{3}$. We did a numerical analysis and found that unfortunately the mixing predicted under the above mentioned limits can not fit the experimental CKM values. The problem lies with the angle θ_{23} which turns out to be only about a third of the experimental value for our best fit. Nevertheless we are able to get a large enough value for the Cabibbo angle, θ_{12}, and also a very small value for the angle θ_{13} as required.

We have shown earlier, Eqs. (3.9, 3.10), that a mass matrix with a large diagonal component and a small circulant component can be used to generate a nearly 2×2-maximal diagonalising matrix. The strategy adopted for the quarks is to assume this form of mass matrix for both the up-type and the down-type quarks. So we get nearly 2×2-maximal unitary contributions from both the up and the down sectors, i.e U_u and U_d are nearly 2×2-maximal. When we take their product to calculate the CKM matrix, $U_{CKM} = U_u U_d^\dagger$, they nearly cancel each other to give a mixing matrix close to the identity. But the individual matrices U_u and U_d are not exactly 2×2-maximal, therefore their cancellations will not be exact. This non-cancellation can be adjusted to give a realistic value for the Cabibbo angle, θ_{12}. However, in U_u and U_d, the mixing contribution coming from outside the 2×2 part is very small by construction. So it becomes impossible to get reasonably large θ_{23}, which essentially vanishes in the limit where U_u and U_d becomes 2×2 mixing matrices.

Chapter 4

Non-zero θ_{13}: Derivation of the "Simplest" Texture from the Discrete Symmetry S_4 and a Model for Majorana Neutrinos

4.1 Introduction

Lepton mixing is characterised by two large mixing angles: $\theta_{12} \simeq 35^\circ$, $\theta_{23} \simeq 45^\circ$, and one small angle: θ_{13}. For several years, the data on neutrino oscillations were compatible with $\theta_{13} = 0$, and the data together were approximated by the tribimaximal (TBM) mixing ansatz, proposed in 2002 [50]. TBM has been used as a starting point for model building. In this ansatz the mixing matrix has three symmetries. The first one is the μ-τ symmetry in which the moduli-squared values of the μ and τ rows are equal. Besides the μ-τ symmetry the second column is democratic, meaning the moduli-squared of the second column elements are equal which also implies that they are 1/3 each due to unitarity. The Tribimaximal mixing also has θ_{13} equal to zero which leaves CP-symmetry conserved. In other words μ-τ symmetry, democracy for the second column and CP conservation uniquely imply Tribimaximal mixing.

The Daya Bay Reactor Neutrino Experiment [23] has recently measured the value for the mixing angle θ_{13}: $\sin^2 2\theta_{13} = 0.092 \pm 0.016\,(\text{stat.}) \pm 0.005\,(\text{syst.})$ and has confirmed that θ_{13} is non-zero. Later the RENO Experiment [24] also made a compatible measurement, $\sin^2 2\theta_{13} = 0.113 \pm 0.013\,(\text{stat.}) \pm 0.019\,(\text{syst.})$. A large number of models based on discrete symmetries have been proposed to reproduce Tribimaximal mixing. It is possible to generate non-zero θ_{13} by introducing higher

order corrections. But in generic cases, the deviations produced should be of the same order for all the mixing angles [63]. Since the experimentally allowed deviation of θ_{12} from $\sin^2\theta_{12} = 1/3$ is small, it is rather difficult to generate a much larger correction to θ_{13} alone as observed in the recent reactor experiments.

A generalisation of Tribimaximal mixing in which only the conditions of μ-τ symmetry and democracy are imposed while the $\theta_{13} = 0$ condition is relaxed is called Triχmaximal mixing [64]. The TχM mixing is given by

$$\mathrm{T}\chi\mathrm{M} = \begin{pmatrix} \sqrt{\frac{2}{3}}\cos\chi & \frac{1}{\sqrt{3}} & \sqrt{\frac{2}{3}}\sin\chi \\ -\frac{\cos\chi}{\sqrt{6}} \mp i\frac{\sin\chi}{\sqrt{2}} & \frac{1}{\sqrt{3}} & \pm i\frac{\cos\chi}{\sqrt{2}} - \frac{\sin\chi}{\sqrt{6}} \\ -\frac{\cos\chi}{\sqrt{6}} \pm i\frac{\sin\chi}{\sqrt{2}} & \frac{1}{\sqrt{3}} & \mp i\frac{\cos\chi}{\sqrt{2}} - \frac{\sin\chi}{\sqrt{6}} \end{pmatrix}. \tag{4.1}$$

The only free parameter in TχM mixing is the angle χ. In the basis where charged-lepton mass matrix is diagonal, a neutrino mass matrix which is hermitian and with μ-τ symmetry and democracy leads to this form of mixing. The general hermitian mass matrix that produces Triχmaximal (TχM) mixing is

$$M_H = a\begin{pmatrix} 1 & \pm ik & \mp ik \\ \mp ik & 0 & 1 \pm ik \\ \pm ik & 1 \mp ik & 0 \end{pmatrix} + b\begin{pmatrix} 0 & 1 & 1 \\ 1 & 0 & 1 \\ 1 & 1 & 0 \end{pmatrix} + c\begin{pmatrix} 1 & 0 & 0 \\ 0 & 1 & 0 \\ 0 & 0 & 1 \end{pmatrix} \tag{4.2}$$

where k, a, b, and c are real parameters.

In the above mentioned mass matrix, the parameter k uniquely determines the angle χ in Eq. (4.1). In fact, only the first term in Eq. (4.2) (with the coefficient a) is sufficient to generate TχM mixing. When diagonalised using the unitary matrix U (the TχM matrix [1]), this term generates three unique eigenvalues. The same matrix (U), when applied to the second term (with the coefficient b), generates two degenerate eigenvalues. The third term (cI), obviously, gives three degenerate eigenvalues. In other words

$$D = U\,M_H\,U^\dagger = a\begin{pmatrix} 1 & 0 & 0 \\ 0 & -\sqrt{1+3k^2} & 0 \\ 0 & 0 & \sqrt{1+3k^2} \end{pmatrix} + b\begin{pmatrix} 2 & 0 & 0 \\ 0 & -1 & 0 \\ 0 & 0 & -1 \end{pmatrix} + c\begin{pmatrix} 1 & 0 & 0 \\ 0 & 1 & 0 \\ 0 & 0 & 1 \end{pmatrix}. \tag{4.3}$$

It is straightforward to obtain the mixing angles in terms of the parameter χ

[1] where we have $|U| = |T\chi M^\dagger|$. The modulus indicates the extra degrees of freedom in the unitary matrix which can be taken out of the four parameter mixing matrix as diagonal phase matrices. These phases do not affect neutrino oscillations and so the phases are ignored here.

using Eq. (4.1). We have $|U| = |T\chi M^\dagger|$ and using the standard PDG parametrisation

$$|U^\dagger_{\tau 3}| = \sin\theta_{13}, \quad |U^\dagger_{\mu 3}| = \sin\theta_{23}\cos\theta_{13}, \quad |U^\dagger_{e2}| = \sin\theta_{12}\cos\theta_{13}. \tag{4.4}$$

we get

$$|U^\dagger_{e3}|^2 = \sin^2\theta_{13} = \frac{2}{3}\sin^2\chi \tag{4.5}$$

$$|U^\dagger_{e2}|^2 = \sin^2\theta_{12}\cos^2\theta_{13} = \frac{1}{3} \tag{4.6}$$

$$|U^\dagger_{\mu 3}|^2 = \sin^2\theta_{23}\cos^2\theta_{13} = \frac{\sin^2\chi}{6} + \frac{\cos^2\chi}{2} \implies \sin^2\theta_{23} = \frac{1}{2} \tag{4.7}$$

$$\delta_{CP} = \pm\frac{\pi}{2} \tag{4.8}$$

As mentioned earlier, the parameter k in the mass matrix, Eq. (4.2), uniquely determines χ. The relation is given by

$$\cos 2\chi = \frac{1}{\sqrt{1+3k^2}}. \tag{4.9}$$

A mass matrix arising from the Majorana mass term for the neutrinos should be complex symmetric. Therefore we would like to determine the general complex symmetric mass matrix that generates TχM mixing. One way to achieve this is to multiply the matrix M_H with the $2-3$ permutation matrix P to get the complex symmetric matrix

$$M_S = M_H\,P = a\begin{pmatrix} 1 & \mp ik & \pm ik \\ \mp ik & 1\pm ik & 0 \\ \pm ik & 0 & 1\mp ik \end{pmatrix} + b\begin{pmatrix} 0 & 1 & 1 \\ 1 & 1 & 0 \\ 1 & 0 & 1 \end{pmatrix} + c\begin{pmatrix} 1 & 0 & 0 \\ 0 & 0 & 1 \\ 0 & 1 & 0 \end{pmatrix} \tag{4.10}$$

where

$$P = \begin{pmatrix} 1 & 0 & 0 \\ 0 & 0 & 1 \\ 0 & 1 & 0 \end{pmatrix} \tag{4.11}$$

and a, b and c are complex in general. So we have

$$D = U\,M_H\,U^\dagger = U\,M_H\,P\,P\,U^\dagger = U\,M_S\,P\,U^\dagger. \tag{4.12}$$

A complex symmetric mass matrix can be diagonalised using a unitary matrix and its transpose,

$$U'\,M_S\,U'^T = |D| \tag{4.13}$$

where D is the same diagonal matrix given in Eq. (4.3). U' can be calculated as the diagonalising matrix for the hermitian matrix $M_S\, M_S^*$

$$U'\, M_S\, M_S^* U'^{\dagger} = D^2. \tag{4.14}$$

It can be shown that the unitary matrix U from Eq. (4.3) itself can be used to diagonalise the symmetric matrix M_S, but this leaves some extra phases on the eigenvalues. The relevant equations are

$$U\, M_S\, U^T = e^{-i\mathrm{Diag}(2\theta_1, 2\theta_2, 2\theta_3)} D \tag{4.15}$$

$$U' = e^{i\mathrm{Diag}(\theta_1, \theta_2, \theta_3)} U. \tag{4.16}$$

The phenomenon of neutrino oscillations is unaffected by the above mentioned phases. Therefore we do not discuss them any further.

The texture of Eq. (4.2), but with $b = 0$, was proposed in 2004 [65] (after having been speculated upon briefly already in 2002 [64]) to obtain a special case of TχM, known as "Simplest" mixing. The eigenvalues of the "simplest" mass matrix are given in terms of the parameters by the RHS of Eq. (4.3), with $b = 0$, and using Eqs. (4.5, 4.9) we get the very straightforward and exact relation between the reactor mixing angle and the eigenvalues (e_i):

$$\sin^2\theta_{13} = \frac{2\,(e_2 - e_1)}{3\,(e_3 - e_1)}. \tag{4.17}$$

In the original publication[65], this texture was proposed for $M_\nu^2 := M_\nu M_\nu^\dagger$, in which case the eigenvalues are the neutrino masses-squared, resulting in the very successful prediction:

$$\sin\theta_{13} = \sqrt{\frac{2}{3}\frac{\Delta m^2_{\mathrm{sol}}}{\Delta m^2_{\mathrm{atm}}}}, \tag{4.18}$$

$$\text{i.e. } \sin^2 2\theta_{13} = 0.086^{+0.003}_{-0.006} \quad \text{(Predicted in 2002/2004 [64, 65])} \tag{4.19}$$

$$\text{cf. } \sin^2 2\theta_{13} = 0.093 \pm 0.010 \quad \text{(Measured in 2012 [23, 24]).} \tag{4.20}$$

Motivated by the success of the "Simplest" mixing texture, here we propose a model based on the symmetric group of degree four (S_4). In order to do this, we must first make the following changes: we adopt the same mass matrix form, but this time for the mass matrix itself (as opposed to its hermitian square), and also assume a Majorana mass term (coupling between two heavy right-handed neutrinos). Thus,

we postulate a Majorana neutrino mass matrix of the following "Simplest" complex-symmetric form:

$$M_\nu(\text{Majorana}) = a \begin{pmatrix} 1 & \mp ik & \pm ik \\ \mp ik & 1 \pm ik & 0 \\ \pm ik & 0 & 1 \mp ik \end{pmatrix} + c \begin{pmatrix} 1 & 0 & 0 \\ 0 & 0 & 1 \\ 0 & 1 & 0 \end{pmatrix}. \tag{4.21}$$

In the following sections we construct such a Majorana mass matrix assuming symmetry under the S_4 group. The neutrino Dirac mass matrix (coupling between the left-handed and the right-handed neutrinos) is assumed to be proportional to the identity. We show that this model has a phenomenology compatible with experiment, and we use it to predict the masses of the light neutrinos. Light neutrinos acquire their masses through the see-saw mechanism. Because the Dirac mass matrix is proportional to the identity, the see-saw mechanism makes light neutrino masses inversely proportional to the eigenvalues of the "Simplest" Majorana matrix. In other words, using Eq. (4.17) we get

$$\sin^2\theta_{13} = \frac{2}{3} \frac{\left(\frac{1}{m_{\nu 2}} - \frac{1}{m_{\nu 1}}\right)}{\left(\frac{1}{m_{\nu 3}} - \frac{1}{m_{\nu 1}}\right)} \tag{4.22}$$

where $m_{\nu 1}$, $m_{\nu 2}$ and $m_{\nu 3}$ are the light neutrino masses.

4.2 The group S_4 and the μ-τ rotated basis

The group of permutation of four objects called the group S_4 [64] is the symmetry group of a cube, Figure 4.1 (and also of an octahedron). It can be constructed using the generators

$$a = \begin{pmatrix} -1 & 0 & 0 \\ 0 & 0 & 1 \\ 0 & 1 & 0 \end{pmatrix}, \tag{4.23a}$$

$$b = \begin{pmatrix} 0 & 1 & 0 \\ 0 & 0 & 1 \\ 1 & 0 & 0 \end{pmatrix}. \tag{4.23b}$$

The generator a corresponds to a rotation about the axis $x = 0$, $y = z$ by an angle π. We have $a.a = I$. The generator b corresponds to the rotation about the axis

$x = y = z$ by an angle $2\pi/3$. So we have $b.b.b = I$. Also the matrix

$$a.b = \begin{pmatrix} 0 & -1 & 0 \\ 1 & 0 & 0 \\ 0 & 0 & 1 \end{pmatrix} \tag{4.24}$$

corresponds to a rotation about the axis $z = 0$, by an angle $\pi/2$. So we have $a.b.a.b.a.b.a.b = I$. All the 24 elements of the group S_4 are generated using a and b. Thus in an abstract form, the group has the presentation

$$\langle a, b | a^2 = b^3 = (ab)^4 = e \rangle. \tag{4.25}$$

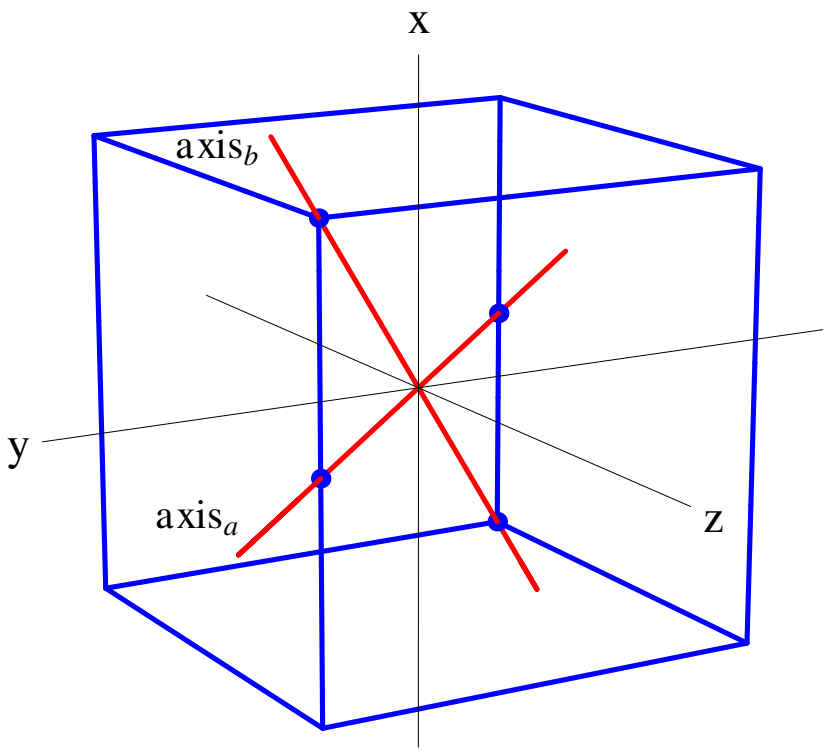

Figure 4.1: Octahedral symmetry as the rotational symmetries of a cube. The generators a and b correspond to rotations about the axes axis$_a$ and axis$_b$ by angles π and $2\pi/3$ respectively.

S_4 symmetry is demonstrated using the rotational symmetries of the cube in Figure 4.1. The characters of S_4 representations are given in Table 4.1. S_4 has

	C_1	C_3	C_6	C_6'	C_8
$\chi_{\mathbf{1}}$	1	1	1	1	1
$\chi_{\mathbf{1'}}$	1	1	-1	-1	1
$\chi_{\mathbf{2}}$	2	2	0	0	-1
$\chi_{\mathbf{3}}$	3	-1	1	-1	0
$\chi_{\mathbf{3'}}$	3	-1	-1	1	0

Table 4.1: Character table for the group S_4

five conjugacy classes. The elements in various conjugacy classes of the group in terms of the generators and also in the defining representation are listed below, Eqs. (4.26-4.30).

$$C_1 = \{a^2\} = \left\{ \begin{pmatrix} 1 & 0 & 0 \\ 0 & 1 & 0 \\ 0 & 0 & 1 \end{pmatrix} \right\} \tag{4.26}$$

This is the identity element.

$$C_3 = \{bab^2ab, (ba)^2, (ab)^2\} = \left\{ \begin{pmatrix} 1 & 0 & 0 \\ 0 & -1 & 0 \\ 0 & 0 & -1 \end{pmatrix}, \begin{pmatrix} -1 & 0 & 0 \\ 0 & 1 & 0 \\ 0 & 0 & -1 \end{pmatrix}, \begin{pmatrix} -1 & 0 & 0 \\ 0 & -1 & 0 \\ 0 & 0 & 1 \end{pmatrix} \right\} \tag{4.27}$$

The class C_3 corresponds to rotations by an angle π about the three axes passing through face centres of the cube.

$$\begin{aligned} C_6 &= \{a, bab^2aba, b^2ab, bab^2abab^2, bab^2, ab^2aba\} \\ &= \left\{ \begin{pmatrix} -1 & 0 & 0 \\ 0 & 0 & 1 \\ 0 & 1 & 0 \end{pmatrix}, \begin{pmatrix} -1 & 0 & 0 \\ 0 & 0 & -1 \\ 0 & -1 & 0 \end{pmatrix}, \begin{pmatrix} 0 & 0 & 1 \\ 0 & -1 & 0 \\ 1 & 0 & 0 \end{pmatrix}, \begin{pmatrix} 0 & 0 & -1 \\ 0 & -1 & 0 \\ -1 & 0 & 0 \end{pmatrix}, \begin{pmatrix} 0 & 1 & 0 \\ 1 & 0 & 0 \\ 0 & 0 & -1 \end{pmatrix}, \begin{pmatrix} 0 & -1 & 0 \\ -1 & 0 & 0 \\ 0 & 0 & -1 \end{pmatrix} \right\} \end{aligned} \tag{4.28}$$

The class C_6 corresponds to rotations by an angle π about the six axes passing through centres of opposite edges. The elements in this class can be grouped in pairs; elements in each pair have axes that lie in a plane parallel to one of the faces. The product of each pair gives a rotation by an angle π about an axis perpendicular that plane, i.e. the product of each pair in C_6 gives the corresponding element in C_3.

$$
\begin{aligned}
C_6' &= \left\{bab, (ab)^2a, ab^2, ba, b^2a, ab\right\} \\
&= \left\{ \begin{pmatrix} 1 & 0 & 0 \\ 0 & 0 & 1 \\ 0 & -1 & 0 \end{pmatrix}, \begin{pmatrix} 1 & 0 & 0 \\ 0 & 0 & -1 \\ 0 & 1 & 0 \end{pmatrix}, \begin{pmatrix} 0 & 0 & -1 \\ 0 & 1 & 0 \\ 1 & 0 & 0 \end{pmatrix}, \begin{pmatrix} 0 & 0 & 1 \\ 0 & 1 & 0 \\ -1 & 0 & 0 \end{pmatrix}, \begin{pmatrix} 0 & 1 & 0 \\ -1 & 0 & 0 \\ 0 & 0 & 1 \end{pmatrix}, \begin{pmatrix} 0 & -1 & 0 \\ 1 & 0 & 0 \\ 0 & 0 & 1 \end{pmatrix} \right\}
\end{aligned} \tag{4.29}
$$

The elements in the class C_6' can also be grouped in pairs; they correspond to rotations by an angle $+\pi/2$ and $-\pi/2$ about the three axes passing through face centres of the cube. Therefore the squares of the elements in C_6' give the corresponding elements in C_3.

$$
\begin{aligned}
C_8 &= \left\{b, b^2, ab^2a, aba, ab^2(ab)^2a, bab^2a, b^2aba, bab^2(ab)^2a\right\} \\
&= \left\{ \begin{pmatrix} 0 & 1 & 0 \\ 0 & 0 & 1 \\ 1 & 0 & 0 \end{pmatrix}, \begin{pmatrix} 0 & 0 & 1 \\ 1 & 0 & 0 \\ 0 & 1 & 0 \end{pmatrix}, \begin{pmatrix} 0 & -1 & 0 \\ 0 & 0 & 1 \\ -1 & 0 & 0 \end{pmatrix}, \begin{pmatrix} 0 & 0 & -1 \\ -1 & 0 & 0 \\ 0 & 1 & 0 \end{pmatrix}, \right. \\
&\qquad \left. \begin{pmatrix} 0 & -1 & 0 \\ 0 & 0 & -1 \\ 1 & 0 & 0 \end{pmatrix}, \begin{pmatrix} 0 & 0 & 1 \\ -1 & 0 & 0 \\ 0 & -1 & 0 \end{pmatrix}, \begin{pmatrix} 0 & 1 & 0 \\ 0 & 0 & -1 \\ -1 & 0 & 0 \end{pmatrix}, \begin{pmatrix} 0 & 0 & -1 \\ 1 & 0 & 0 \\ 0 & -1 & 0 \end{pmatrix} \right\}
\end{aligned} \tag{4.30}
$$

The elements in the class C_8 correspond to rotations by $2\pi/3$ and $-2\pi/3$ about the four axes passing through the opposite corners of the cube.

Models are usually constructed where the neutrinos transform as a triplet

$$
\nu = \begin{pmatrix} \nu_e \\ \nu_\mu \\ \nu_\tau \end{pmatrix} \tag{4.31}
$$

under the postulated symmetry group. While using the S_4 group, the basis given in Eq. (4.23) is used frequently in model building. Here the coordinate system is oriented such that the coordinate axes are normal to the faces of the cube as shown in Figure 4.1. So the x, y and z coordinate axes are the symmetry axes of $\frac{\pi}{2}$-rotations. In a model constructed with a neutrino triplet ν, Eq. (4.31), defined parallel to the coordinate axes (x, y, z) in the above basis, ν_e, ν_μ and ν_τ can be thought of as simply the invariant eigenstates (eigenstates with eigenvalue equal to $+1$) of the corresponding π-rotations about the axes passing through face centres (conjugacy class C_3). These states are shown in Figure 4.2. Note that they are also invariant eigenstates of the elements of the conjugacy class C_6' ($\frac{\pi}{2}$-rotations).

This choice of neutrino eigenstates is straightforward, and is the one used in most models using this group so far. It is however, by no means the only choice, and there is no reason why we should not define the neutrino flavour basis states in a different way. To construct a model with μ-τ symmetry, for example, it will prove useful to define ν_μ and ν_τ eigenstates rotated by an angle $\frac{\pi}{4}$ relative to the x, y and

z coordinate axes defined above, using the rotation matrix

$$R = \begin{pmatrix} 1 & 0 & 0 \\ 0 & \frac{1}{\sqrt{2}} & \frac{1}{\sqrt{2}} \\ 0 & -\frac{1}{\sqrt{2}} & \frac{1}{\sqrt{2}} \end{pmatrix}. \tag{4.32}$$

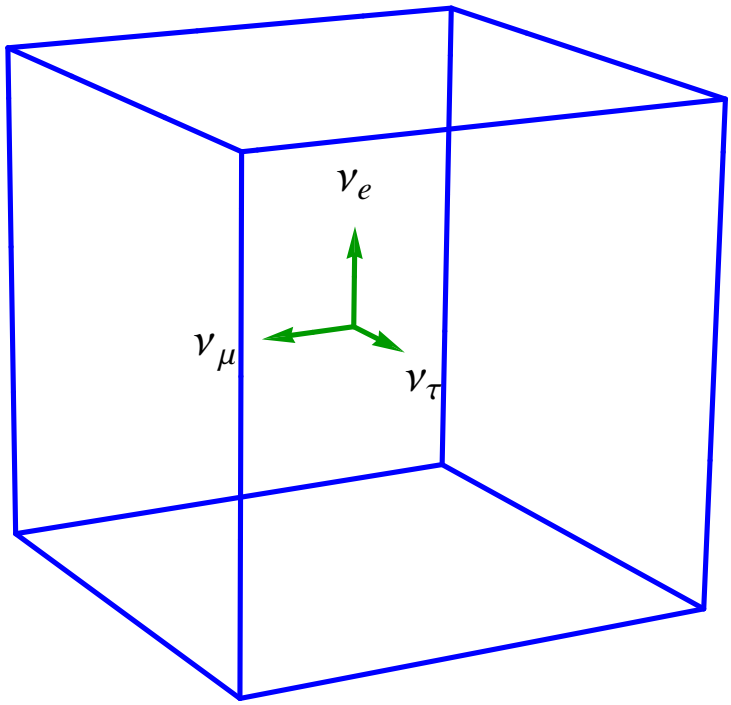

Figure 4.2: The neutrino eigenstates ν_e, ν_μ and ν_τ defined as invariant eigenstates of $\frac{\pi}{2}$-rotations of the cube are normal to the three faces of the cube

The matrix R represents a rotation about the x axis by an angle $\pi/4$ relative to the cube, and this rotation will make a difference to the physical predictions of our model. This redefinition of ν_μ and ν_τ eigenstates is shown in Figure 4.3. The state ν_e is still the invariant eigenstate of the π as well as $\frac{\pi}{2}$ rotations about the axis passing normal to the upper and lower faces of the cube. Now that the states ν_μ and ν_τ have been redefined, do they still form some symmetry axes of the cube? Yes, they do. From Figure 4.3 it is clear that they are aligned along the edge centres of the cube. So they are the invariant eigenstates of π-rotation about the above mentioned edge-centred axes. It is to be noted that S_4 is the smallest group where this works i.e. a pair of invariant eigenstates after a rotation using the matrix R gives another pair of invariant eigenstates. The new definition of the neutrino eigenstates

can be stated abstractly as follows: "ν_e is the eigenstate of one of the elements in the conjugacy class C_3 and ν_μ and ν_τ are the eigenstates of the pair of elements in C_6 whose product is the earlier mentioned the element in C_3".

In model building, specific textures of mass matrices are obtained by coupling the flavons to the fermions and then imposing necessary vacuum alignments for the flavons. Redefining the fermion flavour eigenstates changes the texture of the mass matrices (unless the flavon VEVs are also changed to get an equivalent result). In our model it is useful to define the fermion flavour states in the rotated basis as shown in Figure 4.3, so that in the end we reproduce the "Simplest" texture for the Majorana mass term and a diagonal mass matrix for the charged-leptons.

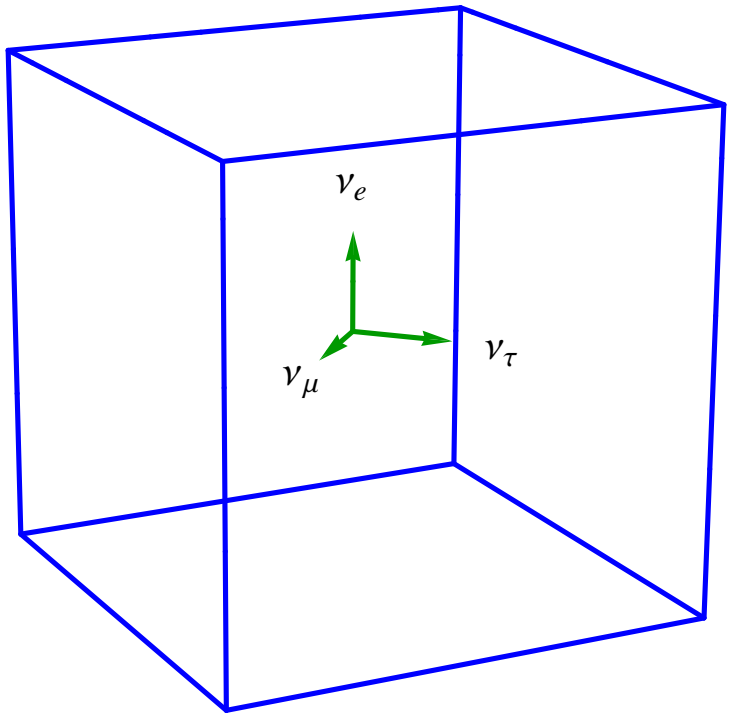

Figure 4.3: Redefinition of the neutrino flavour eigenstates ν_μ and ν_τ. Note that the new states are aligned such that they pass through the edge centres of the cube.

We rotate the coordinate system to reflect this physical rotation of the flavour eigenstates. In other words, we rotate the y and z coordinate axes to align with the new ν_μ and ν_τ flavour eigenstates respectively as shown in Figure 4.4.

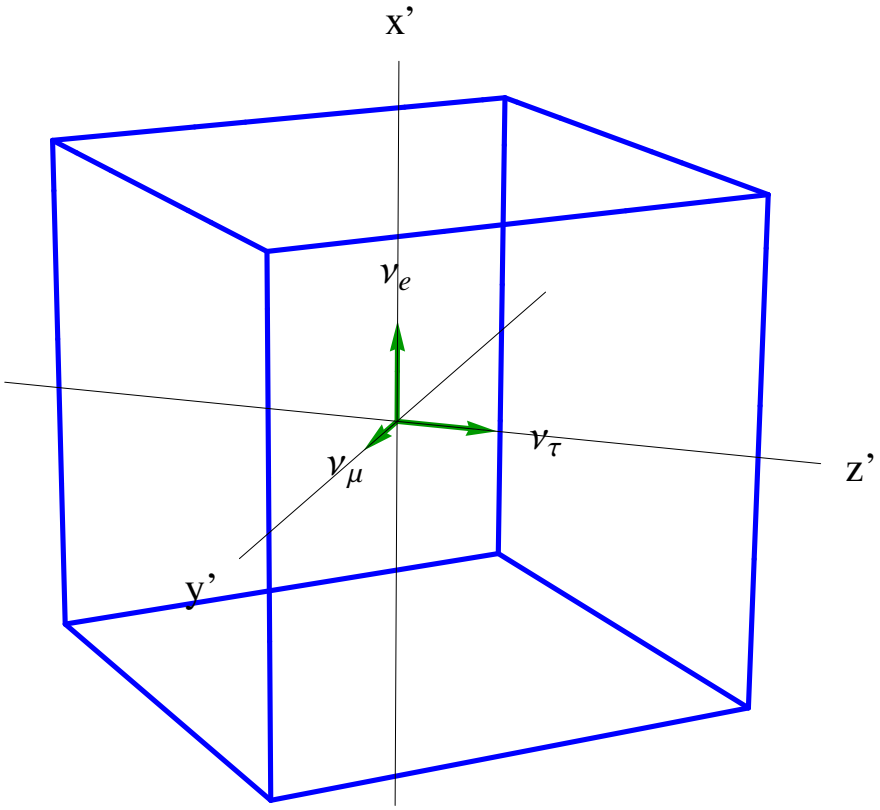

Figure 4.4: Rotation of the coordinate system to align along with the newly defined ν_μ and ν_τ flavour eigenstates

We call this the μ-τ-rotated co-ordinate basis. The rotation of the coordinate system from (x, y, z) to (x', y', z') transforms the group generators as: $a \to R.a.R^\dagger$ and $b \to R.b.R^\dagger$. Thus we have the generators a' and b' in the new (x', y', z') basis as follows:

$$a' = \begin{pmatrix} -1 & 0 & 0 \\ 0 & 1 & 0 \\ 0 & 0 & -1 \end{pmatrix} \tag{4.33a}$$

$$b' = \begin{pmatrix} 0 & \frac{1}{\sqrt{2}} & -\frac{1}{\sqrt{2}} \\ \frac{1}{\sqrt{2}} & \frac{1}{2} & \frac{1}{2} \\ \frac{1}{\sqrt{2}} & -\frac{1}{2} & -\frac{1}{2} \end{pmatrix}. \tag{4.33b}$$

The elements of the conjugacy classes in the new basis are listed below:

$$C_1 = \left\{ \begin{pmatrix} 1 & 0 & 0 \\ 0 & 1 & 0 \\ 0 & 0 & 1 \end{pmatrix} \right\} \tag{4.34a}$$

$$C_3 = \left\{ \begin{pmatrix} 1 & 0 & 0 \\ 0 & -1 & 0 \\ 0 & 0 & -1 \end{pmatrix}, \begin{pmatrix} -1 & 0 & 0 \\ 0 & 0 & -1 \\ 0 & -1 & 0 \end{pmatrix}, \begin{pmatrix} -1 & 0 & 0 \\ 0 & 0 & 1 \\ 0 & 1 & 0 \end{pmatrix} \right\} \tag{4.34b}$$

$$\begin{aligned} C_6 = \Bigg\{ & \begin{pmatrix} -1 & 0 & 0 \\ 0 & 1 & 0 \\ 0 & 0 & -1 \end{pmatrix}, \begin{pmatrix} -1 & 0 & 0 \\ 0 & -1 & 0 \\ 0 & 0 & 1 \end{pmatrix}, \begin{pmatrix} 0 & \frac{1}{\sqrt{2}} & \frac{1}{\sqrt{2}} \\ \frac{1}{\sqrt{2}} & -\frac{1}{2} & \frac{1}{2} \\ \frac{1}{\sqrt{2}} & \frac{1}{2} & -\frac{1}{2} \end{pmatrix}, \\ & \begin{pmatrix} 0 & -\frac{1}{\sqrt{2}} & -\frac{1}{\sqrt{2}} \\ -\frac{1}{\sqrt{2}} & -\frac{1}{2} & \frac{1}{2} \\ -\frac{1}{\sqrt{2}} & \frac{1}{2} & -\frac{1}{2} \end{pmatrix}, \begin{pmatrix} 0 & \frac{1}{\sqrt{2}} & -\frac{1}{\sqrt{2}} \\ \frac{1}{\sqrt{2}} & -\frac{1}{2} & -\frac{1}{2} \\ -\frac{1}{\sqrt{2}} & -\frac{1}{2} & -\frac{1}{2} \end{pmatrix}, \begin{pmatrix} 0 & -\frac{1}{\sqrt{2}} & \frac{1}{\sqrt{2}} \\ -\frac{1}{\sqrt{2}} & -\frac{1}{2} & -\frac{1}{2} \\ \frac{1}{\sqrt{2}} & -\frac{1}{2} & -\frac{1}{2} \end{pmatrix} \Bigg\} \end{aligned} \tag{4.34c}$$

$$\begin{aligned} C_6' = \Bigg\{ & \begin{pmatrix} 1 & 0 & 0 \\ 0 & 0 & 1 \\ 0 & -1 & 0 \end{pmatrix}, \begin{pmatrix} 1 & 0 & 0 \\ 0 & 0 & -1 \\ 0 & 1 & 0 \end{pmatrix}, \begin{pmatrix} 0 & -\frac{1}{\sqrt{2}} & -\frac{1}{\sqrt{2}} \\ \frac{1}{\sqrt{2}} & \frac{1}{2} & -\frac{1}{2} \\ \frac{1}{\sqrt{2}} & -\frac{1}{2} & \frac{1}{2} \end{pmatrix}, \\ & \begin{pmatrix} 0 & \frac{1}{\sqrt{2}} & \frac{1}{\sqrt{2}} \\ -\frac{1}{\sqrt{2}} & \frac{1}{2} & -\frac{1}{2} \\ -\frac{1}{\sqrt{2}} & -\frac{1}{2} & \frac{1}{2} \end{pmatrix}, \begin{pmatrix} 0 & \frac{1}{\sqrt{2}} & -\frac{1}{\sqrt{2}} \\ -\frac{1}{\sqrt{2}} & \frac{1}{2} & \frac{1}{2} \\ \frac{1}{\sqrt{2}} & \frac{1}{2} & \frac{1}{2} \end{pmatrix}, \begin{pmatrix} 0 & -\frac{1}{\sqrt{2}} & \frac{1}{\sqrt{2}} \\ \frac{1}{\sqrt{2}} & \frac{1}{2} & \frac{1}{2} \\ -\frac{1}{\sqrt{2}} & \frac{1}{2} & \frac{1}{2} \end{pmatrix} \Bigg\} \end{aligned} \tag{4.34d}$$

$$\begin{aligned} C_8 = \Bigg\{ & \begin{pmatrix} 0 & \frac{1}{\sqrt{2}} & -\frac{1}{\sqrt{2}} \\ \frac{1}{\sqrt{2}} & \frac{1}{2} & \frac{1}{2} \\ \frac{1}{\sqrt{2}} & -\frac{1}{2} & -\frac{1}{2} \end{pmatrix}, \begin{pmatrix} 0 & \frac{1}{\sqrt{2}} & \frac{1}{\sqrt{2}} \\ \frac{1}{\sqrt{2}} & \frac{1}{2} & -\frac{1}{2} \\ -\frac{1}{\sqrt{2}} & \frac{1}{2} & -\frac{1}{2} \end{pmatrix}, \begin{pmatrix} 0 & -\frac{1}{\sqrt{2}} & \frac{1}{\sqrt{2}} \\ -\frac{1}{\sqrt{2}} & \frac{1}{2} & \frac{1}{2} \\ -\frac{1}{\sqrt{2}} & -\frac{1}{2} & -\frac{1}{2} \end{pmatrix}, \begin{pmatrix} 0 & -\frac{1}{\sqrt{2}} & -\frac{1}{\sqrt{2}} \\ -\frac{1}{\sqrt{2}} & \frac{1}{2} & -\frac{1}{2} \\ \frac{1}{\sqrt{2}} & \frac{1}{2} & -\frac{1}{2} \end{pmatrix}, \\ & \begin{pmatrix} 0 & -\frac{1}{\sqrt{2}} & \frac{1}{\sqrt{2}} \\ \frac{1}{\sqrt{2}} & -\frac{1}{2} & -\frac{1}{2} \\ \frac{1}{\sqrt{2}} & \frac{1}{2} & \frac{1}{2} \end{pmatrix}, \begin{pmatrix} 0 & \frac{1}{\sqrt{2}} & \frac{1}{\sqrt{2}} \\ -\frac{1}{\sqrt{2}} & -\frac{1}{2} & \frac{1}{2} \\ \frac{1}{\sqrt{2}} & -\frac{1}{2} & \frac{1}{2} \end{pmatrix}, \begin{pmatrix} 0 & \frac{1}{\sqrt{2}} & -\frac{1}{\sqrt{2}} \\ -\frac{1}{\sqrt{2}} & -\frac{1}{2} & -\frac{1}{2} \\ -\frac{1}{\sqrt{2}} & \frac{1}{2} & \frac{1}{2} \end{pmatrix}, \begin{pmatrix} 0 & -\frac{1}{\sqrt{2}} & -\frac{1}{\sqrt{2}} \\ \frac{1}{\sqrt{2}} & -\frac{1}{2} & \frac{1}{2} \\ -\frac{1}{\sqrt{2}} & -\frac{1}{2} & \frac{1}{2} \end{pmatrix} \Bigg\}. \end{aligned} \tag{4.34e}$$

The neutrino triplet, Eq. (4.31) transforms as a $\mathbf{3'}$ in the μ-τ-rotated basis. Define a unitary matrix U as given in Eq. (4.37). The matrix U can be used to do the transformation from the tensor product basis of two $\mathbf{3'}$s to the irreducibly decomposed basis. In other words, we have

$$U.Kr(g,g).U^\dagger = g_{\text{block}} \tag{4.35}$$

where the Kronecker product, $Kr(g,g)$ is the group element representing the tensor product of two $\mathbf{3'}$s and the block-diagonalised element, g_{block} is the sum $\mathbf{1}\oplus\mathbf{2}\oplus\mathbf{3}\oplus\mathbf{3'}$,

$$\mathbf{3'} \otimes \mathbf{3'} = \mathbf{1} \oplus \mathbf{2} \oplus \mathbf{3} \oplus \mathbf{3'}. \tag{4.36}$$

For the generators a and b, the block diagonalised matrices are given in Eqs. (4.38).

$$U = \begin{pmatrix} \frac{1}{\sqrt{3}} & 0 & 0 & 0 & \frac{1}{\sqrt{3}} & 0 & 0 & 0 & \frac{1}{\sqrt{3}} \\ -\sqrt{\frac{2}{3}} & 0 & 0 & 0 & \frac{1}{\sqrt{6}} & 0 & 0 & 0 & \frac{1}{\sqrt{6}} \\ 0 & 0 & 0 & 0 & 0 & \frac{1}{\sqrt{2}} & 0 & \frac{1}{\sqrt{2}} & 0 \\ 0 & 0 & 0 & 0 & \frac{1}{\sqrt{2}} & 0 & 0 & 0 & -\frac{1}{\sqrt{2}} \\ 0 & \frac{1}{\sqrt{2}} & 0 & \frac{1}{\sqrt{2}} & 0 & 0 & 0 & 0 & 0 \\ 0 & 0 & \frac{1}{\sqrt{2}} & 0 & 0 & 0 & \frac{1}{\sqrt{2}} & 0 & 0 \\ 0 & 0 & 0 & 0 & 0 & \frac{1}{\sqrt{2}} & 0 & -\frac{1}{\sqrt{2}} & 0 \\ 0 & 0 & -\frac{1}{\sqrt{2}} & 0 & 0 & 0 & \frac{1}{\sqrt{2}} & 0 & 0 \\ 0 & \frac{1}{\sqrt{2}} & 0 & -\frac{1}{\sqrt{2}} & 0 & 0 & 0 & 0 & 0 \end{pmatrix} \tag{4.37}$$

$$a_{\text{block}} = \begin{pmatrix} 1 & 0 & 0 & 0 & 0 & 0 & 0 & 0 & 0 \\ 0 & 1 & 0 & 0 & 0 & 0 & 0 & 0 & 0 \\ 0 & 0 & -1 & 0 & 0 & 0 & 0 & 0 & 0 \\ 0 & 0 & 0 & 1 & 0 & 0 & 0 & 0 & 0 \\ 0 & 0 & 0 & 0 & -1 & 0 & 0 & 0 & 0 \\ 0 & 0 & 0 & 0 & 0 & 1 & 0 & 0 & 0 \\ 0 & 0 & 0 & 0 & 0 & 0 & -1 & 0 & 0 \\ 0 & 0 & 0 & 0 & 0 & 0 & 0 & 1 & 0 \\ 0 & 0 & 0 & 0 & 0 & 0 & 0 & 0 & -1 \end{pmatrix} \tag{4.38a}$$

$$b_{\text{block}} = \begin{pmatrix} 1 & 0 & 0 & 0 & 0 & 0 & 0 & 0 & 0 \\ 0 & -\frac{1}{2} & \frac{\sqrt{3}}{2} & 0 & 0 & 0 & 0 & 0 & 0 \\ 0 & -\frac{\sqrt{3}}{2} & -\frac{1}{2} & 0 & 0 & 0 & 0 & 0 & 0 \\ 0 & 0 & 0 & 0 & \frac{1}{\sqrt{2}} & \frac{1}{\sqrt{2}} & 0 & 0 & 0 \\ 0 & 0 & 0 & \frac{1}{\sqrt{2}} & \frac{1}{2} & -\frac{1}{2} & 0 & 0 & 0 \\ 0 & 0 & 0 & -\frac{1}{\sqrt{2}} & \frac{1}{2} & -\frac{1}{2} & 0 & 0 & 0 \\ 0 & 0 & 0 & 0 & 0 & 0 & 0 & \frac{1}{\sqrt{2}} & -\frac{1}{\sqrt{2}} \\ 0 & 0 & 0 & 0 & 0 & 0 & \frac{1}{\sqrt{2}} & \frac{1}{2} & \frac{1}{2} \\ 0 & 0 & 0 & 0 & 0 & 0 & \frac{1}{\sqrt{2}} & -\frac{1}{2} & -\frac{1}{2} \end{pmatrix} \tag{4.38b}$$

Therefore for the representation **2** we have

$$a = \begin{pmatrix} 1 & 0 \\ 0 & -1 \end{pmatrix} \tag{4.39a}$$

$$b = \begin{pmatrix} -\frac{1}{2} & \frac{\sqrt{3}}{2} \\ -\frac{\sqrt{3}}{2} & -\frac{1}{2} \end{pmatrix} \tag{4.39b}$$

and for the representation **3** we have

$$a = \begin{pmatrix} 1 & 0 & 0 \\ 0 & -1 & 0 \\ 0 & 0 & 1 \end{pmatrix} \tag{4.40a}$$

$$b = \begin{pmatrix} 0 & \frac{1}{\sqrt{2}} & \frac{1}{\sqrt{2}} \\ \frac{1}{\sqrt{2}} & \frac{1}{2} & -\frac{1}{2} \\ -\frac{1}{\sqrt{2}} & \frac{1}{2} & -\frac{1}{2} \end{pmatrix} \tag{4.40b}$$

as the generators.

Using Eq. (4.37) , we get

$$\xi_1 = \frac{1}{\sqrt{3}}(\nu_e.\nu_e + \nu_\mu.\nu_\mu + \nu_\tau.\nu_\tau) \tag{4.41}$$

$$\xi_2 = \begin{pmatrix} -\sqrt{\frac{2}{3}}\nu_e.\nu_e + \frac{1}{\sqrt{6}}\nu_\mu.\nu_\mu + \frac{1}{\sqrt{6}}\nu_\tau.\nu_\tau \\ \frac{1}{\sqrt{2}}(\nu_\mu.\nu_\tau + \nu_\tau.\nu_\mu) \end{pmatrix} \tag{4.42}$$

$$\xi_3 = \begin{pmatrix} \frac{1}{\sqrt{2}}(\nu_\mu.\nu_\mu - \nu_\tau.\nu_\tau) \\ \frac{1}{\sqrt{2}}(\nu_e.\nu_\mu + \nu_\mu.\nu_e) \\ \frac{1}{\sqrt{2}}(\nu_\tau.\nu_e + \nu_e.\nu_\tau) \end{pmatrix} \tag{4.43}$$

$$\xi'_3 = \begin{pmatrix} \frac{1}{\sqrt{2}}(\nu_\mu.\nu_\tau - \nu_\tau.\nu_\mu) \\ \frac{1}{\sqrt{2}}(\nu_\tau.\nu_e - \nu_e.\nu_\tau) \\ \frac{1}{\sqrt{2}}(\nu_e.\nu_\mu - \nu_\mu.\nu_e) \end{pmatrix} \tag{4.44}$$

$$\tag{4.45}$$

where the product $\nu_i.\nu_j$ is the Lorentz invariant product of the neutrino fields, i.e. $\nu_i.\nu_j = \nu_{i\alpha}\nu_j^\alpha$. The expressions ξ_1, ξ_2, ξ_3 and ξ'_3 transform as **1**, **2**, **3** and **3′** respectively.

Note that the expressions ξ_1, ξ_2 and ξ_3 are symmetric and the expression ξ'_3 is antisymmetric under the exchange of the two **3′**s in the LHS of Eq. (4.36). Since we have only a single set of right handed neutrino fields (only one type of **3′**), the

antisymmetric combination vanishes, i.e. $\xi'_3 = 0$.

We define three kinds of flavons ϕ_1, $\phi_2 = (\phi_2^1, \phi_2^2)^T$ and $\phi_3 = (\phi_3^1, \phi_3^2, \phi_3^3)^T$ that transform as **1**, **2**, and **3** respectively. Then the general invariant term takes the form

$$\text{Inv} = c_1\xi_1\phi_1 + c_2\xi_2^T\phi_2 + c_3\xi_3^T\phi_3 \tag{4.46}$$

where c_1, c_2 and c_3 are constants. In a matrix form Eq. (4.46) can be written as

$$\text{Inv} = \nu_\alpha^T M \nu^\alpha \tag{4.47}$$

where

$$M = c_1\phi_1 I + c_2 \begin{pmatrix} -\sqrt{\frac{2}{3}}\phi_2^1 & 0 & 0 \\ 0 & \frac{1}{\sqrt{6}}\phi_2^1 & \frac{1}{\sqrt{2}}\phi_2^2 \\ 0 & \frac{1}{\sqrt{2}}\phi_2^2 & \frac{1}{\sqrt{6}}\phi_2^1 \end{pmatrix} + c_3 \begin{pmatrix} 0 & \frac{1}{\sqrt{2}}\phi_3^3 & \frac{1}{\sqrt{2}}\phi_3^2 \\ \frac{1}{\sqrt{2}}\phi_3^3 & \frac{1}{\sqrt{2}}\phi_3^1 & 0 \\ \frac{1}{\sqrt{2}}\phi_3^2 & 0 & -\frac{1}{\sqrt{2}}\phi_3^1 \end{pmatrix}. \tag{4.48}$$

If the flavons get VEVs $\langle\phi_1\rangle = 1$, $\langle\phi_2\rangle = (-\frac{1}{2}, \frac{\sqrt{3}}{2})^T$ and $\langle\phi_3\rangle = (1, -1, 1)^T$, the mass matrix will become

$$M = c_1 I + \frac{c_2\sqrt{3}}{2\sqrt{2}} \begin{pmatrix} \frac{2}{3} & 0 & 0 \\ 0 & -\frac{1}{3} & 1 \\ 0 & 1 & -\frac{1}{3} \end{pmatrix} + \frac{c_3}{\sqrt{2}} \begin{pmatrix} 0 & -1 & 1 \\ -1 & 1 & 0 \\ 1 & 0 & -1 \end{pmatrix} \tag{4.49}$$

which is in the same form as Eq. (4.21) assuming c_1 and c_2 to be real and c_3 to be imaginary. Unlike in Eq. (4.21), here the trace is removed from the second term and is absorbed into the first. In the next section we study the above mentioned VEVs.

The most general case of the coefficients, where c_1, c_2 and c_3 are imaginary, corresponds to the 'democratic' mixing ansatz. In this ansatz one row or column of the mixing matrix is trimaximally mixed, i.e. the moduli of all the three elements of that particular row or column will be $\frac{1}{\sqrt{3}}$. The phenomenologically acceptable case is the one in which the second column of the mixing matrix is trimaximal so that we have $|U_{\text{PMNS}}|_{e2} = \frac{1}{\sqrt{3}}$ consistent with the solar oscillation data. The TχM mixing is a special case of the democratic mixing where we have the extra constraint of maximal CP-violation ($\delta_{CP} = \pm\frac{\pi}{2}$). The earlier mentioned assumption - 'c_1 and c_2 real and c_3 imaginary' - imposes this maximal CP-violation constraint. However it should be noted that here we do not provide a theoretical origin for this choice of coefficients.

4.3 Flavon vacuum alignments

The VEV for ϕ_1 being proportional to 1 is trivial. What is special about ϕ_2 and ϕ_3 having the VEVs $(-\frac{1}{2}, \frac{\sqrt{3}}{2})^T$ and $(1,-1,1)^T$ respectively? To understand it, we need to examine the group elements of the representations **2** and **3**.

The elements of **3** are listed below:

$$C_1 = \left\{ \begin{pmatrix} 1 & 0 & 0 \\ 0 & 1 & 0 \\ 0 & 0 & 1 \end{pmatrix} \right\} \tag{4.50a}$$

$$C_3 = \left\{ \begin{pmatrix} 1 & 0 & 0 \\ 0 & -1 & 0 \\ 0 & 0 & -1 \end{pmatrix}, \begin{pmatrix} -1 & 0 & 0 \\ 0 & 0 & 1 \\ 0 & 1 & 0 \end{pmatrix}, \begin{pmatrix} -1 & 0 & 0 \\ 0 & 0 & -1 \\ 0 & -1 & 0 \end{pmatrix} \right\} \tag{4.50b}$$

$$C_6 = \left\{ \begin{pmatrix} 1 & 0 & 0 \\ 0 & -1 & 0 \\ 0 & 0 & 1 \end{pmatrix}, \begin{pmatrix} 1 & 0 & 0 \\ 0 & 1 & 0 \\ 0 & 0 & -1 \end{pmatrix}, \begin{pmatrix} 0 & -\frac{1}{\sqrt{2}} & \frac{1}{\sqrt{2}} \\ -\frac{1}{\sqrt{2}} & \frac{1}{2} & \frac{1}{2} \\ \frac{1}{\sqrt{2}} & \frac{1}{2} & \frac{1}{2} \end{pmatrix}, \begin{pmatrix} 0 & \frac{1}{\sqrt{2}} & -\frac{1}{\sqrt{2}} \\ \frac{1}{\sqrt{2}} & \frac{1}{2} & \frac{1}{2} \\ -\frac{1}{\sqrt{2}} & \frac{1}{2} & \frac{1}{2} \end{pmatrix}, \begin{pmatrix} 0 & \frac{1}{\sqrt{2}} & \frac{1}{\sqrt{2}} \\ \frac{1}{\sqrt{2}} & \frac{1}{2} & -\frac{1}{2} \\ \frac{1}{\sqrt{2}} & -\frac{1}{2} & \frac{1}{2} \end{pmatrix}, \begin{pmatrix} 0 & \frac{1}{\sqrt{2}} & \frac{1}{\sqrt{2}} \\ \frac{1}{\sqrt{2}} & \frac{1}{2} & -\frac{1}{2} \\ \frac{1}{\sqrt{2}} & -\frac{1}{2} & \frac{1}{2} \end{pmatrix} \right\} \tag{4.50c}$$

$$C_6' = \left\{ \begin{pmatrix} -1 & 0 & 0 \\ 0 & 0 & 1 \\ 0 & -1 & 0 \end{pmatrix}, \begin{pmatrix} -1 & 0 & 0 \\ 0 & 0 & -1 \\ 0 & 1 & 0 \end{pmatrix}, \begin{pmatrix} 0 & \frac{1}{\sqrt{2}} & -\frac{1}{\sqrt{2}} \\ -\frac{1}{\sqrt{2}} & -\frac{1}{2} & -\frac{1}{2} \\ \frac{1}{\sqrt{2}} & -\frac{1}{2} & -\frac{1}{2} \end{pmatrix}, \begin{pmatrix} 0 & -\frac{1}{\sqrt{2}} & \frac{1}{\sqrt{2}} \\ \frac{1}{\sqrt{2}} & -\frac{1}{2} & -\frac{1}{2} \\ -\frac{1}{\sqrt{2}} & -\frac{1}{2} & -\frac{1}{2} \end{pmatrix}, \begin{pmatrix} 0 & -\frac{1}{\sqrt{2}} & -\frac{1}{\sqrt{2}} \\ \frac{1}{\sqrt{2}} & -\frac{1}{2} & \frac{1}{2} \\ \frac{1}{\sqrt{2}} & \frac{1}{2} & -\frac{1}{2} \end{pmatrix}, \begin{pmatrix} 0 & \frac{1}{\sqrt{2}} & \frac{1}{\sqrt{2}} \\ -\frac{1}{\sqrt{2}} & -\frac{1}{2} & \frac{1}{2} \\ -\frac{1}{\sqrt{2}} & \frac{1}{2} & -\frac{1}{2} \end{pmatrix} \right\} \tag{4.50d}$$

$$C_8 = \left\{ \begin{pmatrix} 0 & \frac{1}{\sqrt{2}} & \frac{1}{\sqrt{2}} \\ \frac{1}{\sqrt{2}} & \frac{1}{2} & -\frac{1}{2} \\ -\frac{1}{\sqrt{2}} & \frac{1}{2} & -\frac{1}{2} \end{pmatrix}, \begin{pmatrix} 0 & \frac{1}{\sqrt{2}} & -\frac{1}{\sqrt{2}} \\ \frac{1}{\sqrt{2}} & \frac{1}{2} & \frac{1}{2} \\ \frac{1}{\sqrt{2}} & -\frac{1}{2} & -\frac{1}{2} \end{pmatrix}, \begin{pmatrix} 0 & -\frac{1}{\sqrt{2}} & -\frac{1}{\sqrt{2}} \\ -\frac{1}{\sqrt{2}} & \frac{1}{2} & -\frac{1}{2} \\ \frac{1}{\sqrt{2}} & \frac{1}{2} & -\frac{1}{2} \end{pmatrix}, \begin{pmatrix} 0 & -\frac{1}{\sqrt{2}} & \frac{1}{\sqrt{2}} \\ -\frac{1}{\sqrt{2}} & \frac{1}{2} & \frac{1}{2} \\ -\frac{1}{\sqrt{2}} & -\frac{1}{2} & -\frac{1}{2} \end{pmatrix}, \begin{pmatrix} 0 & -\frac{1}{\sqrt{2}} & -\frac{1}{\sqrt{2}} \\ \frac{1}{\sqrt{2}} & -\frac{1}{2} & \frac{1}{2} \\ -\frac{1}{\sqrt{2}} & -\frac{1}{2} & \frac{1}{2} \end{pmatrix}, \begin{pmatrix} 0 & \frac{1}{\sqrt{2}} & -\frac{1}{\sqrt{2}} \\ -\frac{1}{\sqrt{2}} & -\frac{1}{2} & -\frac{1}{2} \\ -\frac{1}{\sqrt{2}} & \frac{1}{2} & \frac{1}{2} \end{pmatrix}, \begin{pmatrix} 0 & \frac{1}{\sqrt{2}} & \frac{1}{\sqrt{2}} \\ -\frac{1}{\sqrt{2}} & -\frac{1}{2} & \frac{1}{2} \\ \frac{1}{\sqrt{2}} & -\frac{1}{2} & \frac{1}{2} \end{pmatrix}, \begin{pmatrix} 0 & -\frac{1}{\sqrt{2}} & \frac{1}{\sqrt{2}} \\ \frac{1}{\sqrt{2}} & -\frac{1}{2} & -\frac{1}{2} \\ \frac{1}{\sqrt{2}} & \frac{1}{2} & \frac{1}{2} \end{pmatrix} \right\} \tag{4.50e}$$

The VEV $(1,-1,1)^T$ is the eigenstate of the matrix

$$\begin{pmatrix} -1 & 0 & 0 \\ 0 & 0 & 1 \\ 0 & 1 & 0 \end{pmatrix} \tag{4.51}$$

with an eigenvalue -1. So ϕ_3 can be said to have acquired a VEV equal to the eigenstate of the second element in the conjugacy class C_3 with an eigenvalue -1. It should be noted that this matrix has one eigenvalue equal to +1 and two others equal to -1. So the eigenstate with an eigenvalue -1 is not unique. We may be able to remove this ambiguity by embedding the group S_4 in a larger group.

The elements of **2** are listed below:

$$C_1 = \{\begin{pmatrix} 1 & 0 \\ 0 & 1 \end{pmatrix}\} \tag{4.52a}$$

$$C_3 = \{\begin{pmatrix} 1 & 0 \\ 0 & 1 \end{pmatrix}, \begin{pmatrix} 1 & 0 \\ 0 & 1 \end{pmatrix}, \begin{pmatrix} 1 & 0 \\ 0 & 1 \end{pmatrix}\} \tag{4.52b}$$

$$C_6 = \left\{ \begin{pmatrix} 1 & 0 \\ 0 & -1 \end{pmatrix}, \begin{pmatrix} 1 & 0 \\ 0 & -1 \end{pmatrix}, \begin{pmatrix} -\frac{1}{2} & -\frac{\sqrt{3}}{2} \\ -\frac{\sqrt{3}}{2} & \frac{1}{2} \end{pmatrix}, \begin{pmatrix} -\frac{1}{2} & -\frac{\sqrt{3}}{2} \\ -\frac{\sqrt{3}}{2} & \frac{1}{2} \end{pmatrix}, \begin{pmatrix} -\frac{1}{2} & \frac{\sqrt{3}}{2} \\ \frac{\sqrt{3}}{2} & \frac{1}{2} \end{pmatrix}, \begin{pmatrix} -\frac{1}{2} & \frac{\sqrt{3}}{2} \\ \frac{\sqrt{3}}{2} & \frac{1}{2} \end{pmatrix} \right\} \tag{4.52c}$$

$$C_6' = \left\{ \begin{pmatrix} 1 & 0 \\ 0 & -1 \end{pmatrix}, \begin{pmatrix} 1 & 0 \\ 0 & -1 \end{pmatrix}, \begin{pmatrix} -\frac{1}{2} & -\frac{\sqrt{3}}{2} \\ -\frac{\sqrt{3}}{2} & \frac{1}{2} \end{pmatrix}, \begin{pmatrix} -\frac{1}{2} & -\frac{\sqrt{3}}{2} \\ -\frac{\sqrt{3}}{2} & \frac{1}{2} \end{pmatrix}, \begin{pmatrix} -\frac{1}{2} & \frac{\sqrt{3}}{2} \\ \frac{\sqrt{3}}{2} & \frac{1}{2} \end{pmatrix}, \begin{pmatrix} -\frac{1}{2} & \frac{\sqrt{3}}{2} \\ \frac{\sqrt{3}}{2} & \frac{1}{2} \end{pmatrix} \right\} \tag{4.52d}$$

$$C_8 = \left\{ \begin{pmatrix} -\frac{1}{2} & \frac{\sqrt{3}}{2} \\ -\frac{\sqrt{3}}{2} & -\frac{1}{2} \end{pmatrix}, \begin{pmatrix} -\frac{1}{2} & -\frac{\sqrt{3}}{2} \\ \frac{\sqrt{3}}{2} & -\frac{1}{2} \end{pmatrix}, \begin{pmatrix} -\frac{1}{2} & \frac{\sqrt{3}}{2} \\ -\frac{\sqrt{3}}{2} & -\frac{1}{2} \end{pmatrix}, \begin{pmatrix} -\frac{1}{2} & -\frac{\sqrt{3}}{2} \\ \frac{\sqrt{3}}{2} & -\frac{1}{2} \end{pmatrix}, \begin{pmatrix} -\frac{1}{2} & \frac{\sqrt{3}}{2} \\ -\frac{\sqrt{3}}{2} & -\frac{1}{2} \end{pmatrix}, \begin{pmatrix} -\frac{1}{2} & -\frac{\sqrt{3}}{2} \\ \frac{\sqrt{3}}{2} & -\frac{1}{2} \end{pmatrix}, \begin{pmatrix} -\frac{1}{2} & \frac{\sqrt{3}}{2} \\ -\frac{\sqrt{3}}{2} & -\frac{1}{2} \end{pmatrix}, \begin{pmatrix} -\frac{1}{2} & -\frac{\sqrt{3}}{2} \\ \frac{\sqrt{3}}{2} & -\frac{1}{2} \end{pmatrix} \right\}. \tag{4.52e}$$

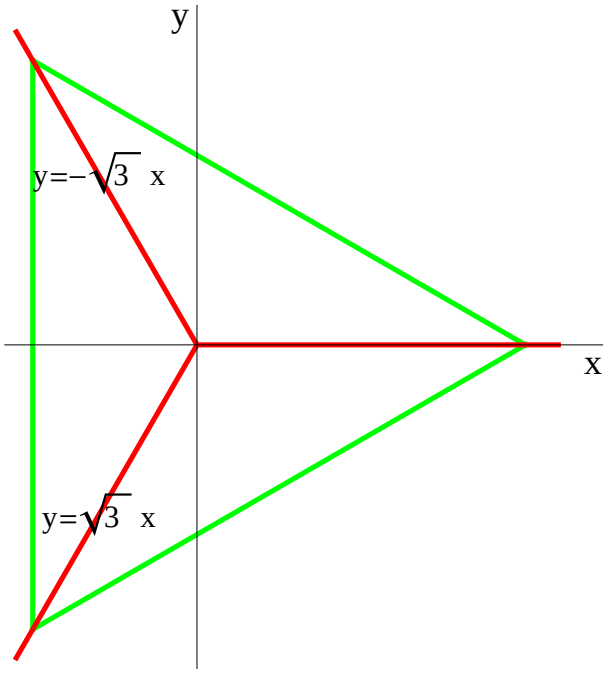

Figure 4.5: S_3 symmetry as the symmetry of an equilateral triangle. The transformations (rotations and reflections) are the same as the unfaithful two dimensional representations **2** of the group S_4

The VEV $(-\frac{1}{2}, \frac{\sqrt{3}}{2})^T$ is the invariant eigenstate of the matrix

$$\begin{pmatrix} -\frac{1}{2} & -\frac{\sqrt{3}}{2} \\ -\frac{\sqrt{3}}{2} & \frac{1}{2} \end{pmatrix}. \tag{4.53}$$

This matrix corresponds to reflection about the line $y = -\sqrt{3}x$. In other words we may say that ϕ_2 acquires a VEV equal to the eigenstate of the second pair of elements in the conjugacy class C_6. As we can see, **2** is not a faithful representation of the group S_4. They form the subgroup S_3 (symmetry group of an equilateral triangle as shown in Figure 4.5).

4.3.1 Minimisation of flavon potentials and flavon VEVs

In the previous section we have shown that the VEVs of the flavons are invariant eigenstates. Thus we used the symmetry arguments alone to explain the origin of the VEVs. Conventionally, the required VEV alignments of the flavons are obtained through spontaneous symmetry breaking using the minimisation procedure of flavon potential terms, for example [66]. In the following discussion we show that such a procedure can be adopted in our model also. This discussion is not an exhaustive analysis of the flavon potentials that can be constructed in our model.

Here it is useful to evaluate the tensor product expansions of various irreducible representations of S_4. We will be working with the μ-τ-rotated basis of the representation $\mathbf{3'}$. The tensor product expansion

$$\mathbf{3'} \otimes \mathbf{3'} = \mathbf{1} \oplus \mathbf{2} \oplus \mathbf{3} \oplus \mathbf{3'}. \tag{4.54}$$

was discussed earlier, Eq. (4.36), and the block-diagonalising matrix U which produces the above tensor product expansion was given in Eq. (4.37). Note that this matrix also defines our basis for the other irreducible representations, **2** and **3**. All the possible non-trivial tensor product expansions of the various irreducible representations and the corresponding block-diagonalising matrices are given below.

$$\mathbf{2} \otimes \mathbf{2} = \mathbf{1} \oplus \mathbf{1'} \oplus \mathbf{2} \tag{4.55a}$$

$$U_{\mathbf{2}\otimes\mathbf{2}} = \begin{pmatrix} \frac{1}{\sqrt{2}} & 0 & 0 & \frac{1}{\sqrt{2}} \\ 0 & \frac{1}{\sqrt{2}} & -\frac{1}{\sqrt{2}} & 0 \\ -\frac{1}{\sqrt{2}} & 0 & 0 & \frac{1}{\sqrt{2}} \\ 0 & \frac{1}{\sqrt{2}} & \frac{1}{\sqrt{2}} & 0 \end{pmatrix} \tag{4.55b}$$

$$\mathbf{3} \otimes \mathbf{3} = \mathbf{1} \oplus \mathbf{2} \oplus \mathbf{3} \oplus \mathbf{3'} \tag{4.56a}$$

$$U_{\mathbf{3}\otimes\mathbf{3}} = \begin{pmatrix} \frac{1}{\sqrt{3}} & 0 & 0 & 0 & \frac{1}{\sqrt{3}} & 0 & 0 & 0 & \frac{1}{\sqrt{3}} \\ \sqrt{\frac{2}{3}} & 0 & 0 & 0 & -\frac{1}{\sqrt{6}} & 0 & 0 & 0 & -\frac{1}{\sqrt{6}} \\ 0 & 0 & 0 & 0 & 0 & \frac{1}{\sqrt{2}} & 0 & \frac{1}{\sqrt{2}} & 0 \\ 0 & 0 & 0 & 0 & -\frac{1}{\sqrt{2}} & 0 & 0 & 0 & \frac{1}{\sqrt{2}} \\ 0 & -\frac{1}{\sqrt{2}} & 0 & -\frac{1}{\sqrt{2}} & 0 & 0 & 0 & 0 & 0 \\ 0 & 0 & \frac{1}{\sqrt{2}} & 0 & 0 & 0 & \frac{1}{\sqrt{2}} & 0 & 0 \\ 0 & 0 & 0 & 0 & 0 & -\frac{1}{\sqrt{2}} & 0 & \frac{1}{\sqrt{2}} & 0 \\ 0 & 0 & \frac{1}{\sqrt{2}} & 0 & 0 & 0 & -\frac{1}{\sqrt{2}} & 0 & 0 \\ 0 & \frac{1}{\sqrt{2}} & 0 & -\frac{1}{\sqrt{2}} & 0 & 0 & 0 & 0 & 0 \end{pmatrix} \tag{4.56b}$$

$$\mathbf{3'} \otimes \mathbf{3} = \mathbf{1'} \oplus \mathbf{2} \oplus \mathbf{3} \oplus \mathbf{3'} \tag{4.57a}$$

$$U_{\mathbf{3'}\otimes\mathbf{3}} = \begin{pmatrix} \frac{1}{\sqrt{3}} & 0 & 0 & 0 & \frac{1}{\sqrt{3}} & 0 & 0 & 0 & -\frac{1}{\sqrt{3}} \\ 0 & 0 & 0 & 0 & 0 & -\frac{1}{\sqrt{2}} & 0 & \frac{1}{\sqrt{2}} & 0 \\ \sqrt{\frac{2}{3}} & 0 & 0 & 0 & -\frac{1}{\sqrt{6}} & 0 & 0 & 0 & \frac{1}{\sqrt{6}} \\ 0 & 0 & 0 & 0 & 0 & -\frac{1}{\sqrt{2}} & 0 & -\frac{1}{\sqrt{2}} & 0 \\ 0 & 0 & \frac{1}{\sqrt{2}} & 0 & 0 & 0 & \frac{1}{\sqrt{2}} & 0 & 0 \\ 0 & -\frac{1}{\sqrt{2}} & 0 & \frac{1}{\sqrt{2}} & 0 & 0 & 0 & 0 & 0 \\ 0 & 0 & 0 & 0 & \frac{1}{\sqrt{2}} & 0 & 0 & 0 & \frac{1}{\sqrt{2}} \\ 0 & \frac{1}{\sqrt{2}} & 0 & \frac{1}{\sqrt{2}} & 0 & 0 & 0 & 0 & 0 \\ 0 & 0 & \frac{1}{\sqrt{2}} & 0 & 0 & 0 & -\frac{1}{\sqrt{2}} & 0 & 0 \end{pmatrix} \tag{4.57b}$$

$$\mathbf{2} \otimes \mathbf{3'} = \mathbf{3} \oplus \mathbf{3'} \tag{4.58a}$$

$$U_{\mathbf{2}\otimes\mathbf{3'}} = \begin{pmatrix} 0 & 0 & 0 & -1 & 0 & 0 \\ 0 & 0 & -\frac{\sqrt{3}}{2} & 0 & \frac{1}{2} & 0 \\ 0 & \frac{\sqrt{3}}{2} & 0 & 0 & 0 & -\frac{1}{2} \\ -1 & 0 & 0 & 0 & 0 & 0 \\ 0 & \frac{1}{2} & 0 & 0 & 0 & \frac{\sqrt{3}}{2} \\ 0 & 0 & \frac{1}{2} & 0 & \frac{\sqrt{3}}{2} & 0 \end{pmatrix} \tag{4.58b}$$

$$\mathbf{2} \otimes \mathbf{3} = \mathbf{3} \oplus \mathbf{3'} \tag{4.59a}$$

$$U_{\mathbf{2}\otimes\mathbf{3}} = \begin{pmatrix} -1 & 0 & 0 & 0 & 0 & 0 \\ 0 & \frac{1}{2} & 0 & 0 & 0 & -\frac{\sqrt{3}}{2} \\ 0 & 0 & \frac{1}{2} & 0 & -\frac{\sqrt{3}}{2} & 0 \\ 0 & 0 & 0 & 1 & 0 & 0 \\ 0 & 0 & -\frac{\sqrt{3}}{2} & 0 & -\frac{1}{2} & 0 \\ 0 & \frac{\sqrt{3}}{2} & 0 & 0 & 0 & \frac{1}{2} \end{pmatrix} \tag{4.59b}$$

$$\mathbf{1'} \otimes \mathbf{3'} = \mathbf{3} \tag{4.60a}$$

$$U_{\mathbf{1'}\otimes\mathbf{3'}} = \begin{pmatrix} 1 & 0 & 0 \\ 0 & 1 & 0 \\ 0 & 0 & -1 \end{pmatrix} \tag{4.60b}$$

$$\mathbf{1'} \otimes \mathbf{3} = \mathbf{3'} \tag{4.61a}$$

$$U_{\mathbf{1'}\otimes\mathbf{3}} = \begin{pmatrix} 1 & 0 & 0 \\ 0 & 1 & 0 \\ 0 & 0 & -1 \end{pmatrix} \tag{4.61b}$$

$$\mathbf{1'} \otimes \mathbf{2} = \mathbf{2} \tag{4.62a}$$

$$U_{\mathbf{1'}\otimes\mathbf{2}} = \begin{pmatrix} 0 & -1 \\ 1 & 0 \end{pmatrix} \tag{4.62b}$$

From Eq. (4.55) it is clear that using the doublet flavon $\phi_2 = (\phi_2^1, \phi_2^2)$ we may construct a second degree doublet $\left(-\frac{1}{\sqrt{2}}(\phi_2^1)^2 + \frac{1}{\sqrt{2}}(\phi_2^2)^2, \sqrt{2}\phi_2^1\phi_2^2\right)$. Now combining this doublet with the original doublet we obtain a third degree singlet (invariant), $-\frac{1}{\sqrt{2}}(\phi_2^1)^3 + \frac{3}{\sqrt{2}}(\phi_2^2)^2\phi_2^1$. Along with the term $(\phi_2^1)^2 + (\phi_2^2)^2$ (which is basically $U(1)$ invariant), we can construct the potential

$$V(\phi_2) \propto \left((\phi_2^1)^2 + (\phi_2^2)^2\right)^3 + c\left(-(\phi_2^1)^3 + 3(\phi_2^2)^2\phi_2^1\right) \tag{4.63}$$

where c is a constant, leading to a VEV of $\langle\phi_2\rangle = (-\frac{1}{2}, \frac{\sqrt{3}}{2})$, as required. The potential V(ϕ_2) is shown in Figure 4.6.

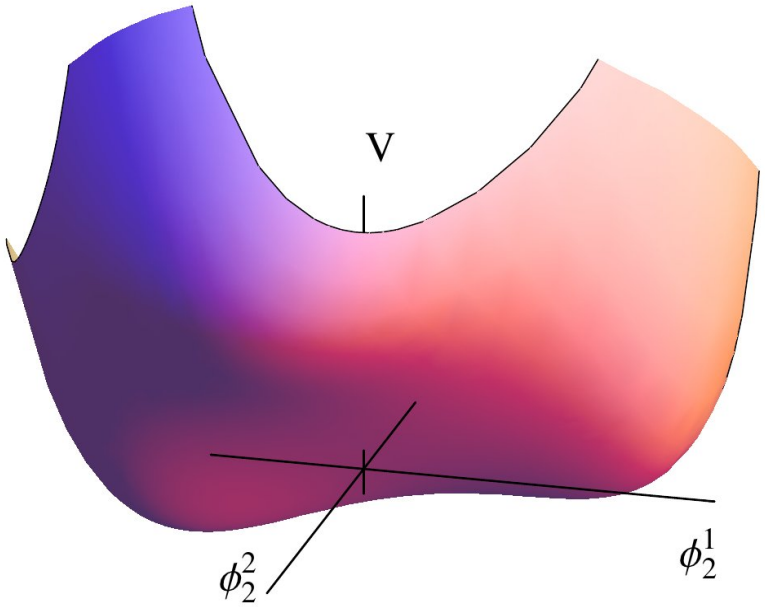

Figure 4.6: The potential, Eq. (4.63), for the flavon field ϕ_2 showing the three points of minima one of which is the required VEV, $(-\frac{1}{2}, \frac{\sqrt{3}}{2})$.

For the flavon ϕ_3, it is easier to work in the non-$\mu-\tau$-rotated basis. Defining $\phi_3 = (\phi_3^1, \phi_3^2, \phi_3^3)$ in this basis (the components are italicised for this non-rotated basis), S_4 invariants can be easily constructed by summing up even powers of ϕ_3^1, ϕ_3^2 and ϕ_3^3 symmetrically. A potential constructed in this way is

$$\begin{aligned} V(\phi_3) \propto \quad & \left((\phi_3^1)^8 + (\phi_3^2)^8 + (\phi_3^3)^8\right) + p\left((\phi_3^1)^6 + (\phi_3^2)^6 + (\phi_3^3)^6\right) \\ & + q\left((\phi_3^1)^4 + (\phi_3^2)^4 + (\phi_3^3)^4\right) + r\left((\phi_3^1)^2 + (\phi_3^2)^2 + (\phi_3^3)^2\right) \\ & + s\left((\phi_3^1)^2(\phi_3^2)^2 + (\phi_3^3)^2(\phi_3^2)^2 + (\phi_3^1)^2(\phi_3^3)^2\right) \end{aligned} \tag{4.64}$$

with the real parameters p, q, r and s under some constraints determined later. This results in $\langle\phi_3\rangle = (1, -\sqrt{2}, 0)$ in the non-rotated basis, corresponding to $\langle\phi_3\rangle = (1, -1, 1)$, in the $\mu-\tau$ rotated basis, as required. At the points of extrema first order derivatives of the potential should vanish, i.e.

$$\frac{\partial V}{\partial \phi_3^1} = 0, \quad \frac{\partial V}{\partial \phi_3^2} = 0, \quad \frac{\partial V}{\partial \phi_3^3} = 0. \tag{4.65}$$

Applying the above conditions at the point $\phi_3 = (1, -\sqrt{2}, 0)$, we get the following

constraints:

$$r = -60 - 21p - 6q \tag{4.66}$$

$$s = 28 + 9p + 2q. \tag{4.67}$$

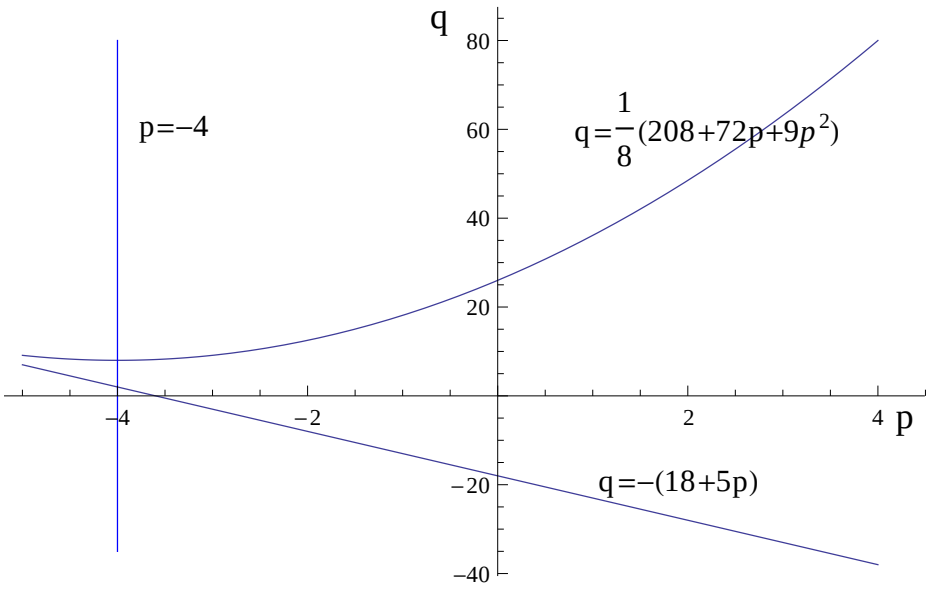

Figure 4.7: Constraints between the variables p and q for a positive definite Hessian matrix. Hessian is positive definite in the region to the right of $p = -1$ and between the curves $q = \frac{1}{8}\left(208 + 72p + 9p^2\right)$ and $q = -(18 + 5p)$.

To ensure that the extrema points are minima, we need to calculate Hessian matrix,

$$H = \begin{pmatrix} \frac{\partial^2 V}{\partial \phi_3^1 \partial \phi_3^1} & \frac{\partial^2 V}{\partial \phi_3^1 \partial \phi_3^2} & \frac{\partial^2 V}{\partial \phi_3^1 \partial \phi_3^3} \\ \frac{\partial^2 V}{\partial \phi_3^2 \partial \phi_3^1} & \frac{\partial^2 V}{\partial \phi_3^2 \partial \phi_3^2} & \frac{\partial^2 V}{\partial \phi_3^2 \partial \phi_3^3} \\ \frac{\partial^2 V}{\partial \phi_3^3 \partial \phi_3^1} & \frac{\partial^2 V}{\partial \phi_3^3 \partial \phi_3^2} & \frac{\partial^2 V}{\partial \phi_3^3 \partial \phi_3^3} \end{pmatrix} \tag{4.68}$$

and impose the condition that H is positive definite. Thus we get the following inequalities:

$$(4 + p) > 0 \tag{4.69}$$

$$(18 + 5p + q) > 0 \tag{4.70}$$

$$(208 + 72p + 9p^2 - 8q) > 0. \tag{4.71}$$

The above constraints are shown in the p-q plot, Figure 4.7. Assuming these constraints, the points of minima obtained for the flavon potential, Eq. (4.64) are shown in Figure 4.8.

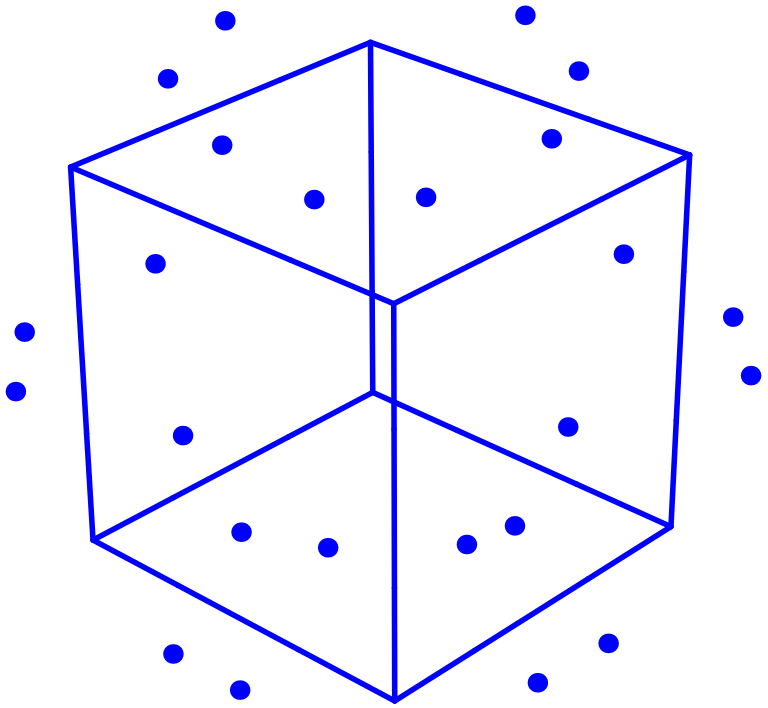

Figure 4.8: The dots represent the points of minima for the flavon potential. The dots are at $(0, \pm 1, \pm\sqrt{2}), (0, \pm\sqrt{2}, \pm 1)$, $(\pm 1, 0, \pm\sqrt{2}), (\pm\sqrt{2}, 0, \pm 1)$, $(\pm 1, \pm\sqrt{2}, 0), (\pm\sqrt{2}, \pm 1, 0)$ (denoted in the non-rotated co-ordinate system i.e. Figure 4.1, for a unit cube)

Note that the potential, Eq. (4.64), contains invariant terms constructed from the triplet flavon up to a degree 8. In general a very large number of terms (here ≈ 50) can be obtained if we allow ourselves to go up this high degree. Analysing all those terms is beyond the scope of this chapter. Moreover the most general potential will contain a large number of free parameters as coefficients of invariant terms. In our potential, Eq. (4.64), we assume that most of these coefficients vanish. Such a simplistic assumption is for demonstrative purpose only, to show that the required VEV can be obtained in the formalism of the extremisation of a flavon potential.

4.4 The model

The model is constructed in the Standard Model framework with the addition of heavy right-handed neutrinos. Through type-1 seesaw mechanism light Majorana neutrinos are produced. The right-handed heavy neutrinos as well as the Standard Model left-handed weak isospin doublets transform as a $\mathbf{3'}$ under the flavour group S_4:

$$\nu_R = \begin{pmatrix} \nu_{Re} \\ \nu_{R\mu} \\ \nu_{R\tau} \end{pmatrix} \equiv \mathbf{3'}, \quad L = \begin{pmatrix} L_e \\ L_\mu \\ L_\tau \end{pmatrix} \equiv \mathbf{3'} \tag{4.72}$$

where

$$L_e = \begin{pmatrix} \nu_{Le} \\ e_L \end{pmatrix} \tag{4.73}$$

etc. Note that throughout this chapter, the indices e, μ, τ are used to denote the three states in the flavour triplets, i.e. they correspond to three families. We assume three families for the right-handed neutrinos which in turn form the triplet, Eq. (4.72), and hence we use the same indices e, μ, τ for right-handed neutrinos also. The right-handed charged leptons transform as flavour singlets.

Apart from the flavons introduced in the last section, we also postulate an S_4 singlet flavon ϕ_1^- along with a C_2 flavour symmetry (Note that the cube also has an additional C_2 symmetry corresponding to reflections). This is done to restrict flavon content of the Dirac mass term for the neutrinos (containing the right-handed neutrinos and the left-handed lepton doublets) to only the singlet flavon ϕ_1^- and thus make the Dirac mass matrix proportional to the identity matrix. Three flavons ϕ_1, ϕ_2 and ϕ_3 that transform as $\mathbf{1}$, $\mathbf{2}$ and $\mathbf{3}$ were introduced in the last section to facilitate the construction of the "Simplest" neutrino Majorana mass matrix. For providing three different masses to the charged leptons, we also introduce three flavons ϕ'_{3e}, $\phi'_{3\mu}$ and $\phi'_{3\tau}$ all of which transform as the triplet $\mathbf{3'}$, corresponding to electron, muon and tau leptons respectively. The fermion and flavon content of the model with representations to which they belong is given in the Table 4.2. The Higgs Boson is a flavour singlet.

	e_R	μ_R	τ_R	L	ν_R	ϕ_1^-	ϕ_1	ϕ_2	ϕ_3	ϕ'_{3e}	$\phi'_{3\mu}$	$\phi'_{3\tau}$
S_4	χ_1	χ_1	χ_1	χ'_3	χ'_3	χ_1	χ_1	χ_2	χ_3	χ'_3	χ'_3	χ'_3
C_2	-1	-1	-1	-1	1	-1	1	1	1	1	1	1

Table 4.2: The flavour structure of the S_4 model

For the charged leptons, the mass term is of the form

$$\left(y_e L^\dagger e_R \phi'_{3e} + y_\mu L^\dagger \mu_R \phi'_{3\mu} + y_\tau L^\dagger \tau_R \phi'_{3\tau}\right) \frac{H}{\Lambda} + H.C. \tag{4.74}$$

where H is the Standard Model Higgs, Λ is the cut-off scale and the y_i are coupling constants. After the spontaneous breaking of the weak gauge symmetry and also the flavour symmetry with the flavons, ϕ'_{3e}, $\phi'_{3\mu}$ and $\phi'_{3\tau}$, getting VEVs of $(1,0,0)^T$, $(0,1,0)^T$ and $(0,0,1)^T$ respectively, we obtain the required masses m_e, m_μ and m_τ for the charged leptons where $m_e = \frac{y_e h_o}{\Lambda}$ etc. with h_o the Higgs VEV.

It is easy to see that $(1,0,0)^T$, $(0,1,0)^T$ and $(0,0,1)^T$, the VEVs for the flavons ϕ'_{3e}, $\phi'_{3\mu}$ and $\phi'_{3\tau}$, are invariant eigenstates. Note that we are in the μ-τ-rotated basis, Figure 4.4. Here the state $(1,0,0)^T$ is aligned along the x-axis which passes through the face centre of the cube. This state is invariant under the $\frac{\pi}{2}$-symmetry rotation of the S_4 group corresponding to the conjugacy class C'_6, Table 4.1. The states $(0,1,0)^T$ and $(0,0,1)^T$ are aligned along the y-axis and the z-axis respectively, which pass through the edge centres of the cube. Therefore these states are the invariant eigenstates of the π-symmetry rotations of the cube corresponding to the conjugacy class C_6.

The basic framework for constructing the Majorana mass term in the model for the right-handed neutrinos was familiarised earlier, Eq. (4.46). Here we write down the mass term along the same lines:

$$\left(y_1 \xi_1 \phi_1 + y_2 \xi_2^T \phi_2 + i y_3 \xi_3^T \phi_3\right) \frac{1}{\Lambda} + H.C., \tag{4.75}$$

where ξ_1, ξ_2 and ξ_3 are the expressions given in Eqs. (4.41-4.43) constructed using the right-handed neutrinos, ν_R. As discussed in the last section, the flavons ϕ_1, ϕ_2 and ϕ_3 get VEVs 1, $(-\frac{1}{2}, \frac{\sqrt{3}}{2})^T$ and $(1,-1,1)^T$ respectively. The couplings y_1, y_2 and y_3 are in the Grand Unification scale. Thus after spontaneous symmetry breaking we get

$$\nu_{R\alpha}\, M_{\text{Maj}}\, \nu_R^\alpha + H.C. \tag{4.76}$$

where

$$M_{\text{Maj}} = \begin{pmatrix} m_1 + \frac{1}{\sqrt{6}} m_2 & -\frac{i}{\sqrt{2}} m_3 & \frac{i}{\sqrt{2}} m_3 \\ -\frac{i}{\sqrt{2}} m_3 & m_1 - \frac{1}{2\sqrt{6}} m_2 + \frac{i}{\sqrt{2}} m_3 & \frac{\sqrt{3}}{2\sqrt{2}} m_2 \\ \frac{i}{\sqrt{2}} m_3 & \frac{\sqrt{3}}{2\sqrt{2}} m_2 & m_1 - \frac{1}{2\sqrt{6}} m_2 - \frac{i}{\sqrt{2}} m_3 \end{pmatrix} \tag{4.77}$$

with $m_1 = \frac{y_1}{\Lambda}$ etc.

The Dirac mass term for the neutrinos takes the form

$$y_w L^\dagger \nu_R \frac{\phi_1^-}{\Lambda} \tilde{H} + H.C. \tag{4.78}$$

where $\tilde{H}$ is the conjugate Higgs and y_w is a coupling of the order of the weak scale. Since L and ν_R belong to $\mathbf{3'}$, we should be able to get terms that transform as a $\mathbf{1}$, a $\mathbf{2}$, a $\mathbf{3}$ and a $\mathbf{3'}$ from their tensor product. But due to the C_2 symmetry from the Table 4.2 it is clear that invariant terms involving a $\mathbf{2}$, a $\mathbf{3}$ or a $\mathbf{3'}$ are not allowed. That is why only the singlet flavon ϕ_1^- can appear in Eq. (4.78). This term after spontaneous symmetry breaking with ϕ_1^- getting a VEV 1, leads to

$$2\nu_{L\alpha}^{*T} M_{\text{Dir}} \nu_R^\alpha + H.C. \tag{4.79}$$

where

$$M_{\text{Dir}} = \begin{pmatrix} m_w & 0 & 0 \\ 0 & m_w & 0 \\ 0 & 0 & m_w \end{pmatrix} \tag{4.80}$$

with $m_w = \frac{y_w h_o}{2\Lambda}$ and

$$\nu_L = \begin{pmatrix} \nu_{Le} \\ \nu_{L\mu} \\ \nu_{L\tau} \end{pmatrix}, \quad \nu_R = \begin{pmatrix} \nu_{Re} \\ \nu_{R\mu} \\ \nu_{R\tau} \end{pmatrix}. \tag{4.81}$$

Thus as promised earlier, the added C_2 symmetry ensures that the Dirac mass matrix is proportional to the identity matrix.

The Dirac and the Majorana mass terms can be combined together and shown using a 6×6 mass matrix M:

$$\nu_\alpha^T M \nu^\alpha + H.C. \tag{4.82}$$

where

$$M = \begin{pmatrix} 0 & M_{\text{Dir}} \\ M_{\text{Dir}} & M_{\text{Maj}} \end{pmatrix} \tag{4.83}$$

and

$$\nu = \begin{pmatrix} \nu_L^* \\ \nu_R \end{pmatrix}. \tag{4.84}$$

In the discussion in the introductory section we showed that right multiplying the mass matrix M_{Maj} with P takes it back to the hermitian form. Let the unitary

matrix U diagonalising this hermitian matrix give the eigenvalues e_1, e_2 and e_3,

$$U M_{\rm Maj} P U^\dagger = D \tag{4.85}$$

where

$$D = \begin{pmatrix} e_1 & 0 & 0 \\ 0 & e_2 & 0 \\ 0 & 0 & e_3 \end{pmatrix}. \tag{4.86}$$

Let

$$\begin{pmatrix} U_{\rm DD} & U_{\rm DM} \\ U_{\rm MD} & U_{\rm MM} \end{pmatrix} \begin{pmatrix} 0 & M_{\rm Dir} \\ M_{\rm Dir} & M_{\rm Maj} \end{pmatrix} \begin{pmatrix} U_{\rm DD} & U_{\rm DM} \\ U_{\rm MD} & U_{\rm MM} \end{pmatrix}^T = \begin{pmatrix} D_{\rm Light} & 0 \\ 0 & D_{\rm Heavy} \end{pmatrix}. \tag{4.87}$$

As stated earlier $M_{\rm Dir}$ is at the weak scale and $M_{\rm Maj}$ is at the GUT scale. Therefore the seesaw mechanism comes into play. It can be shown that [67], to a very good approximation, we have

$$D_{\rm light} = \begin{pmatrix} \frac{m_w^2}{|e_1|} & 0 & 0 \\ 0 & \frac{m_w^2}{|e_2|} & 0 \\ 0 & 0 & \frac{m_w^2}{|e_3|} \end{pmatrix}, \quad D_{\rm heavy} = \begin{pmatrix} |e_1| & 0 & 0 \\ 0 & |e_2| & 0 \\ 0 & 0 & |e_3| \end{pmatrix}. \tag{4.88}$$

The matrices $U_{\rm DM}$ and $U_{\rm MD}$ are very small and can be ignored. The matrices $U_{\rm DD}$ and $U_{\rm MM}$ are approximately equal to the U, Eq. (4.3, 4.85), with some additional phase factors

$$|U_{\rm DD}| = |U_{\rm MM}| = |U|. \tag{4.89}$$

In other words the left handed neutrinos and the light neutrinos are related through the unitary transformation involving U:

$$\begin{aligned} \nu_{\rm i} &= U_{\rm DD} \nu_L \\ &= \Phi_i U \, \Phi_\alpha \nu_L \end{aligned} \tag{4.90}$$

where

$$\nu_{\rm i} = \begin{pmatrix} \nu_1 \\ \nu_2 \\ \nu_3 \end{pmatrix}, \quad \nu_L = \begin{pmatrix} \nu_{Le} \\ \nu_{L\mu} \\ \nu_{L\tau} \end{pmatrix} \tag{4.91}$$

and Φ_i and Φ_α are diagonal matrices with phases like the ones shown in Eqs. (4.15, 4.16). The states ν_1, ν_2 and ν_3 are mass eigenstates with masses $\frac{m_w^2}{|e_1|}$, $\frac{m_w^2}{|e_2|}$ and $\frac{m_w^2}{|e_3|}$ respectively. Thus after spontaneous symmetry breaking and seesaw mechanism, the

mass term takes the form

$$\frac{m_w^2}{|e_1|}\nu_1.\nu_1 + \frac{m_w^2}{|e_2|}\nu_2.\nu_2 + \frac{m_w^2}{|e_3|}\nu_3.\nu_3 + H.C.. \tag{4.92}$$

4.5 Fitting the model with experimental data

The Daya Bay Reactor Neutrino Experiment and the RENO Experiment recently measured a non-zero value of θ_{13}. In this section we fit the model with this value. We will use this information along with the experimentally measured mass-squared differences of the neutrinos to predict the unknown overall neutrino mass offset.

We have earlier stated that given a Majorana mass matrix, M_{Maj}, Eq. 4.77, with eigenvalues e_1, e_2, e_3, then the three light neutrino masses will be proportional to the reciprocal of the eigenvalues, Eq. 4.88,

$$m_1 \propto \frac{1}{|e_1|}, \qquad m_2 \propto \frac{1}{|e_2|}, \qquad m_3 \propto \frac{1}{|e_3|}. \tag{4.93}$$

Using the model we have obtained a Majorana mass matrix of the form given in Eq. (4.21). Using the result given in Eq. (4.3), it is clear that the eigenvalues are

$$e_1 = c - a\sqrt{1+3k^2} \tag{4.94a}$$

$$e_2 = c \tag{4.94b}$$

$$e_3 = c + a\sqrt{1+3k^2}. \tag{4.94c}$$

The squared differences of neutrino masses are experimentally known. The PDG values are

$$m_2^2 - m_1^2 = 75.9 \pm 2.1\text{meV}^2 \tag{4.95a}$$

$$|m_3^2 - m_2^2| = 2430 \pm 130\text{meV}^2. \tag{4.95b}$$

Therefore from Eqs. (4.93-4.95) we have

$$\begin{aligned}\frac{m_2^2 - m_1^2}{m_3^2 - m_2^2} &= \frac{\frac{1}{e_2}^2 - \frac{1}{e_1}^2}{\frac{1}{e_3}^2 - \frac{1}{e_2}^2} \\ &= \frac{(\sqrt{1+3k^2} - r)^2(3k^2 + 2(-1+\sqrt{1+3k^2})r)}{(\sqrt{1+3k^2} + r)^2(-3k^2 + 2(1+\sqrt{1+3k^2})r)} \\ &= \pm\frac{75.9 \pm 2.1}{2430 \pm 130}\end{aligned} \tag{4.96}$$

where $r = c/a$. The parameters a and c are assumed to be real, so that the eigenvalues given in Eq. (4.94) are also real.

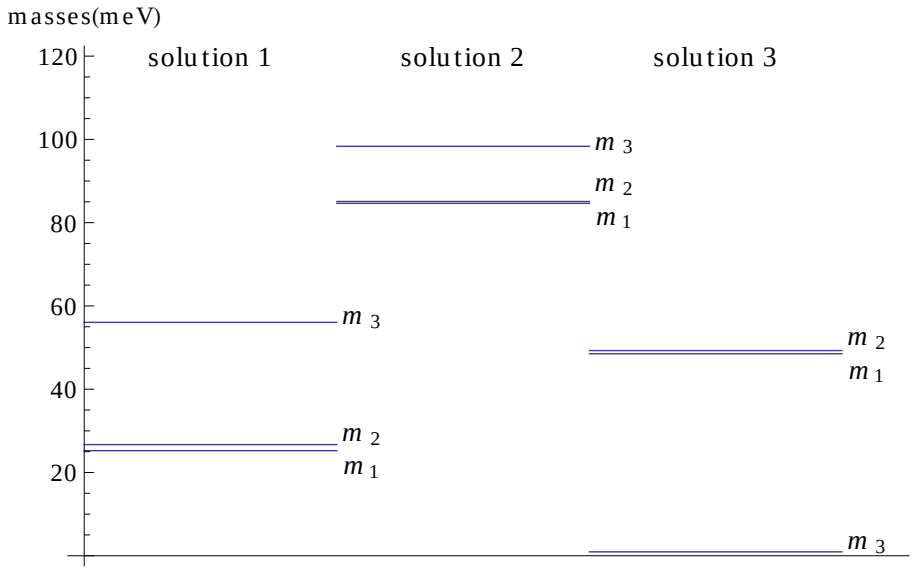

Figure 4.9: The predicted values of the neutrino masses are shown. Solution 1 ($r = 0.4101$) and solution 2 ($r = 14.452$) correspond to normal hierarchy. Solution 3 ($r = -1.0405$) corresponds to inverted hierarchy.

The observations made by Daya Bay [23] and RENO [24] experiments are $\sin^2 2\theta_{13} = 0.092 \pm 0.016(\text{stat}) \pm 0.005(\text{syst})$ and $\sin^2 2\theta_{13} = 0.113 \pm 0.013(\text{stat.}) \pm 0.019(\text{syst.})$ respectively. Given the value of θ_{13}, we use Eqs. (4.5, 4.9) to solve for k^2. For the weighted average value of $\sin^2 2\theta_{13} = 0.098$, we get

$$k^2 = 0.238. \tag{4.97}$$

Substituting the value of k^2 in Eq. (4.96) we can solve for r. Eq. (4.96) being cubic in r, gives three solutions each for positive and negative mass-squared-difference ratios. For the ratio $+\frac{75.9}{2430}$ we have

$$r = -1.0411, \quad r = 0.4101, \quad r = 14.452 \tag{4.98}$$

and for the ratio $-\frac{75.9}{2430}$ we have

$$r = -1.0405, \quad r = 0.362 - i\,0.707, \quad r = 0.362 + i\,0.707. \tag{4.99}$$

The solution $r = -1.0411$ corresponds to negative sign for the mass-squared difference $m_2^2 - m_1^2$ and so it is not admissible. Also the complex solutions are not valid. Thus we have two solutions $r = 0.4101$ and $r = 14.452$ corresponding to the normal hierarchy and one solution $r = -1.0405$ corresponding to the inverted hierarchy. The respective neutrino masses are shown in Figure 4.9. The three solutions for m_1 along with the errors are shown in Figure 4.10.

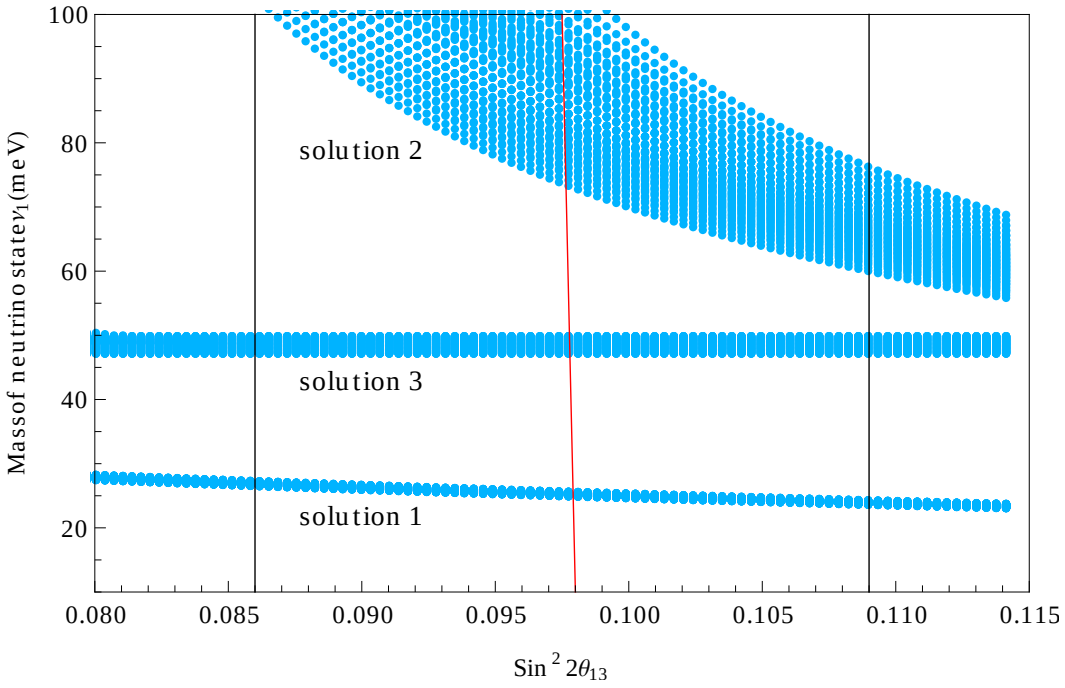

Figure 4.10: The predicted value of m_1 (the mass of the neutrino eigenstate ν_1) vs the measured value of $\sin^2 2\theta_{13}$. The finite thickness of the bands is due to the errors in the measurement of the neutrino mass-squared differences. The red and the black lines indicate the best fit value and the errors of $\sin^2 2\theta_{13}$ respectively

Of course in Triχmaximal mixing (TχM), given the three mixing angles θ_{12}, θ_{23}, θ_{13}, maximal CP violation ($|\delta_{CP}| = 90^o$) is always guaranteed. The positive and negative signs in $\pm ik$ correspond to the CP-violating phase $\delta_{CP} = \pm 90°$.

Summary

The introductory chapter gives a review of flavour physics with emphasis on neutrino oscillations. In the next chapter we discuss the Koide formula and its possible extension. Later we shift our attention to renormalisation and its effect on flavour physics. A set of exact Standard Model renormalisation group evolution invariants which link quark masses and mixing parameters are constructed based on the considerations of flavour symmetry. We study their phenomenology and find that a simple combination of Yukawa coupling matrices plays a unique role in the Standard Model, suggesting a possible new insight into the observed spectrum of quark masses. Our evolution invariants are readily generalised to the leptons in the case of Dirac neutrinos. We also look into the RG evolution equations in the MSSM and find that invariants similar to the ones in the Standard Model cannot be constructed for the MSSM.

In Chapter 3, we present a model of neutrino mixing based on the flavour group $C_3 \times C_3 \rtimes C_3$ in order to account for the recent observation of a non-zero reactor mixing angle (θ_{13}). The model provides a common flavour structure for the charged-lepton and the neutrino sectors, giving their mass matrices a 'circulant-plus-diagonal' form. Mass matrices of this form readily lead to mixing patterns with realistic deviations from Tribimaximal mixing, including non-zero θ_{13}. With the parameters constrained by existing measurements, our model predicts an inverted neutrino mass hierarchy with the lightest neutrino mass, $m_3 \simeq 65$ meV, and a maximal CP phase giving CP asymmetries in neutrino oscillations of up to 40%.

Chapter 4 is motivated by the "Simplest" neutrino mass matrix proposed in 2004 which predicted $\sin\theta_{13} = \sqrt{2\Delta m^2_{sol}/3\Delta m^2_{atm}}$. We remark that this prediction

is consistent with today's measured value of θ_{13}. The "Simplest" mixing being a special case of Triχmaximal mixing also leads to $\delta_{CP} = \pm\frac{\pi}{2}$. In this chapter a model based on S_4 symmetry is constructed to include this specific texture as the Majorana mass matrix. In building the model we define the flavour eigenstates in a non-conventional way and thus work in the "μ-τ-rotated" basis of S_4. We explore its phenomenology in the context of the see-saw mechanism and use it to predict the unknown light neutrino mass.

Bibliography

[1] P. F. Harrison, R. Krishnan, and W. G. Scott. Exact One-Loop Evolution Invariants in the Standard Model. *Phys. Rev. D*, 82:096004, 2010.

[2] Particle Data Group. The Review of Particle Physics. *Phys. Rev. D*, 86:010001, 2012.

[3] Lincoln Wolfenstein. Parametrization of the Kobayashi-Maskawa Matrix. *Phys. Rev. Lett.*, 51:1945, 1983.

[4] C. Jarlskog. Commutator of the Quark Mass Matrices in the Standard Electroweak Model and a Measure of Maximal CP Nonconservation. *Phys. Rev. Lett.*, 55:1039, 1985.

[5] C.L. Cowan, Jr. F. Reines, F.B. Harrison, H.W. Krue, and A.D. McGuire. Detection of the Free Neutrino: a Confirmation. *Science*, 124:103, 1956.

[6] G. Danby, J. M. Gaillard, K. Goulianos, L. M. Lederman, N. Mistry, M. Schwartz, and J. Steinberger. Observation of High-Energy Neutrino Reactions and the Existence of Two Kinds of Neutrinos. *Phys. Rev. Lett.*, 9:36–44, 1962.

[7] DONUT Collaboration. Observation of Tau Neutrino Interactions. *Phys. Lett. B*, 504:218–224, 2001.

[8] http://upload.wikimedia.org/wikipedia/commons/6/64/KATRIN_Spectrum.svg.

[9] E. W. Otten and C. Weinheimer. Neutrino mass limit from tritium beta decay. *Rept. Prog. Phys.*, 71:086201, 2008.

[10] Steven R. Elliott and Petr Vogel. Double Beta Decay. *Annu. Rev. Nucl. Part. Sci.*, 52:115–151, 2002.

[11] NEMO-3 Collaboration. Results of the NEMO-3 Double Beta Decay Experiment. *Proceeding - 22nd Rencontres de Blois - 2010*, arXiv:1105.2435, 2011.

[12] Yvonne Y. Y. Wong. Neutrinos and Cosmology. *LAUNCH, Heidelberg, 9-12 Nov 2009*.

[13] WiggleZ Collaboration. The WiggleZ Dark Energy Survey: Cosmological neutrino mass constraint from blue high-redshift galaxies. *Phys. Rev. D*, 85:081101, 2012.

[14] S. M. Bilenky, C. Giunti, and W. Grimus. Phenomenology of Neutrino Oscillations. *Prog. Part. Nucl. Phys.*, 43:1–86, 1999.

[15] A. Yu. Smirnov. The MSW Effect and Matter Effects in Neutrino Oscillations. *Physica Scripta.*, T121:57–64, 2005.

[16] P.F. Harrison, D.H. Perkins, and W.G. Scott. No Mikheyev-Smirnov-Wolfenstein Effect in Maximal Mixing. *Phys. Lett. B*, 374:111–115, 1996.

[17] John N Bahcall and Carlos Pena-Garay. Solar models and solar neutrino oscillations. *New J. Phys.*, 6:63, 2004.

[18] K. S. Hirata *et al.* Real-time, directional measurement of B-8 solar neutrinos in the Kamiokande II detector. *Phys. Rev. D*, 44:2241–2260, 1991.

[19] K. S. Hirata *et al.* Constraints on neutrino-oscillation parameters from the Kamiokande-II solar-neutrino data. *Phys. Rev. Lett*, 65:1301–1304, 1990.

[20] SNO Collaboration. Combined Analysis of all Three Phases of Solar Neutrino Data from the Sudbury Neutrino Observatory. *Phys. Rev. C (Submitted)*, arXiv:1109.0763, 2011.

[21] The Super-Kamiokande Collaboration. Atmospheric neutrino oscillation analysis with subleading effects in Super-Kamiokande I, II, and III. *Phys. Rev. D*, 81:092004, 2010.

[22] Thierry Lasserre and Henry W. Sobel. Reactor Neutrinos. *Comptes Rendus Physique*, 6:749–757, 2005.

[23] F. P. An *et al.* [Daya Bay Collaboration]. Observation of electron-antineutrino disappearance at Daya Bay. *Phys. Rev. Lett.*, 108:171803, 2012.

[24] J. K. Ahn *et al.* [RENO Collaboration]. Observation of Reactor Electron Antineutrino Disappearance in the RENO Experiment. *Phys. Rev. Lett.*, 108:191802, 2012.

[25] D. V. Forero, M. Tortola, and J. W. F. Valle. Global status of neutrino oscillation parameters after Neutrino-2012. *Phys. Rev. D*, 86:073012, 2012.

[26] Y. Koide. A fermion-boson composite model of quarks and leptons. *Phys. Lett. B*, 120:161–165, 1983.

[27] C. Amsler *et al.* Review of particle physics. *Phys. Lett. B*, 667:1, 2008.

[28] Zhi-zhong Xing, H. Zhang, and S. Zhou. Updated Values of Running Quark and Lepton Masses. *Phys. Rev. D*, 77:113016, 2008.

[29] Nan Li and Bo-Qiang Ma. Energy scale independence of Koide's relation for quark and lepton masses. *Phys. Rev. D*, 73:013009, 2006.

[30] M. E. Peskin and D. V. Schroeder. *An introduction to Quantum Field Theory.* Perseus Books, 1995.

[31] Marie E. Machacek and Michael T. Vaughn. Two-loop renormalization group equations in a general quantum field theory : (I). Wave function renormalization. *Nuclear Physics B*, 222:83, 1983.

[32] K. S. Babu. Renormalization-group analysis of the Kobayashi-Maskawa matrix. *Z. Phys. C*, 35:69, 1987.

[33] K. Sasaki. Renormalization group equations for the Kobayashi-Maskawa matrix. *Z. Phys. C*, 32:149, 1986.

[34] Marie E. Machacek and Michael T. Vaughn. Two-loop renormalization group equations in a general quantum field theory (II). Yukawa couplings. *Nuclear Physics B*, 236:221, 1984.

[35] Durmus A. Demir. Renormalization group invariants in the MSSM and its extensions. *JHEP*, 11:003, 2005.

[36] Sanghyeon Chang and T. K. Kuo. Renormalization Invariants of the Neutrino Mass Matrix. *Phys. Rev. D*, 66:111302, 2002.

[37] Lu-Xin Liu. Renormalization Invariants and Quark Flavor Mixings. *Int. J. Mod. Phys. A*, 25:4975, 2010.

[38] Zhi-zhong Xing and Shu Luo. Radiative Corrections to the CKM Unitarity Triangles. *J. Phys. G: Nucl. Part. Phys.*, 37:075018, 2010.

[39] P. F. Harrison and W. G. Scott. Generation Permutation Symmetry and the Quark Mixing Matrix. *Phys. Lett. B*, 333:471, 1994.

[40] P. F. Harrison and W. G. Scott. Covariant extremisation of flavour-symmetric jarlskog invariants and the neutrino mixing matrix. *Phys. Lett. B*, 628:93, 2005.

[41] P. F. Harrison, D. R. J. Roythorne, and W. G. Scott. Plaquette Invariants and the Flavour Symmetric Description of Quark and Neutrino Mixings. *Phys. Lett. B*, 657:210, 2007.

[42] C. Jarlskog. A Basis Independent Formulation of the Connection Between Quark Mass Matrices, CP Violation and Experiment. *Z. Phys. C*, 29:491, 1985.

[43] Gregory G. Athanasiu, Savas Dimopoulos, and Frederick J. Gilman. CP Non-conservation at the Unification Scale. *Phys. Rev. Lett.*, 57:1982, 1986.

[44] Yu. F. Pirogov and O. V. Zenin. Two-loop renormalization group restrictions on the standard model and the fourth chiral family. *Eur. Phys. J. C.*, 10:629, 1999.

[45] P. F. Harrison, D. R. J. Roythorne, and W. G. Scott. Flavour Permutation Symmetry and Fermion Mixing. *Proceedings of the 43rd Rencontres de Moriond on electroweak interactions and Unified Theories, La Thuile, Italy*, arXiv:0805.3440, 2008.

[46] P. F. Harrison, W. G. Scott, and T. J. Weiler. Real Invariant Matrices and Flavour-Symmetric Mixing Variables with Emphasis on Neutrino Oscillations. *Phys. Lett. B*, 641:372, 2006.

[47] A. Davidson, T. Schwartz, and K. C. Wali. Light-Heavy Symmetry: Geometric Mass Hierarchy for Three Families. *J. Phys. G*, 24:L55–L62, 1998.

[48] S. Abe *et al.* [KamLAND Collaboration]. Precision Measurement of Neutrino Oscillation Parameters with KamLAND. *Phys. Rev. Lett.*, 100:221803, 2008.

[49] Y. Ashie *et al.* [Super-Kamiokande Collaboration]. A Measurement of Atmospheric Neutrino Oscillation Parameters by Super-Kamiokande I. *Phys. Rev. D*, 71:112005, 2005.

[50] P. F. Harrison, D. H. Perkins, and W. G. Scott. Tri-Bimaximal Mixing and the Neutrino Oscillation Data. *Phys. Lett. B*, 530:167–173, 2002.

[51] P. F. Harrison, W. G. Scott, and D. H. Perkins. Threefold Maximal Lepton Mixing and the Solar and Atmospheric Neutrino Deficits". *Phys. Lett. B*, 349:137–144, 1995.

[52] P. F. Harrison, W. G. Scott, and D. H. Perkins. A Redetermination of the Neutrino Mass-Squared Difference in Tri-Maximal Mixing with Terrestrial Matter Effects. *Phys. Lett. B*, 458:79–92, 1999.

[53] Jean-Pierre Serre. *Linear Representations of Finite Groups*. Springer, 1977.

[54] I. de Medeiros Varzielas, S. F. King, and G. G. Ross. Neutrino tri-bi-maximal mixing from a non-Abelian discrete family symmetry. *Phys. Lett. B*, 648:201–206, 2007.

[55] Ernest Ma. Near Tribimaximal Neutrino Mixing with Delta(27) Symmetry. *Phys. Lett. B*, 660:505–507, 2008.

[56] Ernest Ma. Neutrino Mass Matrix from Delta(27) Symmetry. *Mod. Phys. Lett. A*, 21:1917–1921, 2006.

[57] Haim Harari, Herve Haut, and Jacques Weyers. Quark Masses and Cabibbo Angles. *Phys. Lett. B*, 78:459–461, 1978.

[58] C.D. Froggatt and H.B. Nielsen. Hierarchy of Quark Masses, Cabibbo Angles and CP Violation. *Nucl. Phys. B*, 147:277–298, 1979.

[59] Miriam Leurer, Yosef Nir, and Nathan Seiberg. Mass Matrix Models. *Nucl. Phys. B*, 398:319–342, 1993.

[60] David B. Kaplan and Martin Schmaltz. Flavor Unification and Discrete Nonabelian Symmetries. *Phys. Rev. D*, 49:3741–3750, 1994.

[61] Thomas Schwetz, Mariam Tortola, and J. W. F. Valle. Global neutrino data and recent reactor fluxes: status of three-flavour oscillation parameters. *New J. Phys.*, 13:063004, 2011.

[62] K. Abe *et al.* [T2K Collaboration]. Indication of Electron Neutrino Appearance from an Accelerator-produced Off-axis Muon Neutrino Beam. *Phys. Rev. Lett.*, 107:041801, 2011.

[63] Guido Altarelli and Ferruccio Feruglio. Discrete Flavor Symmetries and Models of Neutrino Mixing. *Rev. Mod. Phys.*, 82:2701–2729, 2010.

[64] P. F. Harrison and W. G. Scott. Symmetries and Generalisations of Tri-Bimaximal Neutrino Mixing. *Phys. Lett. B*, 535:163–169, 2002.

[65] P. F. Harrison and W. G. Scott. The Simplest Neutrino Mass Matrix. *Phys. Lett. B*, 594:324–332, 2004.

[66] Stephen F. King and Christoph Luhn. A new family symmetry for SO(10) GUTs. *Nucl. Phys. B*, 820:269–289, 2009.

[67] Alexei Yu. Smirnov. See-saw Enhancement of Lepton Mixing. *Phys. Rev. D*, 48:3264–3270, 1993.